EXPERIMENTAL AND NUMERICAL CHARACTERIZATION OF THE FATIGUE AND FRACTURE PROPERTIES OF FRICTION PLUG WELDS IN 2195-T8 ALUMINUM LITHIUM ALLOY

by

DAVID FRANCIS METZ

MARK E. BARKEY, COMMITTEE CHAIR
RICHARD C. BRADT
JAMES P. HUBNER
MARK L. WEAVER
JOHN E. JACKSON
YUEBIN GUO

A DISSERTATION

Submitted in partial fulfillment of the requirements
for the degree of Doctor of Philosophy
in the Department of Aerospace Engineering and Mechanics
in the Graduate School of
The University of Alabama

TUSCALOOSA, ALABAMA

2013

ABSTRACT

The mechanical, fatigue, and fracture properties of friction stir welded 2195-T8 Al-Li alloy plates that contained friction plug welds were investigated. The friction plug weld process is currently being developed for use in the fabrication of aerospace pressure vessels. The friction plug welds in this study used double-tapered plugs that were machined from extruded 2195-T8 Al-Li alloy.

The mechanical properties were determined from uni-axial tensile tests of 2195-T8 base metal, friction stir welded 2195-T8, and friction stir welded 2195-T8 that contained friction plug welds made with 2195-T8 plugs. The microstructure and microhardness of the friction plug weld interfaces with the base metal and friction stir welded material were studied to identify the thermal, thermomechanical, and mechanical effects that the friction plug welding process introduced to the surrounding region.

Microhardness measurements of the plug weld interface, base metal, friction stir weld, and heat affected zones that surround the plug weld were made with a Knoop indenter operated at a 100g load. The results of hardness tests showed the largest decrease in hardness was found at the plug weld interface and ranged from 110-130 HK_{100g}. Metallographic images of the microhardness specimens were examined and a recrystallized zone that surrounds the plug weld was identified. The size of the recrystallized zone was measured to be 30-122 μm.

The fatigue properties were examined by the use of constant amplitude fatigue tests for friction stir welded specimens and friction stir welded specimens that contained a friction plug weld. The fracture surfaces were examined to identify the crack origin and crack path. Results from the fatigue tests showed that the process parameters for the friction plug weld can directly influence the fatigue properties of friction plug welds.

The unique weld geometry of the friction plug weld repair precluded the use of ASTM standard compact specimens C(T), so the fatigue crack growth test was performed in a non-conventional manner using a dog-bone style fatigue specimen and crack mouth opening displacement as a means of measuring the fatigue crack growth rate. The crack mouth opening displacement was obtained during testing from a clip gage mounted at the fatigue crack. The crack mouth opening data was then used to correlate the crack mouth opening displacement obtained experimentally with that of the crack mouth opening displacement determined from a finite element model of the specimen with a crack located at the plug weld.

The crack depth, which was unobservable during testing, was determined by a correlation of the crack mouth opening data with the crack mouth opening calculated from finite element model for a specific crack geometry. The stress amplitude level used during the fatigue crack growth test was 70-90% of the ultimate strength for the friction plug welds tested.

LIST OF ABBREVIATIONS AND SYMBOLS

a	crack depth
K	Stress intensity factor
ΔK	K_{max} - K_{min}
S	Stress
ΔS	S_{max} - S_{min}
ε	Strain
ϕ	Angle of fracture path from axial load direction
θ	Angle measured from center-line of friction plug weld
θ_1, θ_2	Angle of crack growth within friction plug weld from specimen centerline
Al-Li	Aluminum lithium alloy
BM	Base metal
CGR	Crack growth rate
COD	Crack opening displacement
FCG	Fatigue crack growth

FEA	Finite element analysis
FEM	Finite element model
FPW	Friction plug weld
FSW	Friction stir weld
HAZ	Heat affected zone
NDE	Non destructive evaluation
SLWT	Super light weight tank
SZ	Stir zone
TMZ	Thermo-mechanical zone
TWI	The Welding Institute
UTS	Ultimate tensile strength
ULCF	Ultra low-cycle fatigue
VPPA	Variable polarity plasma arc

ACKNOWLEDGEMENTS

There is little I can say with words to express my gratitude for all the help, advice and the never-ending encouragement that my advisor Dr. Mark E. Barkey has provided during the writing of this dissertation. Thank you Dr. Barkey for everything you have done for me. Special thanks to all my committee members, Dr. Jackson, Dr, Hubner, Dr. Guo, Dr. Weaver, and Dr. Bradt for your time, advice, and assistance.

I would like to thank Doug Wells and Carolyn Russell of Marshall Space Flight Center for providing the opportunity to conduct this study. Also, thank you to Preston McGill for his assistance. Thank you to Dr. Greg Thorwald of Quest Integrity Group for his assistance with FEACrack software and finite element modeling techniques.

I would like to thank Dr. Eric Weishaupt for all of his expertise and assistance. Dr. Stan E. Jones also deserves a note of thanks for helping me get to this moment in time. Tim Connell of the UA AEM department provided much help and especially humor when needed. Thank you to Ben Fairbee as well.

Thank you to my parents for being supportive of all my ambitions throughout life. Lastly, but most certainly not the least, I want to thank my wife, Melissa. Thank you for all the wonderful years together...I look forward to the many years ahead with you. You never give up on me.

CONTENTS

LIST OF TABLES

LIST OF FIGURES

CHAPTER 1

INTRODUCTION

The friction stir welding (FSW) process is a solid-state welding process that relies on gross plastic deformation and localized heating from friction to join the base materials. The welding process differs from traditional fusion welding processes in that the base material is not completely melted and re-solidified in a fusion zone. Additionally, friction stir welding does not require the use of a filler material, as usually is common to with fusion welding processes.

The friction stir welding process was used successfully in the fabrication of the Super Light Weight External Tank (SLWT) for NASA's Space Shuttle program [1]. Prior to the use of friction stir welding, the primary welding process used in the fabrication of the SLWT was variable polarity plasma arc welding (VPPA). The VPPA welding process was prone to the introduction of several weld defects that required several grinding and re-welding passes, a planishing operation to remove residual stresses, and non-destructive evaluation (NDE) [1]. The introduction of the friction stir welding process reduced the number of joining defects found in the welded structure; however, defects still occur with the friction stir welding process, and a suitable method of repair for defects is required [2].

The use of a friction plug welding process is one of the proposed methods used to the repair defects that may occur during the friction stir welding process. Figure 1.1 shows a schematic view of the friction plug weld process.

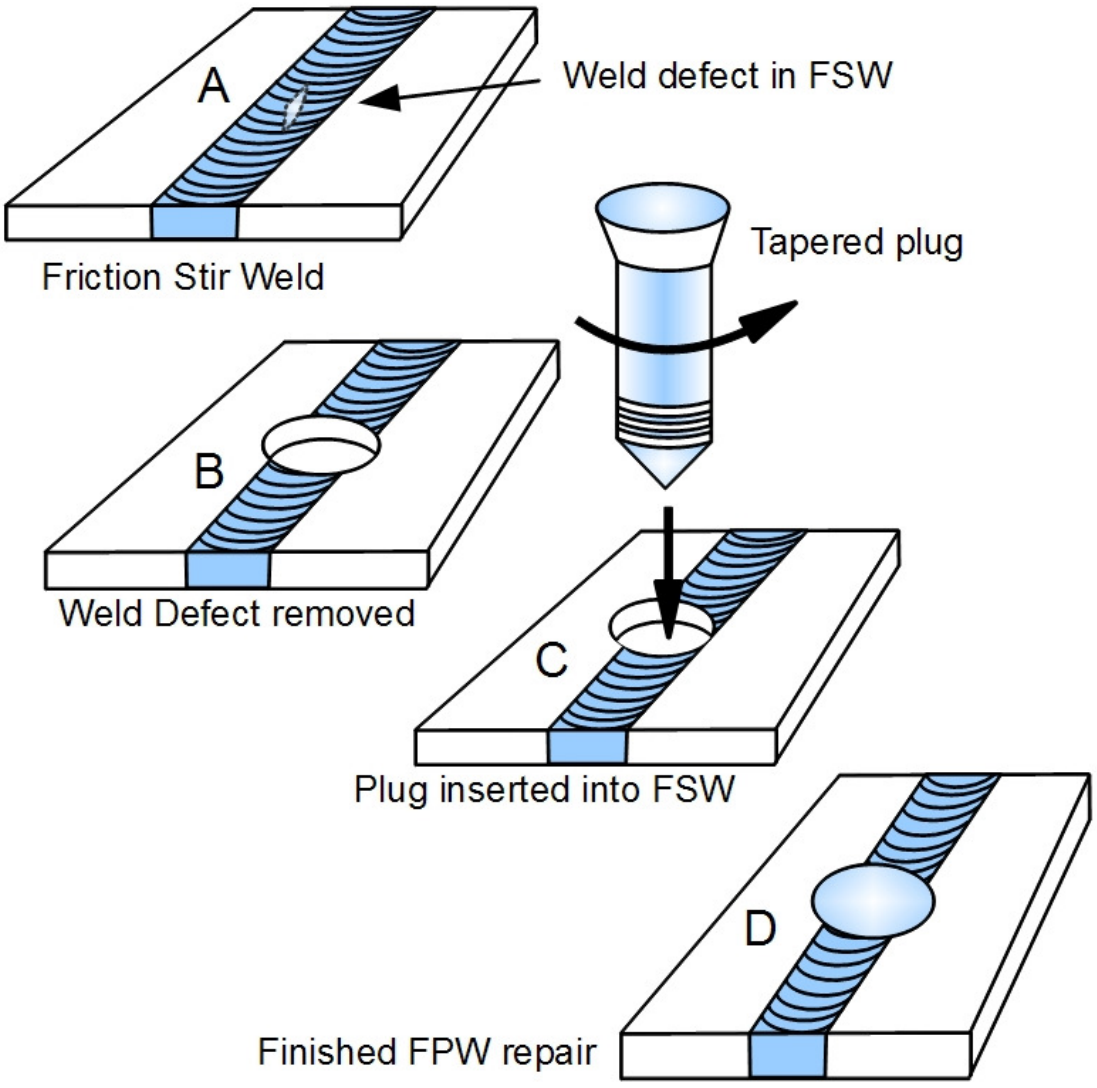

Figure 1.1. Friction plug weld process.

Friction plug welding (FPW) was first developed by Lockheed Martin as a method of repairing both 2219 Al-Li and 2195 Al-Li alloys [3-5]. The process involves using a tapered plug with a threaded end that is simultaneously spun and pulled by a special welding head. The tapered plug end has a specially designed profile to reduce and eliminate plug weld defects. When the size of a defect or crack exceeds the repair size of the plug, a stitch weld may be used wherein overlapping plug welds are made to effectively repair the defect.

The purpose of this research is to characterize the mechanical, fatigue, and fracture properties of friction stir welded 2195-T8 Al-Li plates which contained friction plug weld repairs. The plug material used in this study was extruded 2195-T8 Al-Li.

The objectives of the research are to:

1. Determination of the tensile strength and microstructural properties of a friction plug weld, made with 2195-T8 plug, in friction stir welded 2195-T8 plate material. Examine the microstructure and microhardness of the plug weld to characterize the thermomechanical effects of the plug weld process.
2. Investigate the fatigue properties of using cyclic loading.
3. Determine the fatigue crack growth rate for a friction plug weld at stress amplitudes of 70 to 90% of the friction plug weld ultimate tensile strength for damage tolerance analysis in aerospace pressure vessel applications.

The organization of this dissertation is as follows:

In Chapter 2, the results of the microstructure and microhardness profiles of the friction stir plug weld are reviewed. The factors that are known to influence the mechanical and fatigue properties will be summarized. Factors affecting the microstructure and microhardness will also be reviewed. Chapter 3 will discuss the uni-axial fatigue properties of friction plug welds and friction stir welds. Comparison of the observed fatigue and fracture characteristics will be presented. Chapter 4 will describe the crack mouth opening displacement method used for fatigue crack growth testing of friction plug welded specimens tested at high stress amplitude levels, and the results will be discussed. The overall conclusions of the study will be presented in Chapter 5.

CHAPTER 2

A MICROSTRUCTURE AND MICROHARDNESS CHARACTERIZATION OF A FRICTION PLUG WELD IN FRICTION STIR WELDED 2195 AL-LI

INTRODUCTION

Friction Plug Welding (FPW) is a solid-state welding process being investigated as a repair method for weld and process defects that occur within a friction stir weld (FSW) [1]. The procedure used in the friction plug weld repair process is as follows. First, a defect that has been identified in the FSW is removed by drilling a though-hole in the area of the defect. Subsequently, a rapidly rotating plug is pulled through the hole to create a friction weld between the plug and the structure. A brief overview of friction stir welding will be given since the plug weld fusion zone contacts the FSW.

Friction stir welding, which is also solid-state welding process, was developed prior to friction plug welding by The Welding Institute (TWI) in 1991 [2]. In the FSW process a rapidly rotating tool is pushed into the joint composed of two butted plates and moved along the joint. As the weld is formed, the material from each plate mix together to create a fusion zone. The tool is

removed from the material at the termination of the weld, leaving a slot width that is approximately the diameter of the rotating tool. This slot is referred to as a "keyhole" defect [3] and is inherent to the FSW process. A friction stir welded plate containing friction plug welds is shown in Figure 2.1. A detailed view of a keyhole defect and a friction stir weld are shown in Figure 2.1, items A and B, respectively.

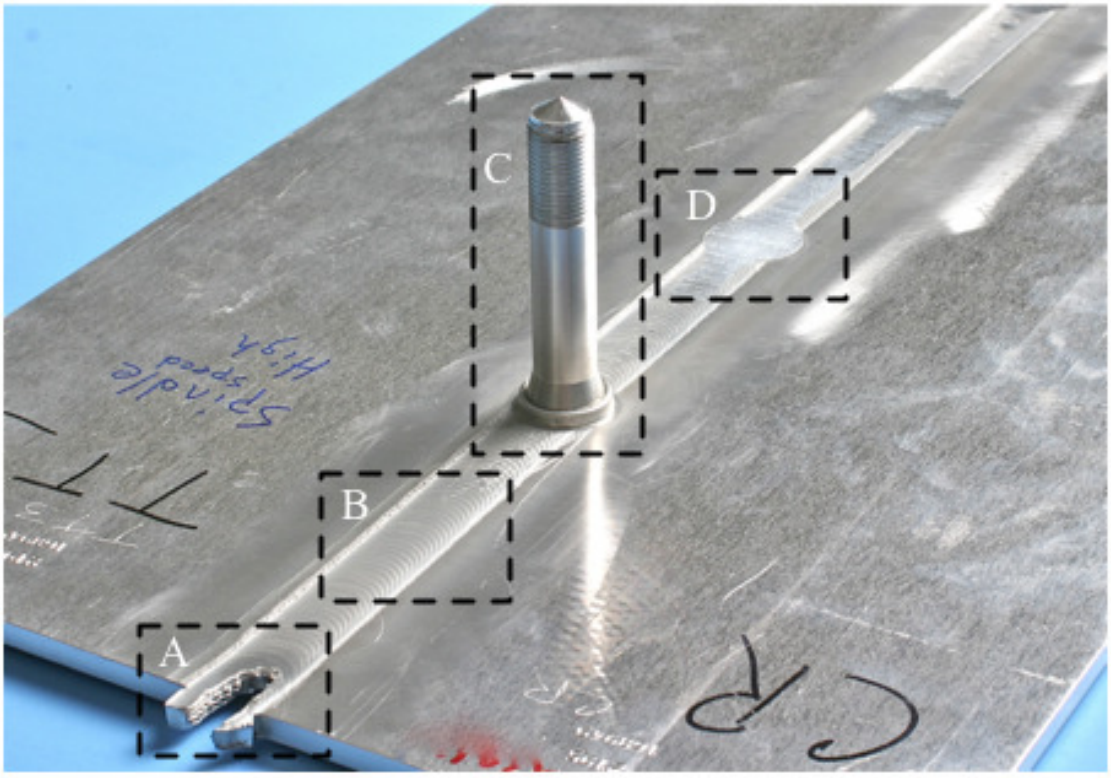

Figure 2.1. Friction stir welded 2195-T8 Al-Li plates with FSW keyhole defect (A), FSW (B), unfinished plug in FSW following joining (C), and FPW after removal of excess plug material (D).

The FSW process has been refined and has been successfully used in the fabrication of spacecraft fuel tanks and pressure vessels. These structures typically consist of curved panels that are

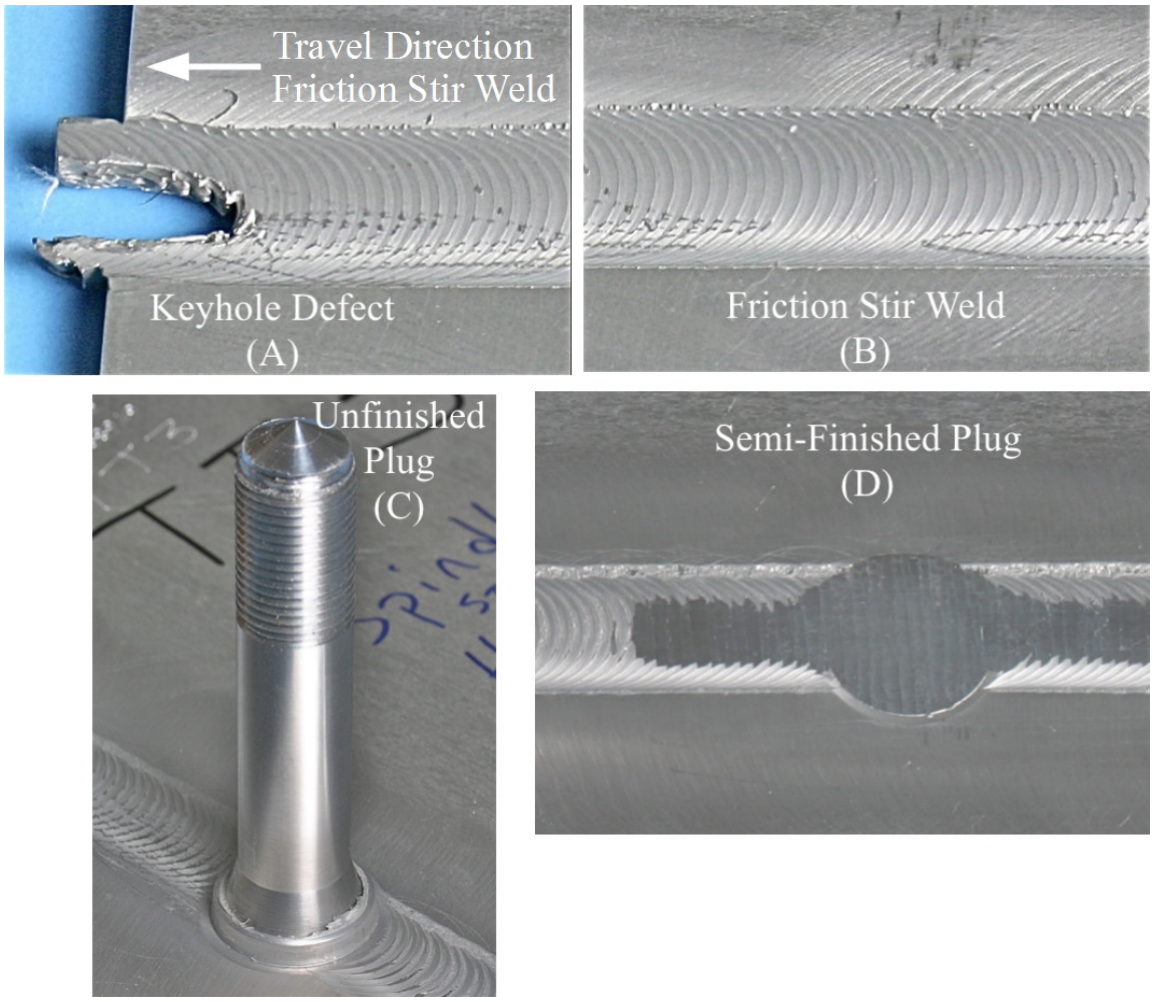

Figure 2.2. Detailed view of keyhole defect (A), FSW (B) , unfinished plug joint (C), and semi-finished plug joint (D).

welded along the longitudinal direction together to form barrel sections.

Keyhole defects in the structure can be avoided in the longitudinal direction by the use of run-out tabs that are trimmed from the final structure [4]. The barrel sections containing the longitudinal welds are joined to each other by welding along the circumferential direction to create the tank.

The use of FSW in the circumferential direction precludes the use of a run-out tab, and when the weld termination point is reached, the keyhole defect must be repaired. Thus, the FPW process is being investigated as a method to finish circumferential welds and also for repair of other defects that occur within the friction stir weld or base metal.

A friction plug weld is made by the use of a specially designed tapered plug that is simultaneously rotated and pulled axially into a pre-machined hole [5, 6]. As the tapered section of the plug begins to contact the top edge of the machined hole, frictional heating and deformation occur at the interface between the plug and the machined hole. After the plug is fully engaged into the hole, the rotation of the plug is rapidly stopped. Finally, a forging stage occurs where the axial load is maintained while the weld begins to cool and recrystallization of the material occurs. No additional heat energy is input into the weld during this final stage of the friction plug welding process.

Different standard plug sizes have been made to accommodate variously sized defects [4, 7]. After a plug weld is inserted into the plate, excess material from the plug is removed during a finishing process. An unfinished plug weld and a plug weld with the excess plug material removed are shown in Figure 2.1, and detailed views of the unfinished plug joint and a semi-finished plug joint are shown in Figure 2.2, items C and D, respectively. The plug weld is subsequently ground smooth in a final finishing operation. When used to terminate a circumferential friction stir weld, the plug is inserted into a hole in the structure containing regions of both friction stir welded material and base metal.

The 2195-T8 aluminum-lithium (Al-Li) alloy has become the preferred material for applications such as the Super Light Weight Tank on the Space Shuttle due to its low density, high tensile strength, and good cryogenic fracture toughness as compared to other aluminum alloys [1, 8-10]. In this study, extruded 2195-T8 plugs that were friction welded into the friction stir weld of 2195-T8 base metal plates were examined. The resulting microstructure and microhardness of the plug weld interfaces with the friction stir welded material and base metal are characterized in an effort to identify the extent of the thermal, thermomechanical, and mechanical effects introduced by the friction plug welding process. By determining the hardness of these zones, insight can be gathered into the transformation of material from the friction plug welding process around the fusion zone, and areas that may control the fatigue behavior of the joint.

Base Metal

The base metal, 2195-T8, is comprised of a banded microstructure with the long axis of the grains oriented in the rolling direction of the plate material [8]. The texture of rolled 2195-T8 has been researched extensively and found to have a predominately brass texture [11,12]. The primary strengthening phase is 60-115 nm long T_1 (Al_2CuLi) precipitated uniformly distributed throughout the matrix [13,14]. The T_1 precipitate phase acts as a non-shearable barrier to hinder dislocation motion and is considered to be responsible for the relatively good strength and fracture toughness properties of 2195-T8 when compared to other Al-Li alloys. The precipitation of the T_1 phase in 2195-T8 will promote homogeneous slip, as opposed to other Al-Li alloys that exhibit localized slip mechanisms. This homogeneous deformation contributes to the increased

strength and fracture toughness of this alloy.

Friction Stir Weld

The cross section of a friction stir weld consists of three zones as shown in Figure 2.3. The weld nugget or stir zone (SZ), which occupies the center region of the weld cross section, is where the material closest to the rotating tool is recrystallized by the stirring action of the tool. The SZ has a fine recrystallized grain structure. Adjacent to the SZ is the thermomechanical zone (TMZ) where both thermal and mechanical affects are found in the weld. The mechanical action results in the distortion of the grains of the base metal into a curved shape from previously flat, elongated grains. The heat affected zone (HAZ) is located between the TMZ and base metal, where mechanical effects are no longer observed [15].

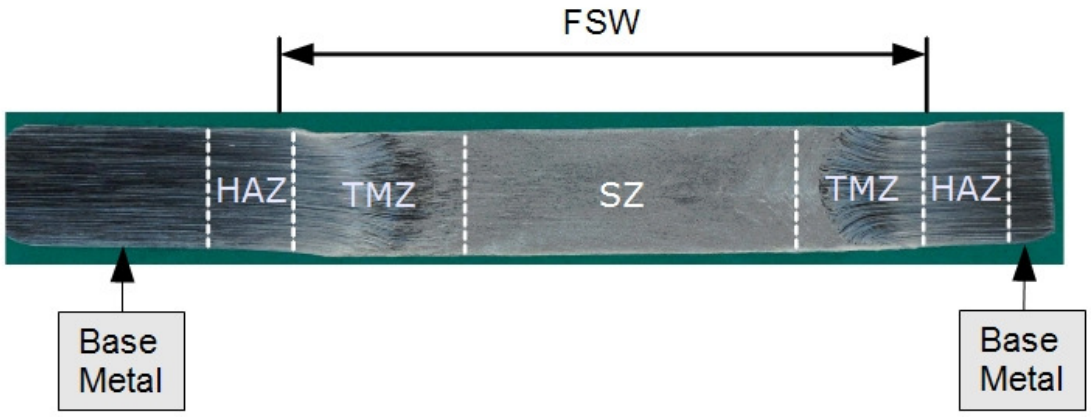

Figure 2.3. Friction stir weld cross-section.

Friction stir welding is commonly used to join plates of 2195. Previous studies by several authors [13,16,17] have indicated that this alloy is capable of producing many secondary precipitates and

that the presence of these precipitates affects the hardness values. Fonda and Bingert [16] found that both the T_1 phase and the θ' (Al_2Cu) phase were present in the HAZ of the FSW. The T_1 and θ' phases were both found to coarsen from the base metal through the HAZ. Temperatures in the TMZ allow for the precipitates to dissolve. Metastable phases δ'(Al_3Li) and β'(Al_3Zr) are found in the SZ or weld nugget. These phases appear to serve as initiation sites for T_B ($Al_{15}Cu_8Li_2$) precipitates. It was also observed that the formation of the T_B phase limits the amount of solute available to form Guinier-Preston (GP) zones, in turn resulting in a lowered value of hardness in the weld nugget.

Fonda et al. [17] found that the primary mechanism for grain refinement in the FSW was subdivision induced by deformation and dynamic recovery processes without the need to invoke a dynamic recrystallization mechanism. Schneider et al. [13] found in a TEM study that strengthening precipitates in the TMZ and the HAZ were overaged while the same precipitates solutionized in the SZ. It was also stated that overaging of the strengthening precipitates in the base metal is associated with a reduction in strength. A possible mechanism for fatigue crack initiation and growth may be attributed to the prevalence of δ' around the weld. Preferential slip may occur near the weld and propagate through the shearable δ' precipitates.

Plug Design and Friction Plug Weld

The plug used in this study was designated by NASA as an M3 plug, shown schematically in Figure 2.4. The plug is comprised of three main parts [6]. The top of the plug consists of a heat sink and annular shoulder. The second part consists of the frusto-conical section that comprises

the main portion of the plug that fills the hole in the plate. This section has a larger or major diameter at the heat sink end, and transitions to a smaller or minor diameter through a double taper. The shank, threaded end, and conical tip comprise the lower section of the plug. The shank has a constant diameter equal to the minor diameter of the frusto-conical section. The threaded section is used as a means to attach the plug to the friction plug welding machine.

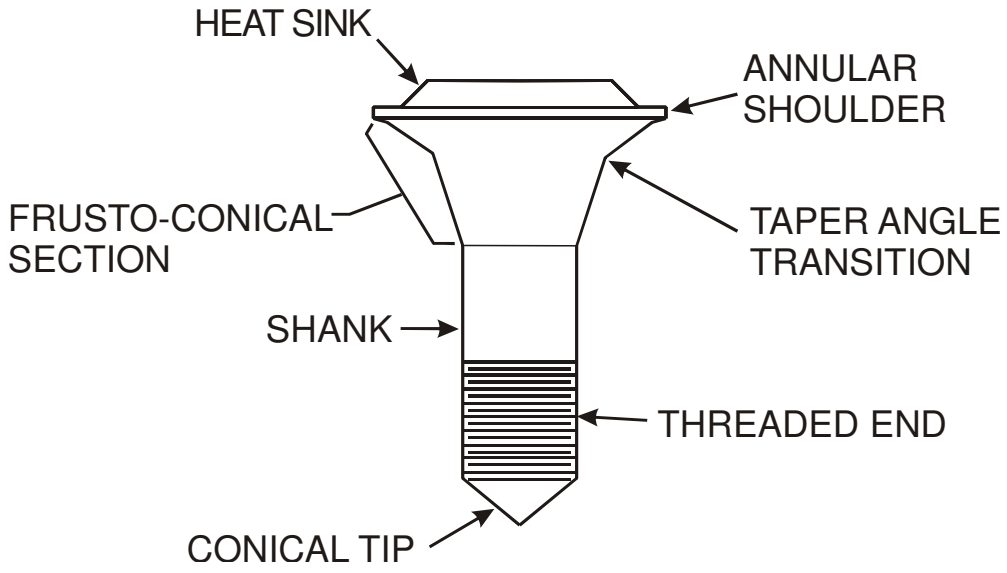

Figure 2.4. Schematic and nomenclature of plug.

The plug was machined from extruded 2195-T8 round stock. Wang (1998) [18] discovered δ′, β′, T_1, and θ′ phases present with the possible presence of Ω (Al_2Cu) and S′ (Al_2CuMg) in extruded 2195-T8. The extruded material exhibits a predominately brass texture which is similar to the base metal. However, the grain shape of the extruded aluminum is “blocky” in contrast to the flattened, elongated grain structure in the base metal.

Similar to a FSW, a FPW has three primary zones associated with the process: a stir zone

(SZ), a thermo-mechanically affected zone (TMZ), and a heat affected zone (HAZ). The size of the stir zone in a FPW is much smaller than found in a FSW due to the fact that a rotating plug is used to create the weld instead of a rotating tool. The placement of a FPW within the FSW complicates the delineation of the three FSW zones. FPW interfaces are now created within the three FSW zones.

The microstructure of a FPW was discussed in the work done by Li [7]. The work investigates sections of the joint taken parallel to FSW joint line and normal to the FPW. Li reported that the microstructure had evidence of T_1 precipitates in the plug and base metal. They found that at the weld interface there was no T_1 or θ' phase apparent. Analysis of the HAZ revealed evidence of T_1 platelets along grain/subgrain boundaries at 2.5 mm from the plug interface. At a distance of 3.8 mm from the plug interface partial dissolution of the T_1 phase was also observed.

In Li's study, the heat affected zone (HAZ) had a reduction in the amount of T_1 present within the zone. The reduction of the T_1 phase in the HAZ resulted in a decreased hardness in the region which would indicate a reduction of strength in the zone. This would correspond to the reduction of T_1 phase found in the HAZ of friction stir welded 2195 as discussed in the aforementioned sections; however, the size of the HAZ is smaller for friction plug welds than for friction stir welds. Coletta et al. [19] also sectioned several FPW and FSW joints in a similar direction as stated above. This study emphasized the effect of plug taper angle on the resulting joint integrity. We wanted to determine if there is significant variation in hardness in relationship to the theta direction of the FPW and/or relationship to the offset of the plug weld from the centerline of the

FSW.

EXPERIMENTAL PROCEDURE

Two plates of 2195-T8 were joined by a friction stir weld. Four friction plug welds were inserted along the friction stir weld line. The centerline of the plug welds was offset from the friction stir weld centerline by a distance of 1.5 mm toward the advancing side of the friction stir weld as shown in Figure 2.5. All welds were performed at NASA Marshall Space Flight Center (MSFC). The welded plate was designated “A” and is shown in the unprepared state in Figure 2.1. These welds were made for a companion study on fatigue of FPW joints. The FSW 2195-T8 plates had a thickness of 6.35 mm, a width of 305 mm, and length of 610 mm. The major diameter of the plug used in the joint was 33 mm and the minor diameter was 15.9 mm.

To investigate the hardness of the material in the vicinity of the friction plug weld joint, twelve rectangular samples were removed from the plug weld area of the fatigue specimen using electrical discharge machining (EDM), as illustrated in Figure 2.5. The samples were removed from 0° through 330° at 30° intervals around the plug. Each sample had a length of 20.3 mm and a width of 2.54 mm. The starting edge of the samples originated 6.35 mm from the center of the plug traversing outward through the plug weld interface and into the base metal, friction stir weld, or both depending on the location of the sample. The samples had a thickness of 6.35 mm which is equal to the 2195-T8 plate thickness.

The hardness samples were mounted in black phenolic using a Struers LaboPress-3 hot mounting

press. The samples were mounted to allow the transverse, or through thickness, direction to be examined. An Allied M-Prep 3 polisher was used to prepare the samples for microhardness testing and metallography. The samples were prepared following standard metallographic procedures stated in ASTM E3 [20].

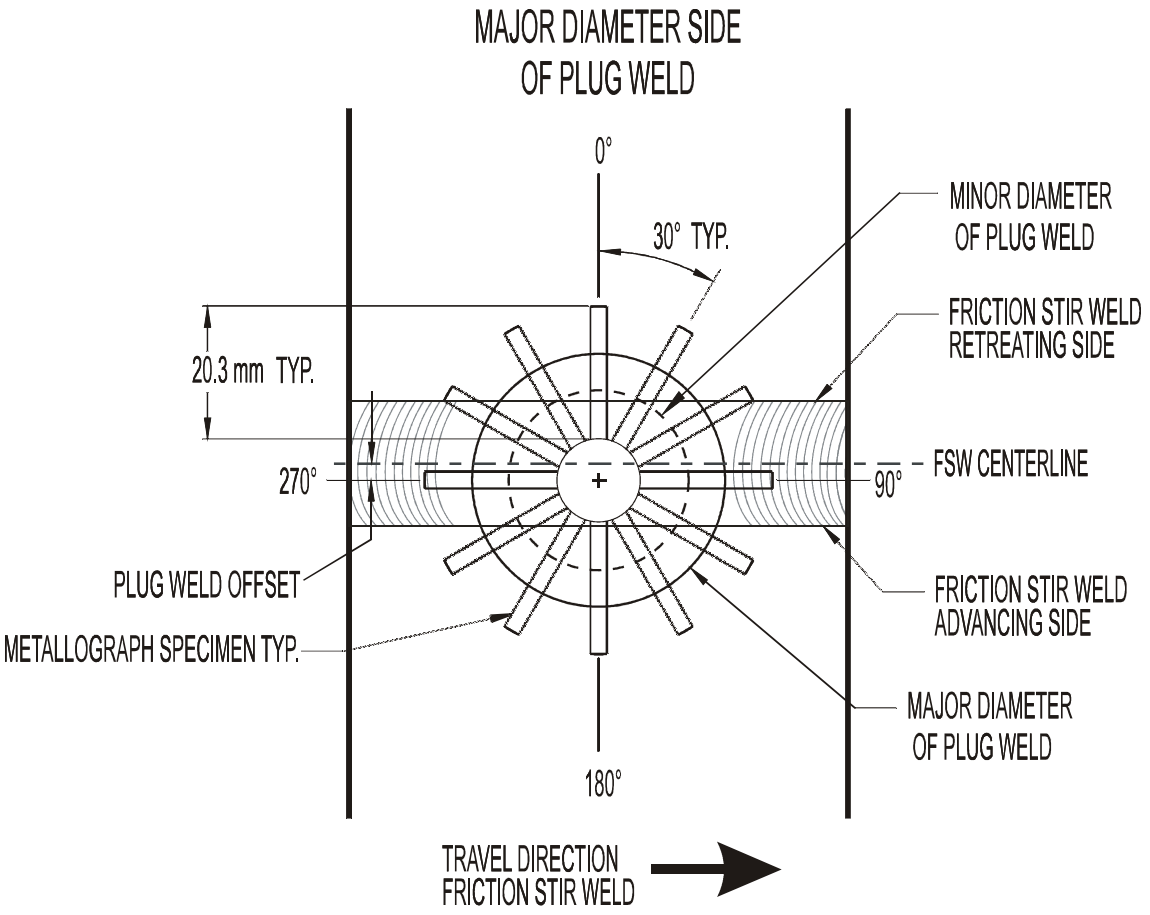

Figure 2.5. Sectioning diagram of specimen.

Knoop microhardness traverses using an interval of 0.5 mm were performed over the length of

each sample by using a Wilson hardness machine. The accuracy of the hardness tester was checked using a calibration block for 100g loading, and found to be ± 8 HK_{100g}. The accuracy was again checked after all samples were hardness tested and found to still be within acceptable limits. The samples were tested under a load of 100 grams. The traverses were performed beginning on the plug side of each sample and traversing radially outward through the base metal/friction stir weld. The hardness samples were etched using Keller's reagent, in order to examine the weld interface, and specifically the interface between the plug and base metal/friction stir weld. Following the application of Keller's reagent, a 5% Nital solution was used to remove staining.

Digital images of each sample were captured at various locations of the plug weld interface and the adjacent areas surrounding the interface including the plug material, TMZ, HAZ, FSW, and base metal. The metallographic inspection was performed using a Nikon metallograph with an integrated digital camera and image analysis software. Multiple images of the plug weld interface on each sample were recorded at 50X magnification and compiled to form a montage of the interface for each sample. Higher magnification images were recorded at 500X and 1000X to investigate and quantify the recrystallized layer near the plug weld interface. Digital image analysis software was used to measure the thickness of the recrystallized material.

RESULTS and DISCUSSION

Recrystallized layer thickness measurements

Thickness measurements of the recrystallized material were recorded at two specific locations of the plug weld interface. A typical image with recrystallized layer thickness measurement is shown in Figure 2.6. The first location was near the plate surface on the minor diameter side of the plug, and the second location was at a section of the weld near the plate's mid-thickness, which corresponds to the location of taper angle change of the plug. Ten thickness measurements were made at each of the two locations for each sample. The measurements were then averaged and are displayed in Figure 2.7.

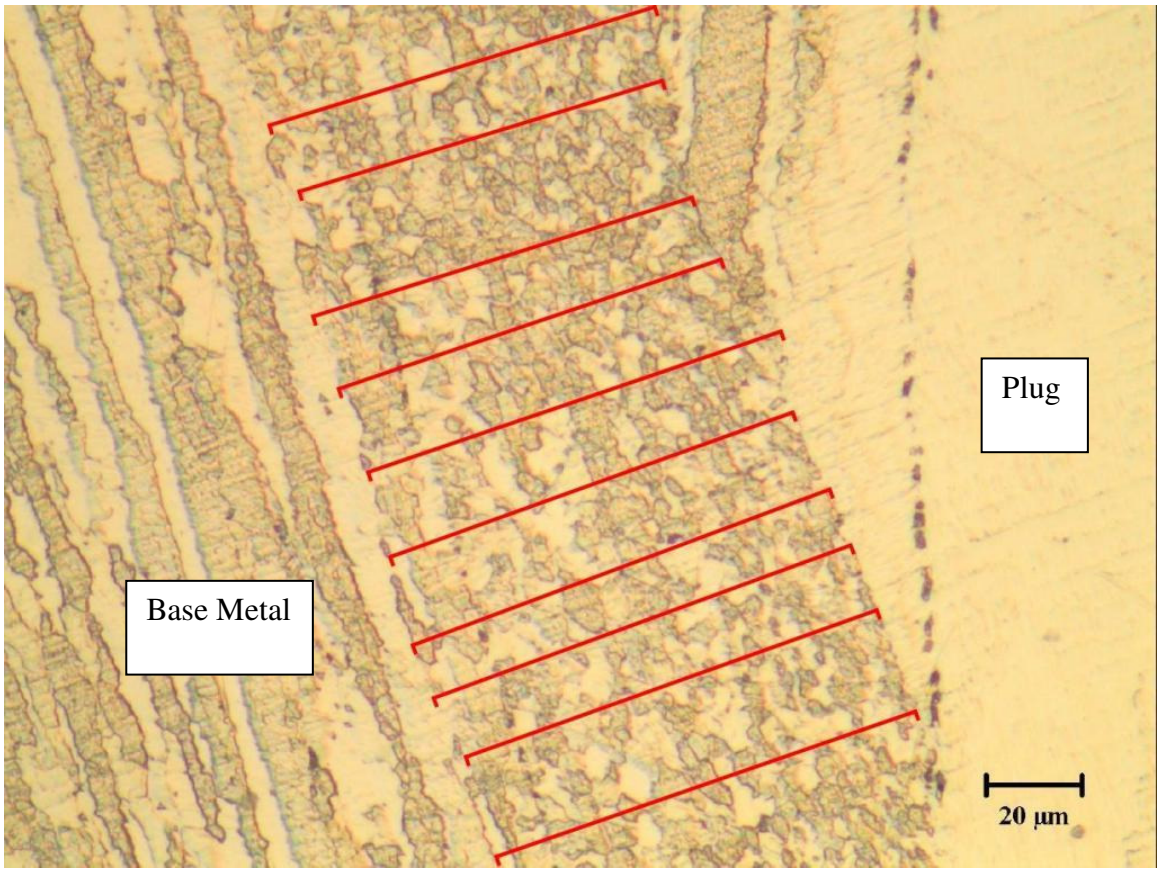

Figure 2.6. Recrystallized zone measurement at minor diameter location for 0° sample.

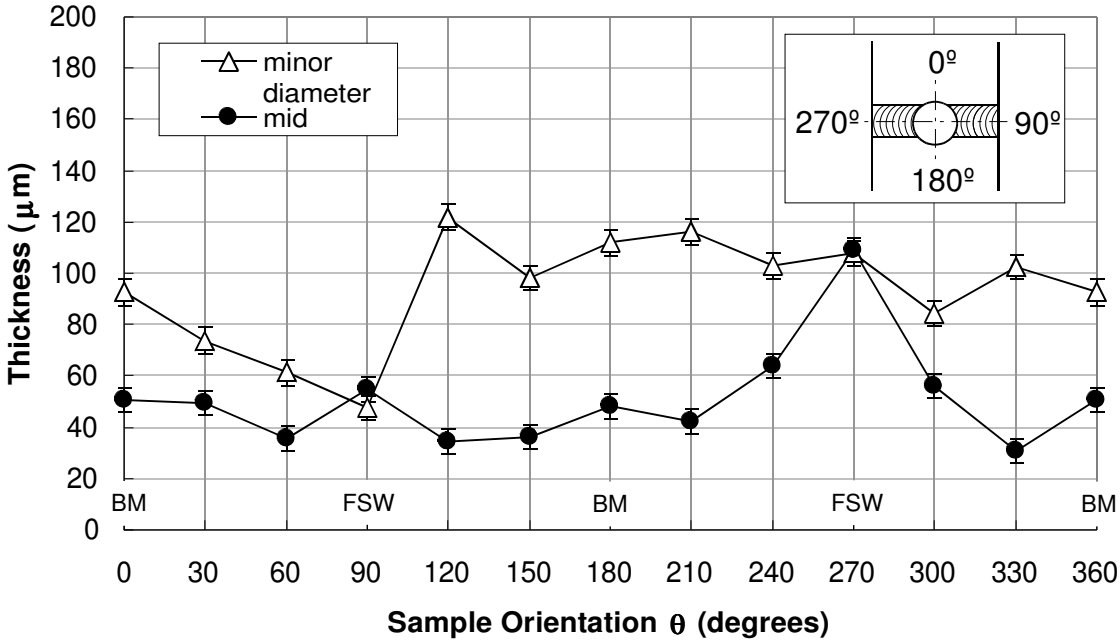

Figure 2.7. Average recrystallized layer thickness.

A distinguishable zone of recrystallized material was observed in each sample around the entire plug weld circumference. This layer of material varied in thickness from 30–122 μm. It was observed that the recrystallized ring surrounding the plug was thickest on the side of the joint corresponding to the minor diameter side of the plug, while the thinnest or least amount of recrystallization occurred in the portion of the plug where the taper angle changes. This layer was observed to have thickness values on the side of the joint corresponding to the major diameter of the plug that was intermediate to that observed at the taper angle change and the minor diameter side of the plug.

The increased amount of recrystallization associated with the minor diameter side of the plug interface is likely due to increased time of contact between the plate and the plug. The plug stays

in contact with the plate for the longest amount of time at the minor diameter side of the plug. This will lead to higher temperatures developing at the minor diameter side of the plug and will result in more recrystallization.

The mechanism that controls the recrystallization process at the mid-thickness depends on the design of the frusto-conical section of the plug. The design of the plug was the result of several revisions and testing trials [7, 19, 21]. During plug welding, cold plug material is continuously introduced into a hot interface as the plug is simultaneously rotated and pulled in the axial direction. When the heat sink at the top of the plug is too large, the result is weak bonding near the major diameter side of the plug. If the heat sink is too small, the plug material becomes too hot at the interface at the major diameter side of the plug weld, and, subsequently, the plug may pull through the plate during the welding process.

It is noted that the recrystallized layer thickness for the minor diameter and mid-thickness locations were similar in values at the 90° and 270° angles. The recrystallized layer thickness values were approximately 50 μm and 110 μm at these angles, respectively. The sections that correspond to 90° and 270° are parallel with the welding direction and lie near the centerline of the FSW. However, the recrystallized layer thickness for the minor diameter and mid-thickness locations diverged at other angles.

Although the exact reason for the difference in recrystallized zone size is not known, slight differences in temperature and pressure may have caused the layer to have different thickness

values at other locations and angles. Temperature and pressure values may differ due to alignment of the plug in the hole during the welding process.

Hardness Measurements

The hardness results are shown in pairings of samples that lie on a common plane passing through them. This was done to allow for comparison of the hardness results of samples that shared similar composition. The hardness results for the 0° and 180° samples, which lie on the plane passing through theta angles of 0° and 180°, are shown in Figure 2.8. This plane is referred to as the 0°/180° plane. At a distance of 20 – 26 mm away from the center-line of the plug weld, the Knoop hardness was 180-200 HK_{100g} and is consistent with the hardness of the base metal. Within 20 mm of the center of the plug weld, the hardness began to drop, corresponding to the TMZ of the plug weld. Moving in the clockwise direction of Figure 2.5, Figure 2.9 shows the hardness results from the 30°/210° plane from the fatigue specimen. The hardness results start in the base metal and move through the FSW and FPW. Figure 2.10 shows the hardness results on a plane through the fatigue specimen at the 60°/240° orientation. In this orientation, the hardness numbers reflect base metal, FSW and FPW. Figure 2.11 shows the 90°/270° hardness results. This orientation lies parallel to the FSW. The hardness of the FSW was 110-130 HK_{100g}, with a slightly increasing hardness into the plug material.

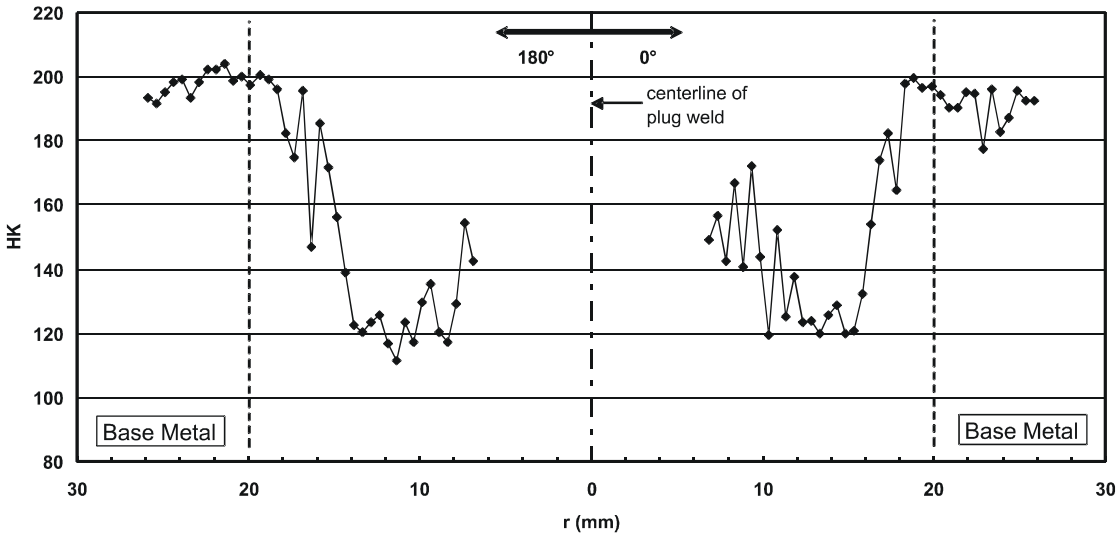

Figure 2.8. Hardness results for the 0°/180° plane.

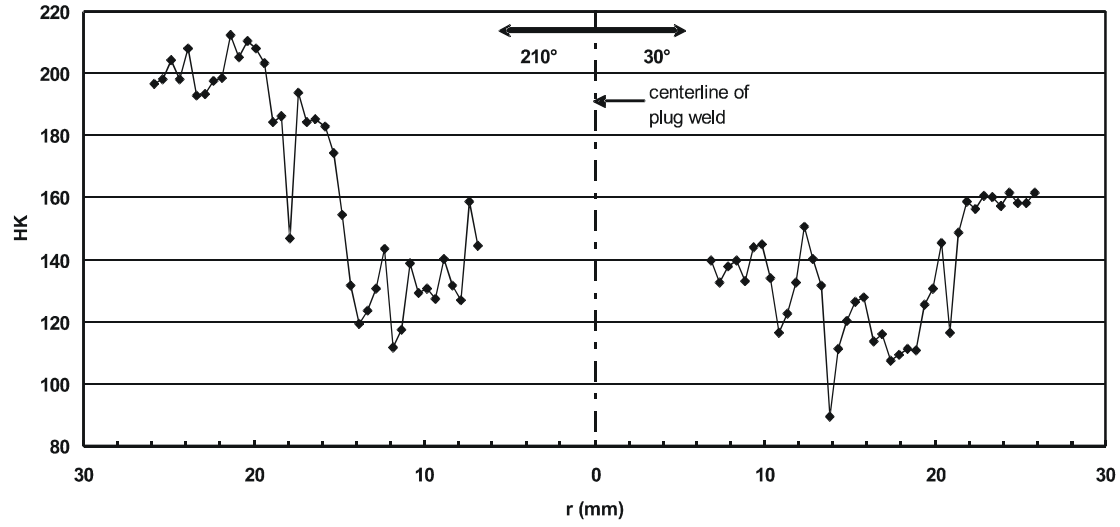

Figure 2.9. Hardness results for the 30°/210° plane.

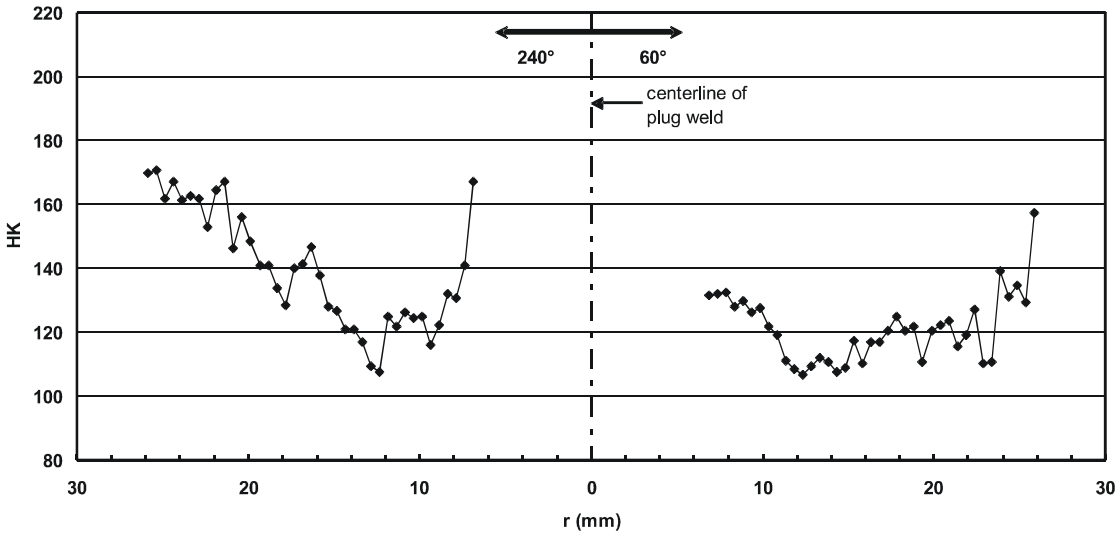

Figure 2.10. Hardness results for the 60°/240° plane.

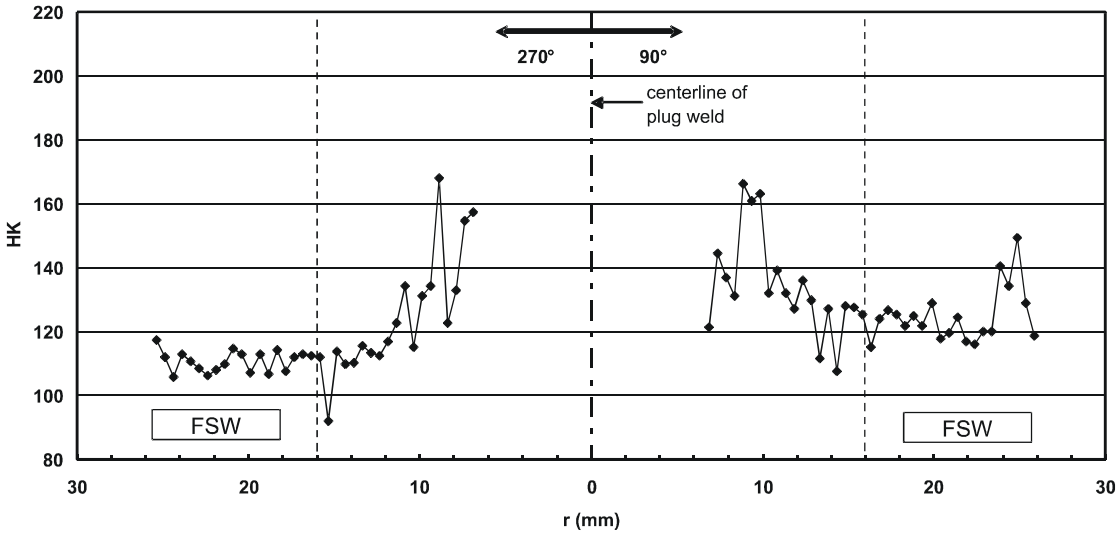

Figure 2.11. Hardness results for the 90°/270° plane.

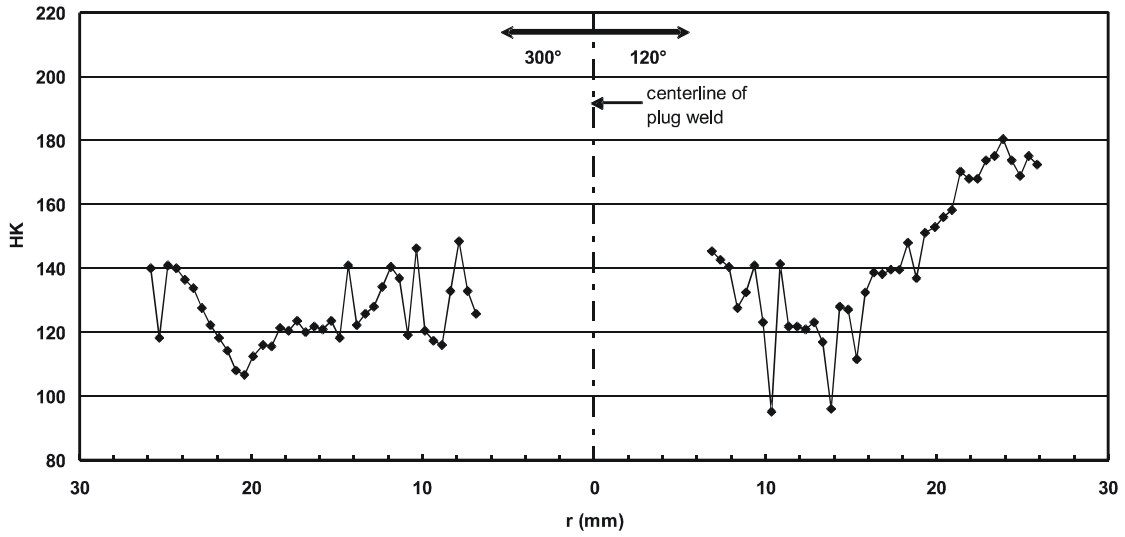

Figure 2.12. Hardness results for the 120°/300° plane.

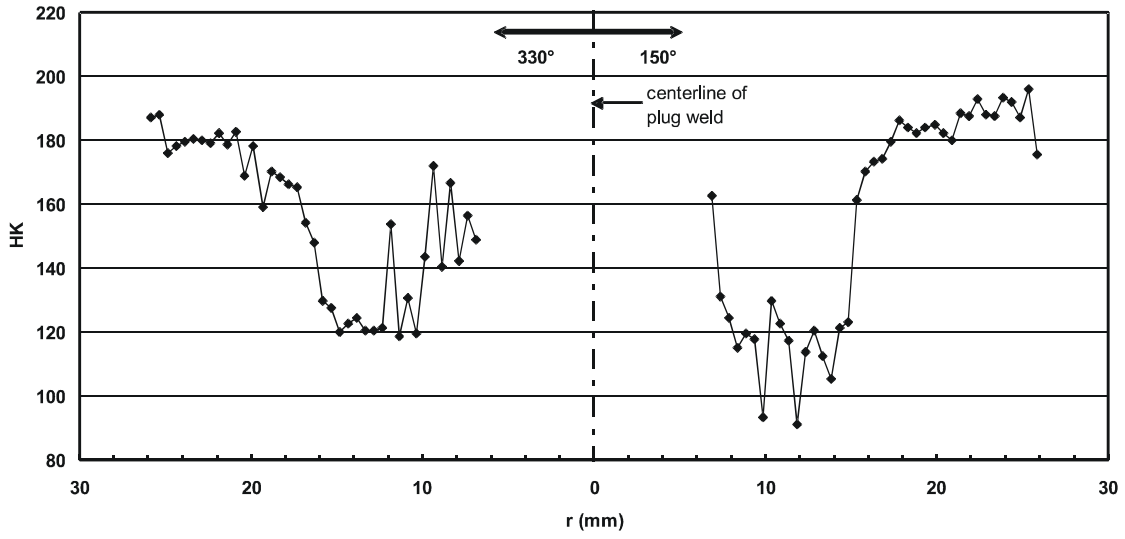

Figure 2.13. Hardness results for the 150°/330° plane.

Figures 2.12-13 are the results of the hardness test on the 120°/300° and 150°/330° directions, respectively. The structure of the FPW in the FSW is asymmetric due to the FPW being offset slightly toward the advancing side of the FSW. The travel direction of the FSW and the plug rotation direction of the FPW also contribute to the non-symmetry of the TMZ for the joint. This is illustrated by the difference in hardness profiles shown in Figure 2.12 and Figure 2.13 as compared with Figure 2.10 and Figure 2.9, respectively.

Figures 2.8-13 show a lower hardness at the friction plug weld interface, which includes the recrystallized layer and the adjacent portion of the TMZ. The hardness measurements within the friction plug weld interface region were consistently lower than the plug material and base metal; however the hardness was similar to that of the FSW regions. The drop in hardness in the plug weld interface region is likely related to the dissolution of the T_1 phase. Hardness test results show that the plug weld interface consistently exhibited lower hardness values of any other zone. The dissolution of the T_1 phase results in more localized slip in the HAZ and TMZ and may result in unfavorable fatigue properties, specifically in the case of high cycle fatigue.

The 60°, 120°, 240°, and 300° samples contained sections of both FPW and FSW. These samples had hardness values of 140-160 HK_{100g}. The difference in the hardness between the FPW and FSW, specifically at the interface between the two, varied by approximately 5-15 HK_{100g}. This would not represent a significant decrease in strength; however it is worth noting that the lowest hardness values were consistently recorded in the FSW/FPW interface.

The placement of a FPW in the FSW produces a thin layer of material which surrounds the entire

plug weld, and corresponds to the location of the lowest hardness values. This thin layer effectively negates the beneficial effects of any prior heat treatment and processing on the base metal. The decrease in hardness between the sections of the FSW and the FPW were measured to be approximately 5-15 HK_{100g}. This observed drop in hardness, which was observed consistently in all tested samples, may prove to be of little consequence with respect to the ultra low and low cycle fatigue behavior of the welded plate.

It has been documented in previous studies that the resulting microstructure in the recrystallized layer of the FPW is devoid of the T_1 phase. As stated previously, the T_1 phase is responsible for the strengthening in the base 2195-T8 microstructure. It is apparent that this recrystallized layer exists continuously in the circumferential direction. The hardness in regions near the recrystallized layer was consistently measured to be 110-130 HK_{100g}. This corresponds to an approximate 35% decrease in hardness from values measured in the base metal. The large variations seen in hardness measurement within the TMZ and plug HAZ were similar to those seen in other microhardness tests for plug welds done by Li, et al. [7]. This variation in the TMZ is also consistent with hardness results for FSW in 2195-T8 reported by Schneider et al. [13].

Figures 2.14-16 are montages of the plug weld interface for the 0°, 240°, and 270° hardness samples respectively. A typical montage is shown in Figure 2.14. This figure is annotated to show the location of the previously mentioned recrystallized layer measurements. The plug material is on the left side of the figure and has the blocky, elongated microstructure characteristic of the extrusion process used to create the plug. The top of the figure is the surface

of the plate where the major diameter of the plug is located and the bottom of the figure is the surface of the plate where the minor diameter of the plug is located. Since Figure 2.14 was taken for the 0° orientation, the far right side of the montage shows the base metal microstructure that is elongated due to rolling of the plate material. The disruption of the microstructure of the plate material is clearly evident at the weld interface, where the grains of the plate become highly deformed. The base material can be seen to flow toward each surface of the plate, with a noticeable material stagnation point which is located near the taper angle change of the plug.

Figure 2.15 is the montage created from the sample taken from the 240° orientation. This orientation is such that both FSW and base metal are shown in the montage. The base metal flow lines are somewhat altered in this region as compared to those shown in Figure 2.14. A montage of the sample cut from the 270° orientation is shown in Figure 2.16. The plug is clearly visible on the left side of the figure and the right side of the figure shows the stir zone of the FSW. Some material flow lines are still visible at the interface between the FPW and the FSW.

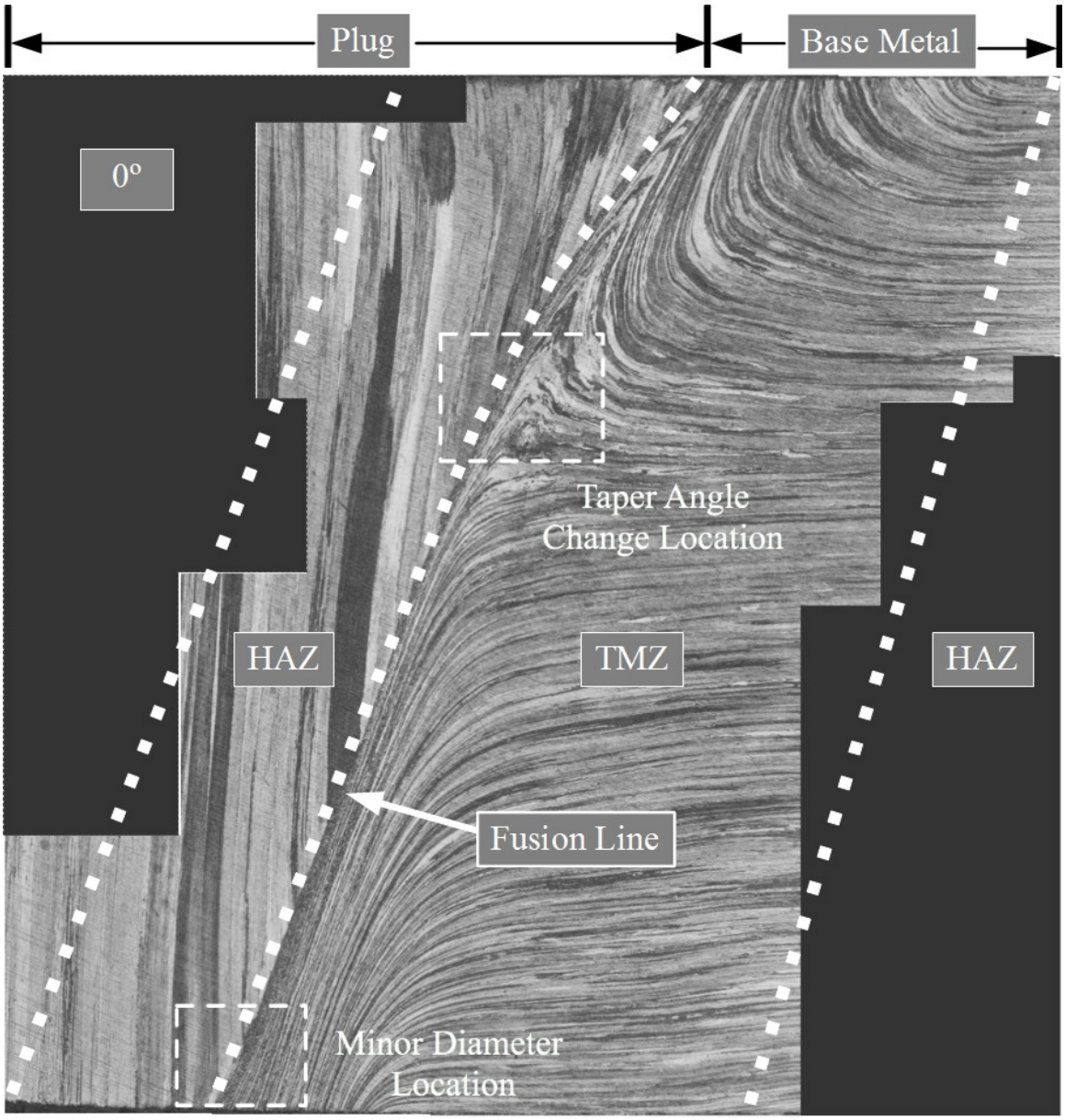

Figure 2.14. Montage of 0° section.

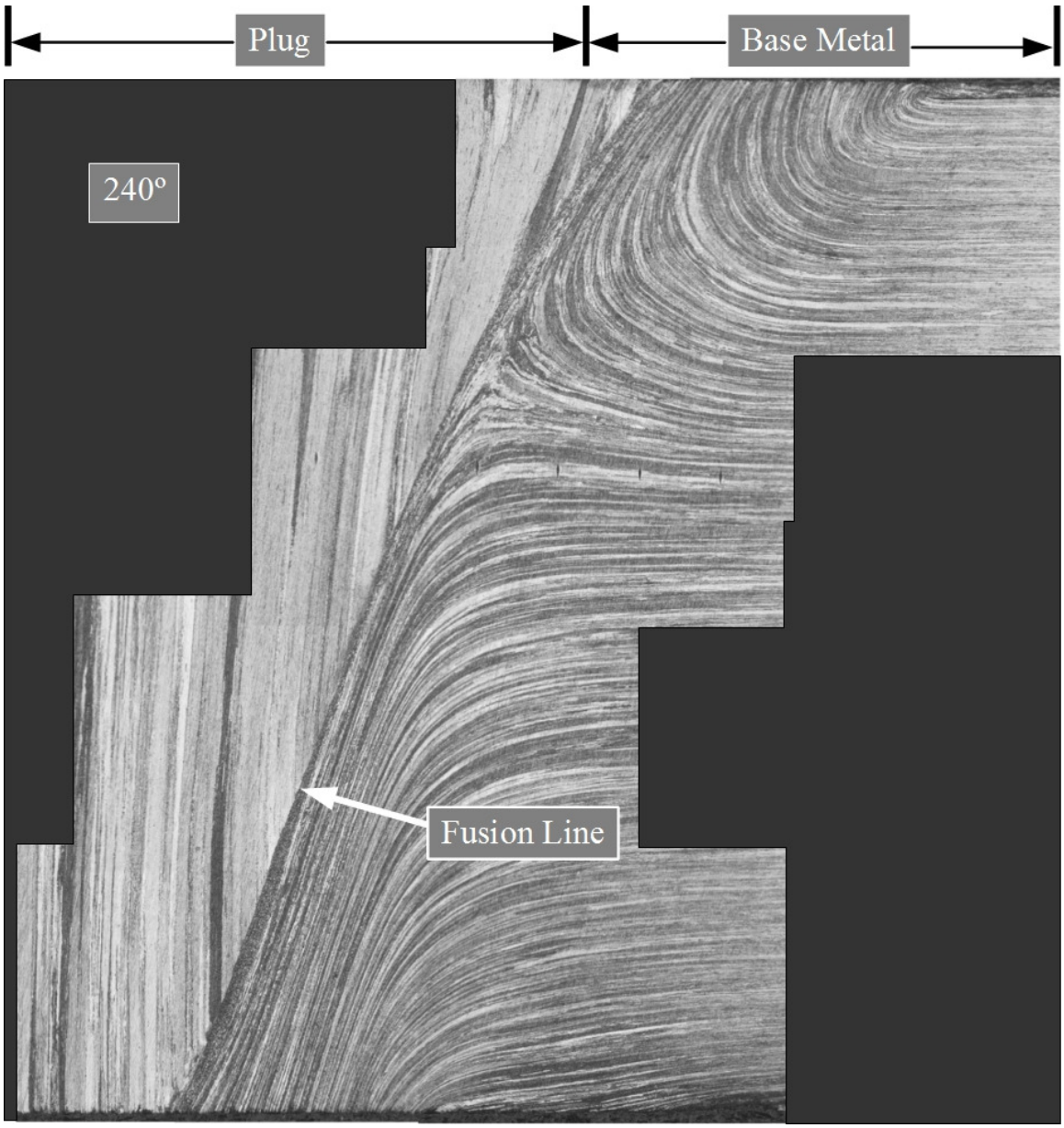

Figure 2.15. Montage of 240° section.

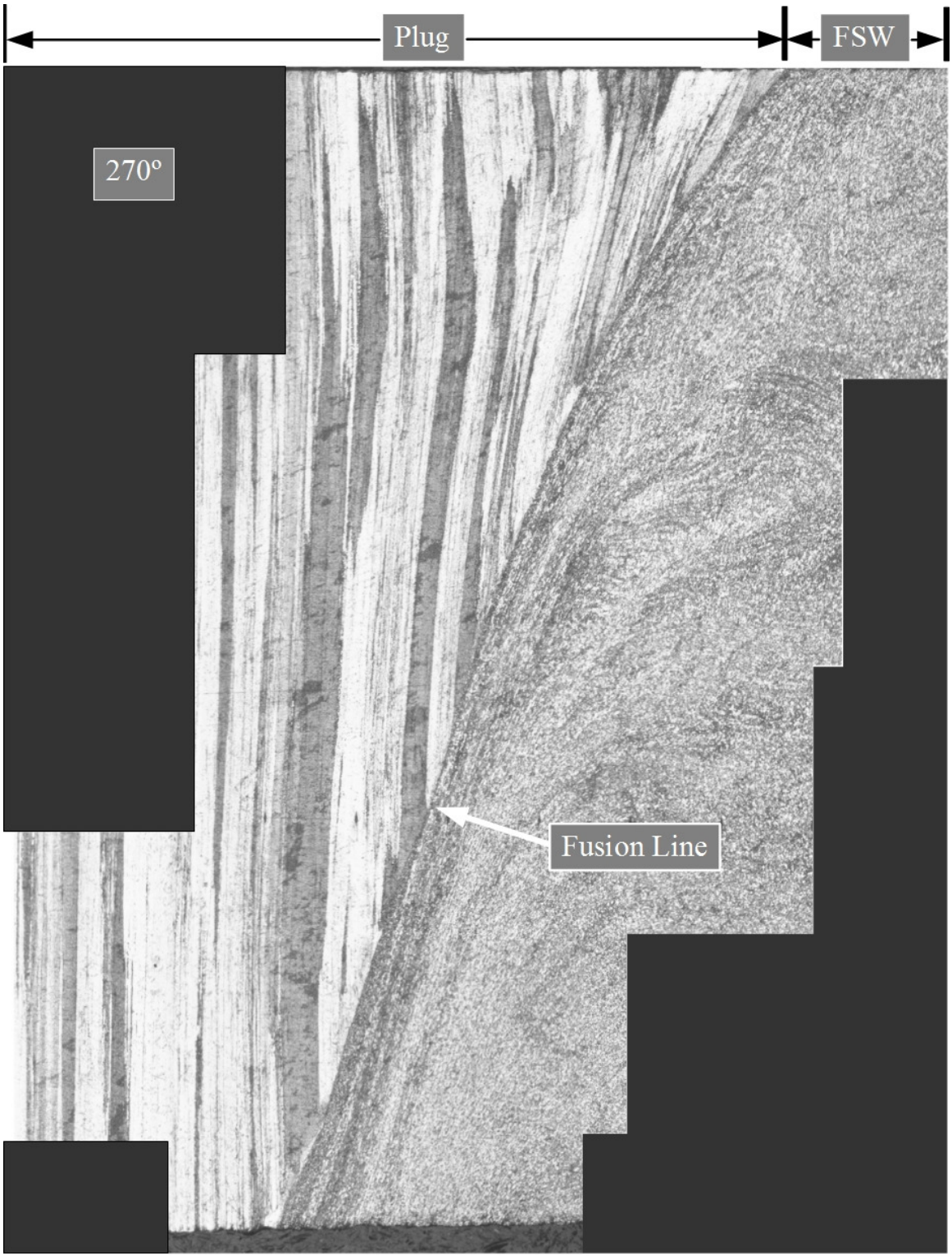

Figure 2.16. Montage of 270° section.

CONCLUSIONS

Measurements made with respect to the recrystallized layer thickness indicate that the plug welding process disrupts the base metal microstructure more extensively on the minor diameter side of the plate than at any other location through the thickness. This is likely due to higher temperatures developed at this side of the plug.

Hardness test results show that the weld interface had the lowest hardness. The TMZ also exhibits a drop in hardness with respect to the base metal. These decreases in hardness are related to the dissolution and over-aging of the T_1 phase. Degradation and over-aging of the T_1 phase is a two-fold process that occurs once during the creation of the FSW and again during the creation of the FPW.

There appears to be a large localized variation within the TMZ and plug HAZ. The large amount of plastic deformation and local elevated temperatures most likely are causing mixing of base metal and FSW material, along with dissolution of T_1 precipitates in the base metal. This result of this mixing and heating results in the local variation of the hardness within the areas adjacent to the plug weld fusion line.

The hardness did not vary drastically within the plug weld interface with respect to the angular (θ) direction. Since hardness is directly related to the presence of strengthening phases, lower hardness values indicate lower strength. The absence of the T_1 phase results in non-homogeneous

slip. This more localized slip mechanism in the plug interface, HAZ, and TMZ is expected to result in lowered high cycle fatigue life due to preferential fatigue crack initiation in areas of decreased strength, specifically with respect to the plug weld interface. Lastly, it is important to note that although the FPW process is considered a solid-state joining process, there are significant metallurgical transitions occurring. It is vital to understand the role of the transitions with respect to the mechanical behavior of the structures created.

Future work in the field should include an extensive study of the effect of the dislocation motion in the plug to the fatigue life and fatigue fracture of the plug weld. Preliminary testing in this field suggests that some long life (lower stress) fatigue tests may result in fatigue crack initiation in the plug. Future research regarding the ultra low cycle fatigue (ULCF) and low cycle fatigue (LCF) behavior of this structure may indicate that failure in these regimes is dependent on geometry.

REFERENCES

[1] Hartley, P. J., 2000, "Friction Plug Weld Repair for the Space Shuttle External Tank," NASA Document ID 20000093962, Johnson Space Center, Marshall Space Flight Center.

[2] Dickerson, T. L., and Przydatek, J., 2003, "Fatigue of Friction Stir Welds in Aluminum Alloys that Contain Root Flaws," International Journal of Fatigue, **25** (2003), pp. 1399-1409.

[3] Khaled, T., 2005, "An Outsider Looks at Friction Stir Welding," Federal Aviation Administration Report ANM-112N-05-06, pp. 14-15.

[4] Wells, D. 2008. NASA MSFC-EM20. Private communication.

[5] Coletta, E. R., and Cantrell, M. A., 2001, "Friction Pull Plug Welding : Top Hat Plug Design," US Patent No. US 6,253,987 B1, July 3, 2001.

[6] Colleta, E. R., and Cantrell, M. A., 2002, "Friction Pull Plug Welding: Chamfered Heat Sink Pull Plug Design," U.S. Patent No. US 6,460,750 B1.

[7] Li, Z. X., Cantrell, M. A., and Brown, R. J., 2000, "Process Development and Microstructural Characterization on Friction Plug Welded 2195 and 2219 Alloys," *AeroMat 2000*.

[8] Chen, P. S., Kuruville, A. K., Malone, T. W., and Stanton, W. P., 1998, "The Effects of Artificial Aging on the Microstructure and Fracture Toughness of Al-Cu-Li Alloy 2195," Journal of Materials Engineering and Performance **7**(5), pp. 682-690.

[9] Li, Z. X., Arbegast, W. J., Hartley, P. J., and Meletis, E. I., 1998, "Microstructural Characterization and Stress Corrosion Evaluation of Friction Stir Welded Al 2195 and Al 2219 Alloys," *Trends in Welding Research*: *Proceedings of the 5th International Conference Pine Mountain Georgia, USA, June 1–5, 1998*, Vitek, J. M., David, S. A., Johnson, J. A. , Smartt, H. B., DebRoy, T., eds., ASM, Cleveland, OH.

[10] Chen, D. L., and Chaturvedi, M. C., 2001, "Effects of Welding and Weld Heat-Affected Zone Simulation on the Microstructure and Mechanical Behavior of a 2195 Aluminum-Lithium Alloy," Metallurgical and Materials Transactions, **32A**, pp. 2729-2741.

[11] Chen, D. L., and Chaturvedi, M. C., 2000. "Near-Threshold Fatigue Crack Growth Behavior of 2195 Aluminum Lithium Alloy Prediction of Crack Propagation Direction and Influence of Stress Ratio," Metallurgical and Materials Transactions, **31A**(6), pp. 1531-1541.

[12] Crooks, R., Wang, Z., Levit, V. I., and Shenoy, R. N., 1998, "Microtexture, Microstructure and Plastic Anisotropy of AA2195," Materials Science and Engineering, **257A**, pp. 145-152.

[13] Schneider, J. A., Nunes, A. C. Jr., Chen, P. S., and Steel, G., 2005, "TEM Study of the FSW Nugget in AA2195-T81," Journal of Materials Science, **40**, pp. 4341-4345.

[14] Shulka, A. K. and Baeslack, W. A. III, 2007, "Study of Microstructural Evolution in Friction-Stir Welded Thin-Sheet Al-Cu-Li Alloy using Transmission-Electron Microscopy," Scripta Materialia, **56**, pp. 513-516.

[15] Subramanian, P., Nirmalan, N., Young, L., Sudkamp, P., Mika, D., Larsen, M., Othon, M., Dupree, P., Walker, S., and Catlin, G., 2003, "Fundamental Studies of Microstructure Evolution during Stir Welding of Aluminum Alloys," NASA Technical Report No. 20031028177.

[16] Fonda, R. W. and Bingert, J. F., 2006, "Precipitation and Grain Refinement in a 2195 Al Friction Stir Weld," Metallurgical and Materials Transactions, **37A**, pp. 3593-3603.

[17] Fonda, R. W., Bingert, J. F., and Colligan, K. J., 2004, "Development of Grain Structure During Friction Stir Welding," Scripta Materialia, **51**, pp. 243-248.

[18] Wang, Z. M. and Shenoy, R. N., 1998, "Microstructural Characterization of Aluminum-Lithium Alloys 1460 and 2195," NASA CR-1998-206914.

[19] Coletta, E. R. and Cantrell, M. A., 2000, "Friction Plug Weld Repair Geometric Innovations," Marshall Space Flight Center, NASA Document ID: 20000112928

[20] ASTM E3, "Standard Guide for Preparation of Metallographic Specimens Annual Book of ASTM Standards," American Society for Testing and Materials, Volume 3.01.

[21] Colleta, E. R. and Cantrell, M. A., 2005, “Friction Pull Plug Welding: Chamfered Heat Sink Pull Plug Design,” U.S. Patent No. US 6,880,743 B1.

CHAPTER 3

FATIGUE BEHAVIOR OF FRICTION PLUG WELDS IN 2195-T8 AL-LI

INTRODUCTION

The aluminum-lithium alloy 2195-T8 has become the preferred material for applications such as the Super Light Weight Tank (SLWT) on the Space Shuttle due to its low density, high tensile strength, and good cryogenic fracture toughness as compared to other aluminum alloys [1-4]. This material will likely be used in the future for both single use and re-usable types of future aerospace cryogenic pressure vessels as well as incorporation into other types of future aeronautical and aerospace structures. [5, 6]

The welding process being investigated to be used to fabricate such future pressure vessels and aerospace structures is friction stir welding (FSW), a solid-state welding process. FSW has already been proven in the use of spacecraft fuel tanks and cryogenic pressure vessels. The aerospace alloys 2195-T8 and 2219, which are used in components of the SLWT, have been successfully joined using the FSW process. The FSW process can be used for both longitudinal welds and circumferential welds in pressure vessel fabrication, with an overall reduction in

welding defects. Although the implementation of FSW has been shown to reduce the number of weld defects, as compared to other processes such as variable polarity plasma arc welding (VPPA), there is still a need for a method to repair FSW defects. [6-8]

One repair method that has been proposed is called Friction Plug Welding (FPW). Friction Plug Welding is a solid-state welding process being investigated as a repair method for weld and process defects that occur within a Friction Stir Weld (FSW) [1]. Also, since the FPW process can be performed with portable equipment, it may be used to repair larger structures fabricated with FSW that may have no means of repair once assembled due to accessibility issues with FSW equipment. For this repair method, a defect that has been identified in the FSW is removed by drilling a though-hole in the area of the defect, and subsequently, by pulling a rapidly rotating plug through the hole to create a friction weld between the plug and the structure. For more detailed information on the FPW process, the reader may refer to the following references [10-13].

The tensile and fatigue properties of the base metal 2195-T8 and friction stir welded 2195-T8 plate have been investigated by several researchers [5, 8, 14-20]. However, little data is available or has been published with regards to the fatigue properties of FSW 2195-T8 plate that has been repaired using the FPW process. Comparison of any reduction in fatigue life due to the FPW process would be of interest to design engineer for stress limits and evaluation of damage tolerance for structures using this repair process.

Low cycle fatigue is of interest for applications in both single use and re-usable cryogenic pressure vessels, in which the pressure vessel has limited life and limited number of load cycles. However, obtaining meaningful low cycle fatigue test data is difficult due to the large amount of plasticity that is inherently found in the low cycle regime. Specimen design for base metal testing in the low cycle regime fatigue is usually restricted to smooth type round specimens, which may not be able to reflect the notch, residual stress, and thermal effects found in the actual structure in the as-welded condition. However, to compare the effect that varying the weld process parameters has on fatigue performance of the joint, fatigue testing in the mid-to-high cycle region may be used [21]. An increase of fatigue lives at the mid-to-high cycle regime indicates that properties within the weld joint are improved.

In this study, plates of FSW 2195-T8 base metal that had friction plug welds located in the FSW were examined. The tensile properties of the base metal, FSW 2195-T8, and FPW 2195-T8 were determined. Fatigue tests were run for FSW 2195-T8 and FPW 2195-T8, and the S-N plots prepared. The location of fracture initiation, mode of crack growth, and comparison of fracture surface characteristics was noted for the FPW 2195-T8 specimens.

The plug design used in the manufacture of the test plates was designated by NASA as an M3 plug, shown schematically in Figure 3.1. The plug is comprised of three main
parts: the top section, main section, and lower section [10]. The top section of the plug contains the heat sink and annular shoulder. The main part consists of a double-tapered, frusto-conical section. The main portion of the plug fills the hole in the plate. This section has a larger or major

diameter at the heat sink end, and transitions to a smaller or minor diameter through a double taper. The lower section is comprised of the shank, threaded end, and conical tip. The shank portion of the plug has a constant diameter. The threaded section is used as a means to attach the plug to the friction plug welding machine. In this study, the plug was machined from extruded 2195-T8 round stock.

EXPERIMENTAL PROGRAM

Overview

Material strength testing was performed to establish baseline ultimate tensile strength (UTS) transverse to the rolling direction for the base metal 2195-T8 Al-Li alloy. The UTS was also determined for the same alloy that had undergone a friction stir welding process. Likewise, the UTS was determined for a friction stir plug welded specimen consisting of a friction plug weld inserted into a friction stir weld. The UTS of the FSW and FPW were used to establish the upper limit of the stress amplitude for the fatigue testing schedule for these specimens. Constant amplitude fatigue testing was used to compare the fatigue life of specimens containing only friction stir welds with that of specimens which contained a friction stir plug weld in the friction stir weld.

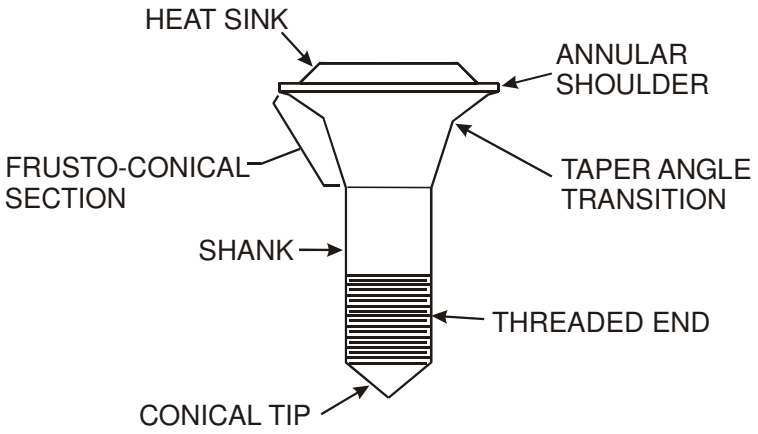

Figure 3.1. Plug diagram and nomenclature.

Material

Two separate groups of friction stir welded plates that contained friction plug welds were provided by the Materials and Processes Laboratory's Metals Engineering Division, EM30, of NASA's Marshall Space Flight Center. All test plates were made from 6.35 mm thick 2195-T8 Al-Li sheet material. The test plate dimensions were 305 mm x 610 mm. The first group of test plates, Group A, comprised of three separate plates, was made with plug weld spindle speeds designated as low, medium and high corresponding to 4000, 5000, and 6000 RPM spindle speeds, respectively. The spindle speed refers to the rotational speed at which the plug is rotated during the FPW process. Each test plate contained four plug welds with a M3 style plug with 15.9 mm shank diameter. The plate made with 4000 RPM of Group A is shown in Figure 3.2. The second set of test plates, Group B, was manufactured according to optimized specifications, with spindle speed of 4250 RPM. The Group B plug welded plates were made with a M-3 Revision A style plug with a shank diameter of 19.1 mm (0.75 inch). The FSW process parameters were consistent between the two groups of plates. The plates had NDE inspection

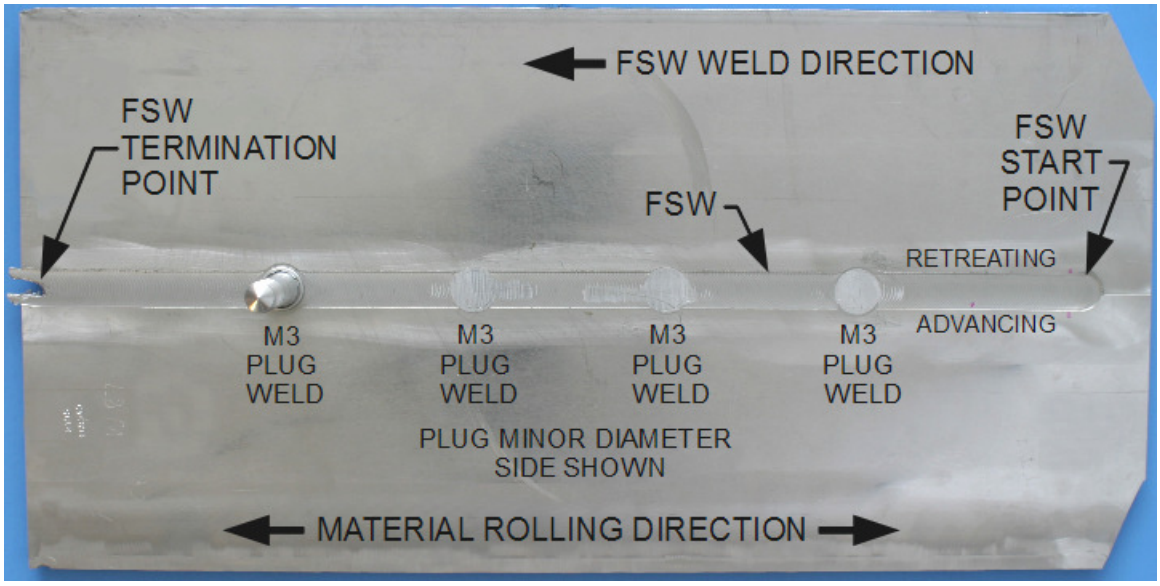

Figure 3.2. Test Plate from Group A.

performed by NASA at Marshall Space Flight Center. The inspection techniques used were visual, dye penetrant and phased-array ultrasound with a threshold defect size of 0.5 mm. All plug welds in both Group A and Group B plates were finish ground prior to the specimens being cut from the test plates.

Base Metal, FSW and FPW Specimen Design

Dog-bone style specimens, as shown in Figure 3.3, were used for the tensile and fatigue testing of the base metal, FSW 2195-T8, and FPW 2195-T8. The physical dimensions for each type of specimen used in the testing are listed in Table 3.1. The orientation of the FSW weld line with respect to the loading axis of the specimen is listed in the second column of Table 3.1. An orientation of 90º for the FSW describes a specimen with the FSW weld line at a right angle to

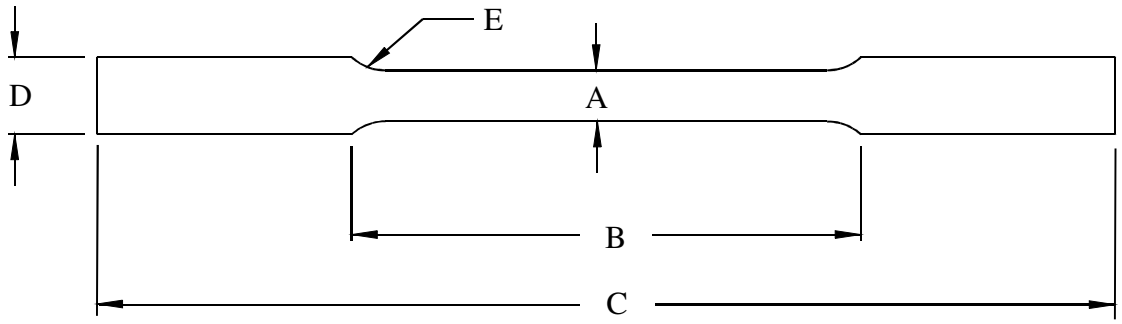

Figure 3.3. Tensile and fatigue test specimen diagram.

Table 3.1. Tensile and fatigue specimen dimensions.

Specimen	FSW orientation	A	B	C	D	E
BM	n/a	6.35	63.5	127	9.52	6.35
FSW	90º	12.7	102	203	19.1	12.7
FPW-0º	0º	76.2	152	254	102	25.4
FPW-90º	90º	76.2	152	305	102	25.4

Note: All dimensions millimeters.

the loading axis of the specimen, while a 0º FSW orientation denotes specimens where the FSW is in-line with the loading axis of the specimen. The base metal specimens were cut from the plate such that the loading axis was transverse to the material rolling direction of the plate. Note that the base metal specimens did not contain FSW, hence there was no FSW orientation angle listed for this type of specimen. The FSW 2195-T8 specimens all had the same orientation of 90º.

The base metal, FSW, and FPW specimens were marked with plate number and plug number where applicable to keep record of which test plate it had been cut from and its location within the test plate.

The base metal tensile specimens were sub-size specimens and the FSW specimens were standard size sheet specimens as specified in ASTM standard E8-04. The base metal specimens were cut so that the load axis was transverse to the base metal plate rolling direction. The base metal specimens were designated A-BM-X where A denotes the Group A test plate, BM denotes base metal, and X denotes the individual specimen number. The FSW specimens were cut for use as tensile and fatigue specimens containing only friction stir weld. The FSW specimens all had the FSW oriented at an angle of 90º to the loading axis. The specimens were designated as A-FSW-X where A denotes the Group A, FSW denotes a friction stir weld specimen, and X is the individual specimen number.

The FPW specimens were modified sheet-type specimens, deviating in specimen width and length from the ASTM E8-04 specification. This deviation was necessary due to the physical size of the plug welds and overall dimensions of the provided test plates, which restricted adherence to the specification. The FPW specimens cut from the Group A plates were numbered A-FPW-90º-X. The letter A denotes the plate is from Group A, FPW denotes a friction plug weld specimen, and 90º indicates the orientation of the load axis with the friction stir weld. Figure 3.4 shows this configuration of FPW specimen. The fatigue specimens that were cut from the Group

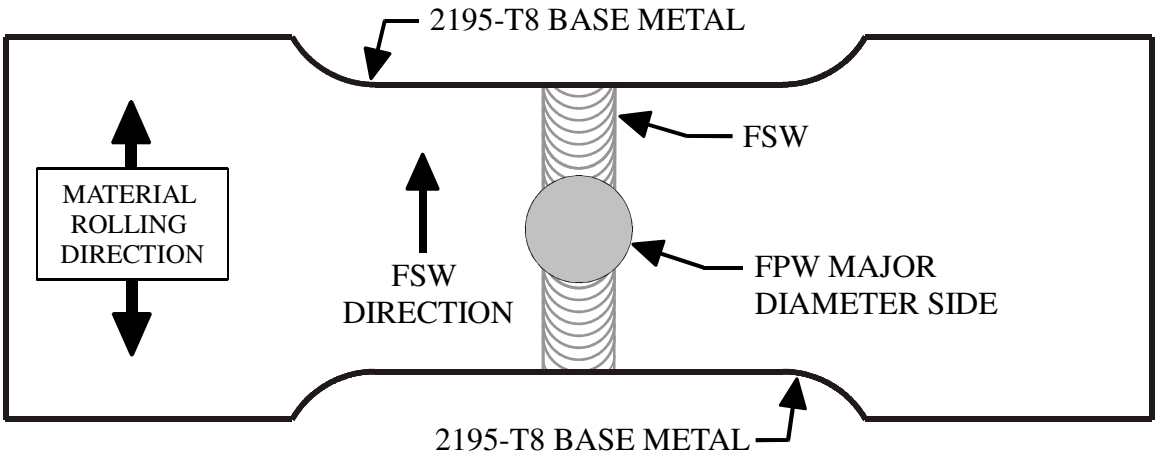

Figure 3.4. FPW 90º specimen.

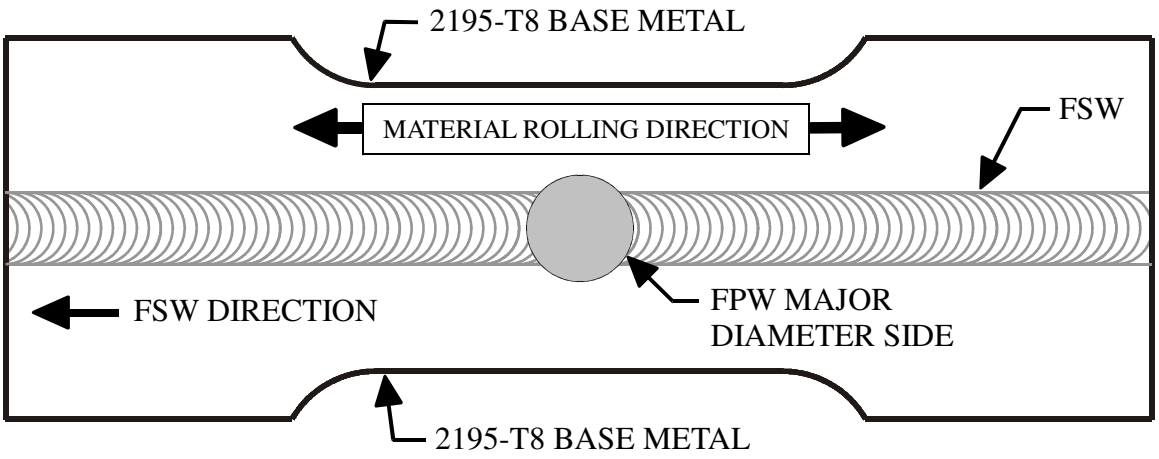

Figure 3.5. FPW 0º specimen.

B plates had two orientations of FSW to the load axis, either 90º or 0º. Fatigue specimens with the load axis at 90º to the FSW were designated B-FPW-90º-X, and specimens with the load axis in line with the FSW were designated as B-FPW-0º-X. Figure 3.5 shows this type of FPW specimen. The layout of the sub-size tensile, FSW, and FPW specimens as cut from the test plates is shown in Figure 3.6, while Figure 3.7 shows the cut locations for the B-FPW-0º-X type specimens (B-FPW-0º-9 through B-FPW-0º-14).

Mechanical Properties

2195-T8 Base Material

The tensile specimens were used to obtain the yield strength, tensile strength, and total elongation of the 2195-T8 base metal. The base metal tensile specimens were cut from the Group A set of friction stir plug welded plates. Figure 3.6 shows the locations from which the tensile specimens were cut from the plates. Fifteen base metal specimens were tension tested in air at room temperature conditions using a Tinius-Olsen 45 kN test frame and an extensometer with 25.4 mm gage length was used to measure the elongation in the gage section of the specimen. The test results were averaged to find the average mechanical properties of the base 2195-T8 Al-Li.

An example stress-strain curve is shown in Figure 3.8. The average UTS was found to be 597 MPa, and the average total elongation was 10.6%.

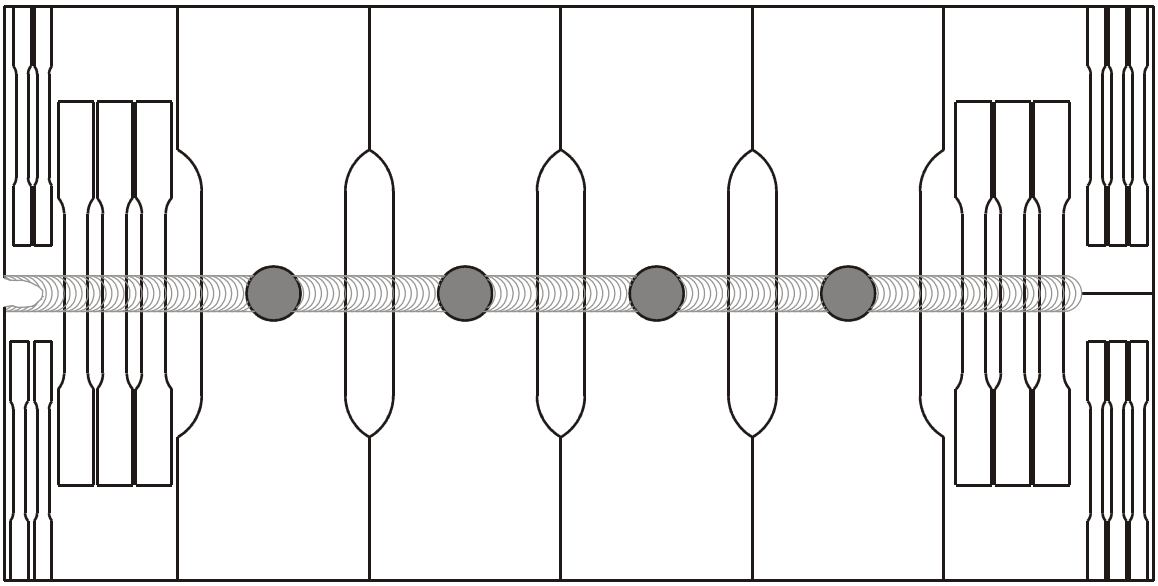

Figure 3.6. Cutting diagram for BM tensile, FSW, and FPW 90º specimens from test panel.

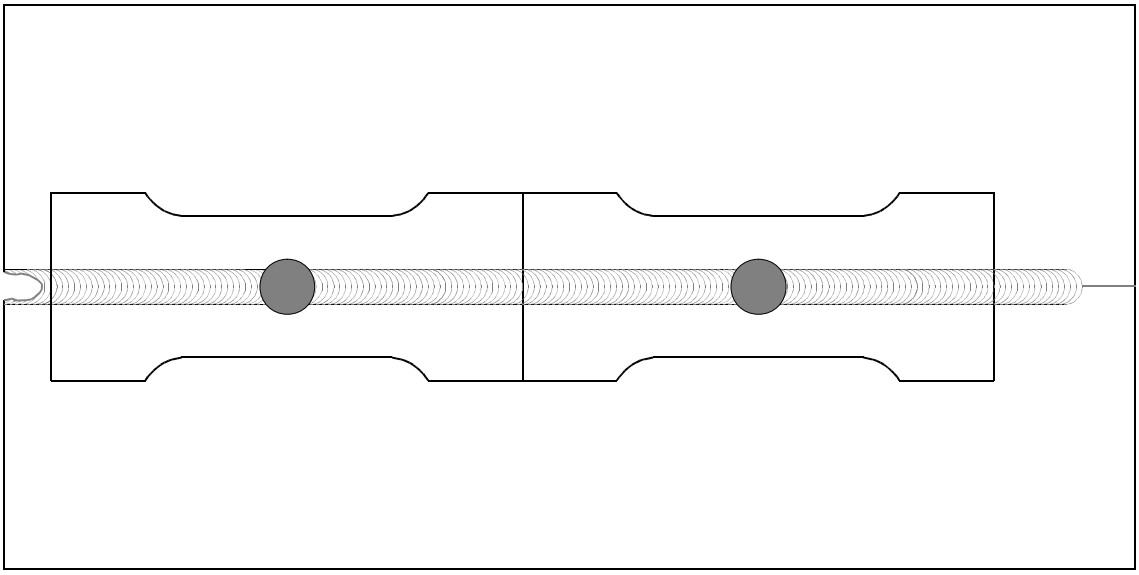

Figure 3.7. Cutting diagram for FPW 0º specimens.

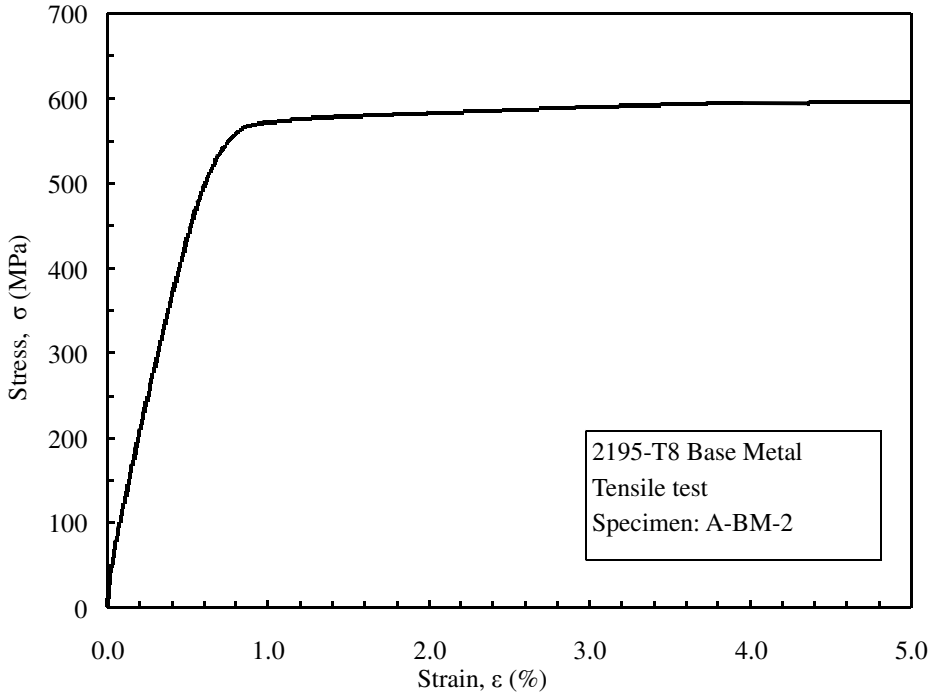

Figure 3.8. Stress-strain curve for 2195-T8 base metal.

Friction Stir Weld

The ultimate tensile strength for the friction stir weld without a plug weld was determined at room temperature for a single specimen A-FSW-1 cut from one of the Group A plates. The specimen was loaded to failure using a SATEC 245 kN test frame. The load and piston displacement was recorded using LabVIEW 6.2 for data acquisition. An extensometer was not used during the test so only the ultimate tensile strength of the friction stir welded 2195-T8 plate was measured. The UTS for the specimen containing friction stir weld only was determined to be 408 MPa, which is 68% of the base material's ultimate tensile strength of 597 MPa.

Friction Plug Weld

The ultimate tensile strength was determined for three of the FPW specimens containing a friction plug weld placed in the friction stir weld. Specimens A-FPW-90º-0 and A-FPW-90º-1 were chosen from the Group A plate with corresponding 6000 RPM spindle speed. Specimen A-FPW-90º-2 was chosen from the Group A plate with 4000 RPM spindle speed. The A-FPW-90º-2 specimen had a visible, circular shaped, surface defect on both the major diameter and minor diameter sides of the plug weld. Figure 3.9 shows the defect located on the minor diameter side. Similar circular shaped, surface defects were present in all of the fatigue specimens cut from plate with 4000 RPM spindle speed.

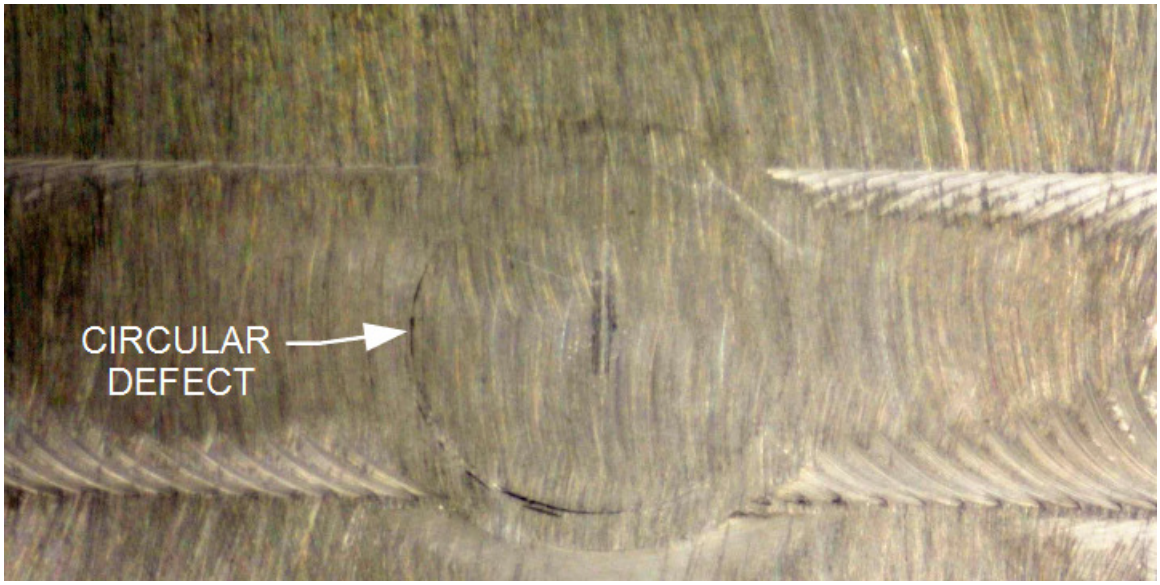

Figure 3.9. Circular surface defect on minor diameter side of A-FPW-90º-2.

The results of the FPW tensile tests are shown in Table 3.2. The average tensile strength of the plug weld was found to be 342 MPa, which corresponds to 57% of the base metal UTS. Specimen A-FPW-90º-0 had the lowest tensile strength, while specimen A-FPW-90º-2 had the highest tensile strength. It should be noted that specimens A-FPW-90º-2, which contained the line defect noted earlier had ultimate tensile strength 10 % greater than the ultimate strength of specimen A-FPW-90º-0. Specimen A-FPW-90º-1 had tensile strength which varied from the maximum tensile strength by less than 0.5 %. This means that a circular, surface defect does not necessarily indicate a significant decrease in tensile strength. The tensile strength of specimen A-FPW-90º-0 would be used as a base-line value for all fatigue testing of friction stir plug weld specimens, including those from the second set of test plates which were Group B.

Table 3.2. FPW tension test results.

FPW Tensile Specimen	Ultimate Tensile Strength (MPa)
A-FPW-90º-0	318
A-FPW-90º-1	354
A-FPW-90º-2	355

The fracture surfaces of the tensile strength friction plug weld specimens A-FPW-90º-1 and A-FPW-90º-2 were found to be similar with regard to appearance and fracture path along the plug weld and FSW. The fracture in these two specimens had a clear separation along the plug weld interface. The fracture initiated on the major diameter side, adjacent to the advancing side of the FSW of the plug at the plug weld/base metal interface. Specimen A-FPW-90º-0 also had initiation on the major diameter side, however, the failure initiated within the plug HAZ, adjacent

to the retreating side of the FSW. The location of fracture initiation for specimens A-FPW-90º-0, A-FPW-90º -1, and A-FPW-90º -2 is shown in Figure 3.10.

The fracture surface of -0 within the plug region had a rough, stepped appearance due to the elongated grain structure due to the extrusion, in contrast to the smooth, inclined surface of specimens A-FPW-90º-1 and A-FPW-90º-2. The initial fracture surface in all tensile specimens had an arced shape, with propagation along the arc of the plug until the crack reached the center-line of the FSW, at which point the fracture path changed to the center-line direction of the FSW as shown in Figure 3.11. Specimen A-FPW-90º-1 had evidence of crack branching near the FSW center-line with branches partially extending into the FSW along a direction slightly angled from the axial direction of the specimen.

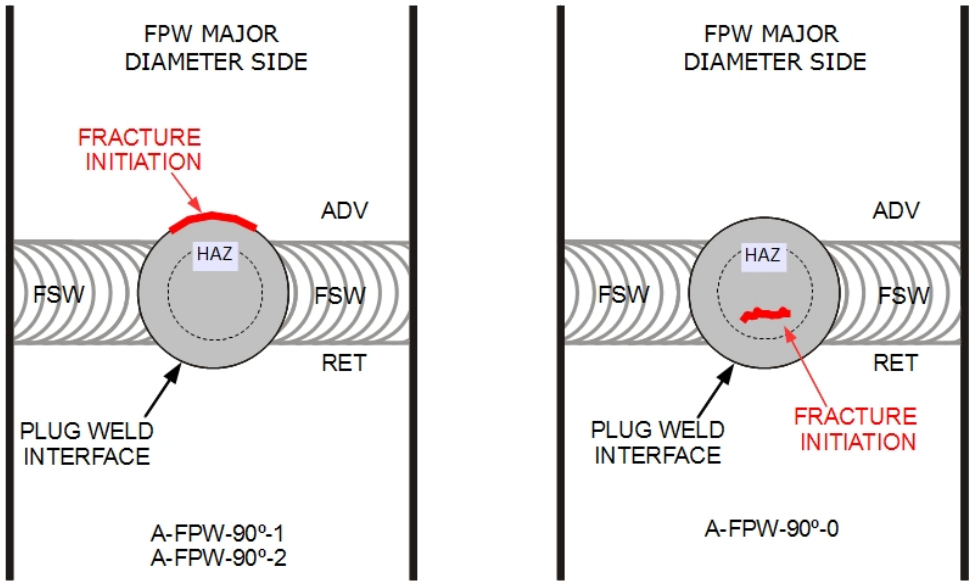

Figure 3.10. Fracture initiation location for specimens A-FPW-90°-0 thru -2.

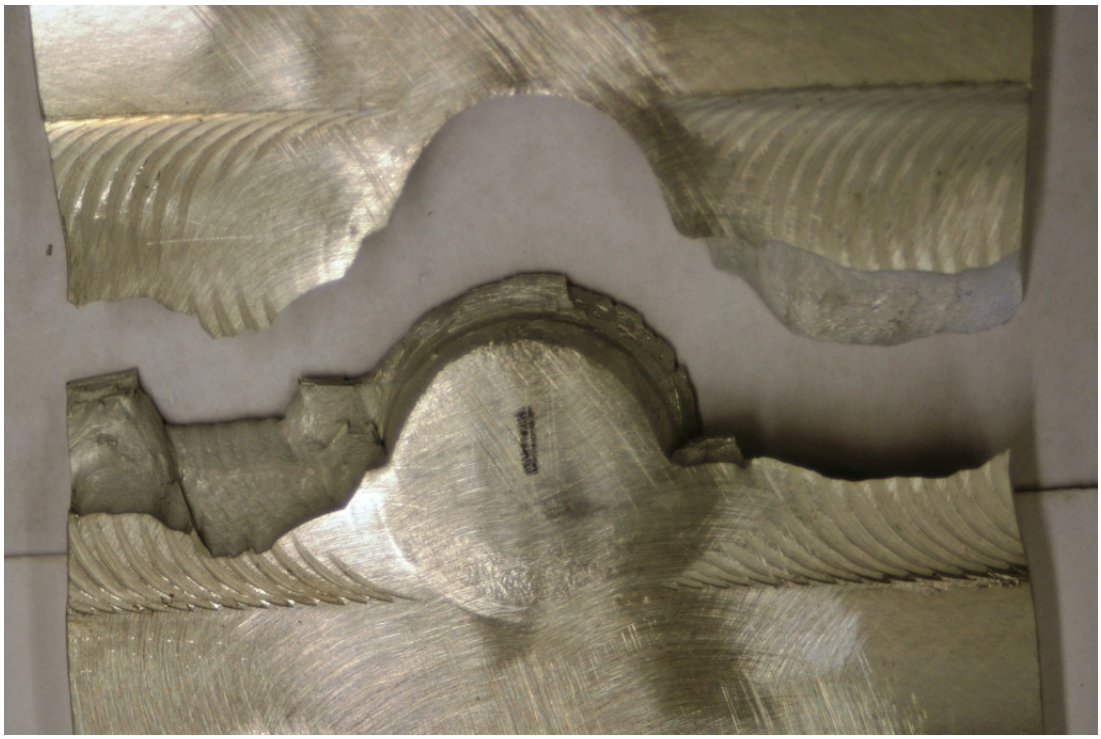

Figure 3.11. Fracture surface of FPW tensile specimen.

Fatigue Testing of Friction Stir Weld and Friction Plug Weld

A total of ten specimens which had friction stir weld only and twenty-two specimens containing friction plug welds were fatigue tested at room temperature conditions on a SATEC 245 kN test frame with a MTS 407 controller. All fatigue testing of the FSW and FPW specimens was conducted under constant amplitude loading conditions using cyclic (sine wave) loading with frequency of 5 Hz for both the FSW and FPW specimens. An R ratio of 0.1 was used for both FSW and FPW specimens. The stress amplitude varied from 55 MPa to 147 MPa for the friction stir weld only specimens, while FPW specimens had stress amplitude that varied from 43 to 158

MPa. Failure of the specimen was specified as a 30% load drop causing interlock of the test machine, a complete fracture, and extension of greater than 2.5 mm specifically for the FPW specimens. The testing machine was set to interlock on any of the mentioned failure conditions. In cases where the interlock was tripped without complete fracture of the specimen, the interlock was cleared and then the specimen was either removed from the test machine, or the specimen was fractured by using the test machine in manual control.

Any FSW or FPW specimens which attained a cycle count of 1 million cycles or greater were considered to be run-out specimens. The pseudo endurance limit of 1 million cycles was chosen due to limited specimen number and that the actual pressure vessel application would not be expected to see this life cycles any greater that this in actual service. The main area of interest for the application was in the low to mid cycle regime. The two observed run-out specimens with more than 1 million cycles exhibited no visible sign of fatigue cracks.

RESULTS

Results of FSW fatigue testing

A plot of the stress amplitude versus cycles to failure for FSW fatigue specimens is shown in Figure 3.12. A linear regression was performed on the data and a best fit line is shown on the FSW S-N curve. The standard error for the linear regression was determined to be 0.0382. The specimen A-FSW-8 was not included in the regression analysis, since this was a run-out specimen (1.4 million cycles) as indicated by the short arrow in Figure 3.12. Additionally, the

two other FSW specimens, A-FSW-1 and A-FSW-4, were also excluded from the data analysis, shown as solid data points. Specimen A-FSW-1 was tested with a stress amplitude of 55 MPa and had failure occur at 38750 cycles. The specimen A-FSW-4 was tested with a stress amplitude of 110 MPa and failure occurred 34584 cycles. Post failure examination of fracture surface for these two specimens revealed the presence of weld voids in the FSW for both specimens.

Visual inspection of the fracture surface using a stereo microscope with magnification of 30X revealed the presence of severe welding defects (voids), and additionally X-ray images of the specimens taken prior to the fatigue testing indicated the presence of weld voids. Specimen A-FSW-1 was cut from the Group A 4000 rpm spindle speed plate, while specimen A-FSW-4 was from the Group A 5000 rpm spindle speed plate. These specimens were sectioned from the test plates at the location near the termination point of the FSW. The area surrounding the termination point of the FSW is prone to have severe welding defects, and these two specimens would not be considered to have been satisfactory friction stir welds [4]. The results of the fatigue test showed that the fatigue life of friction stir weld specimens was adversely affected by the presence of such weld voids similar to those found in specimens A-FSW-1 and A-FSW-4. Specimens cut at locations in the plate away from the FSW termination point did not contain any visibly detectable signs of weld defects in both X-ray images and visual inspection of the fracture surfaces.

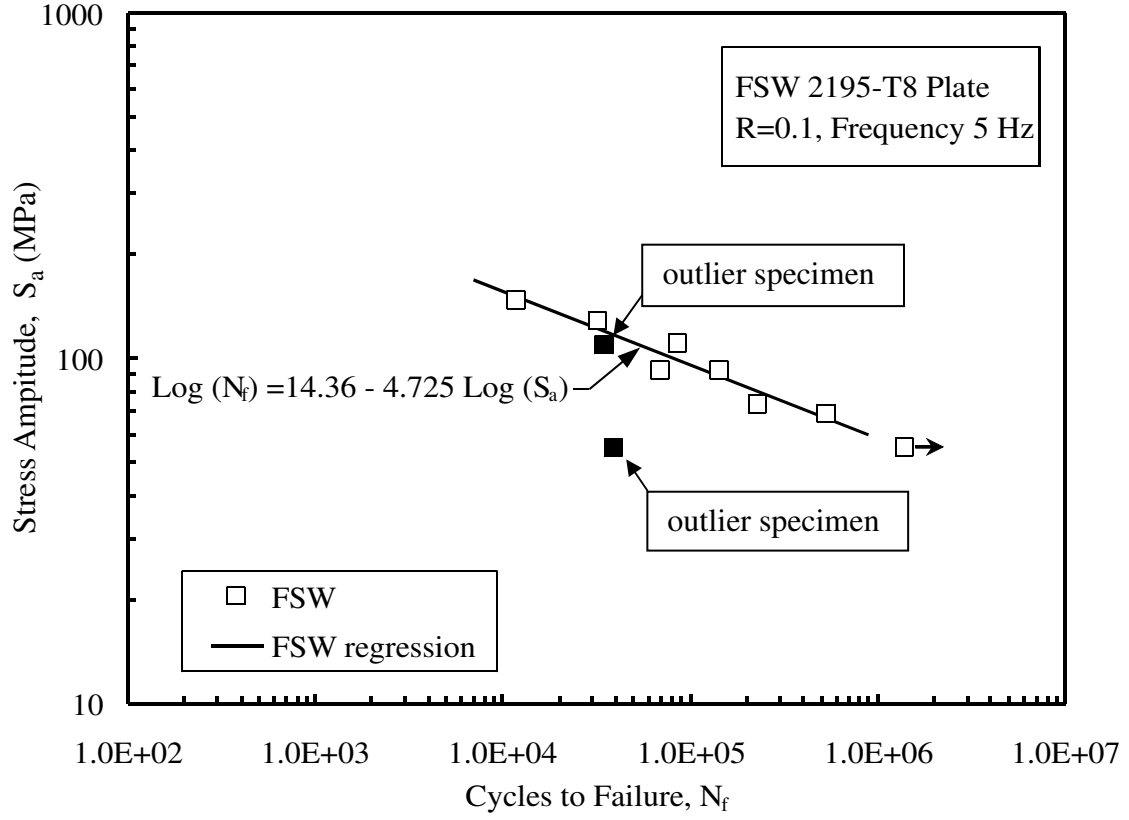

Figure 3.12. S-N curve for FSW 2195-T8

Results of FPW fatigue testing

Figure 3.13 shows a plot of the stress amplitude versus cycles to failure for the Group A FPW 90º specimens. A linear regression analysis was performed and the best fit line is indicated on the plot. The standard error for the regression line was 0.0469. The regression line for FSW specimens is also shown on the S-N plot for the purpose of comparison of FPW to FSW fatigue properties. The FPW specimens A-FPW-90º-7 and A-FPW-90º-8 were run-out specimens as indicated with arrows in Figure 3.13. These run-out specimens were excluded from the linear

regression analysis. Additionally, the specimens A-FPW-90º-9 and A-FPW-90º-10, shown as solid data points, were also excluded from the linear regression analysis due to these specimens having plug welds having a circular defect at the FPW interface. The defects on these two specimens were similar to defect exhibited on the FPW tensile specimen A-FPW-90º-2 that is shown in Figure 3.9. Visual inspection of the fracture surfaces of the two specimens showed a lack of fusion at the FPW interface. The data for these two specimens are shown in Figure 3.13 in order to illustrate the effect that poor weld fusion had with respect to fatigue life for the other Group A FPW 90º specimens.

The S-N plot for the Group B FPW 90º specimens is shown in Figure 3.14. The linear regression for the data points is shown on the plot. The linear regression was found to have a standard error of 0.0393. The specimen B-FPW-90º-2, shown as a solid data point, was not included in the regression. This specimen was determined to be an outlier. Comparison with the FSW regression line shows the Group B 90º specimens had similar fatigue properties to the FSW fatigue specimens, although the standard error of the regression was 0.0393, which is slightly larger than the value for the FSW regression.

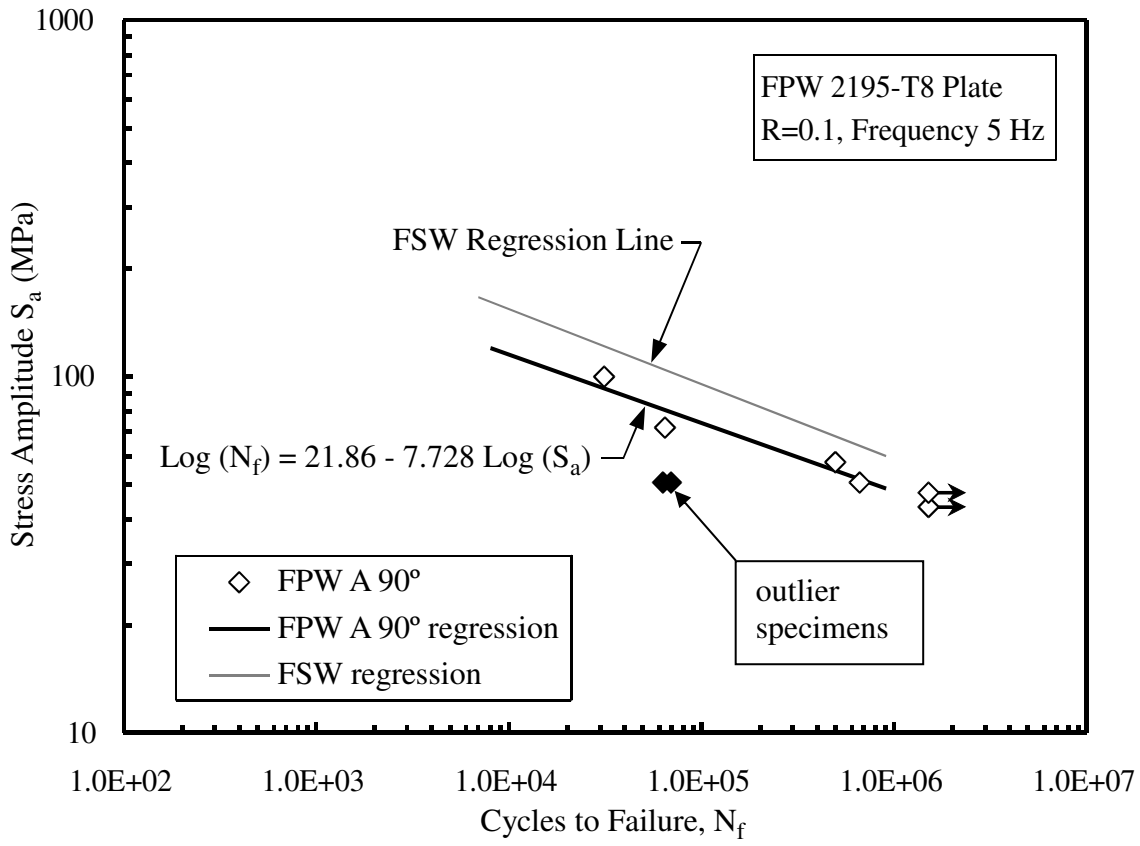

Figure 3.13. S-N curve for FPW A 90º specimens.

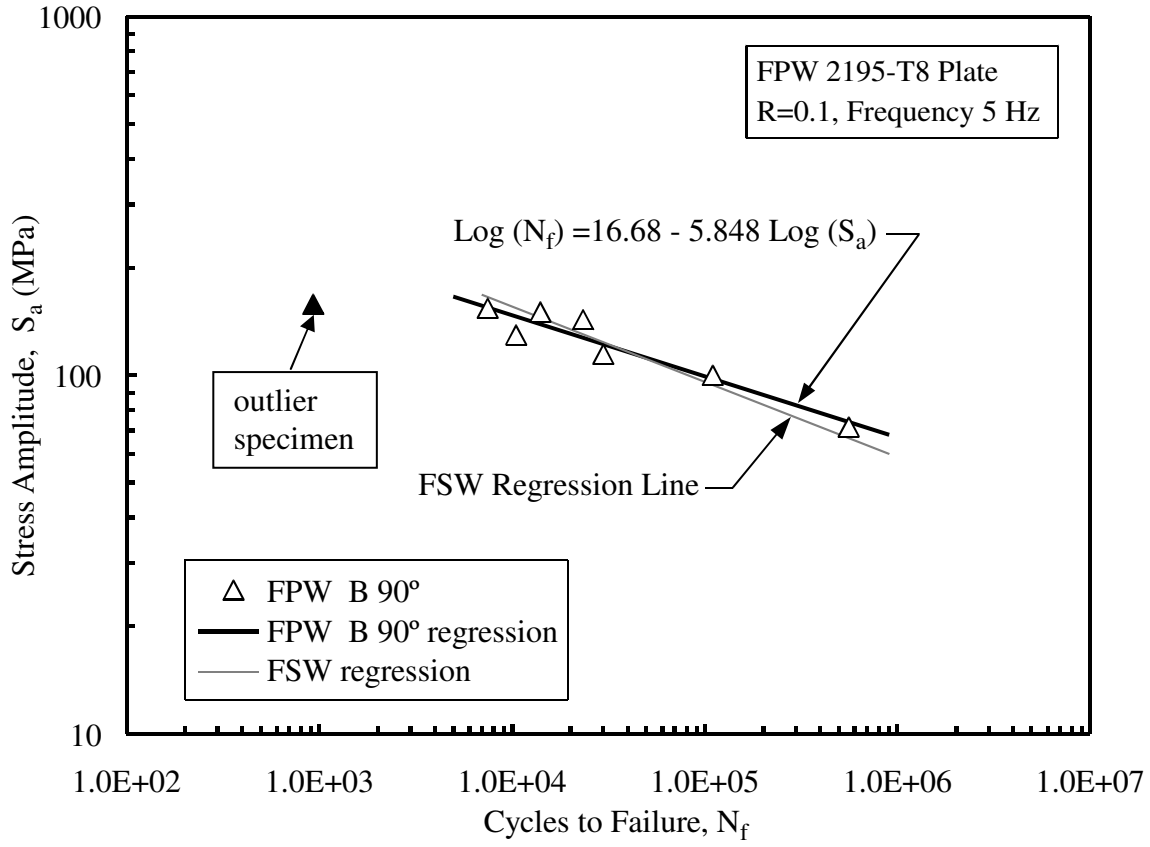

Figure 3.14. S-N curve for FPW B-90º specimens.

Figure 3.15 shows the S-N plot for the Group B FPW 0º specimens. Linear regression was performed on the data and the regression line shown on the plot. The regression line is similar to both the Group B FPW 90º specimens and the FSW specimens. However the error associated with the regression for the B FPW 0º was found to be 0.0963, which is more than twice as large as the error for Group B 90º. The three data points around 10^5 cycles were checked for randomness, and found to be within the statistical test for randomness.

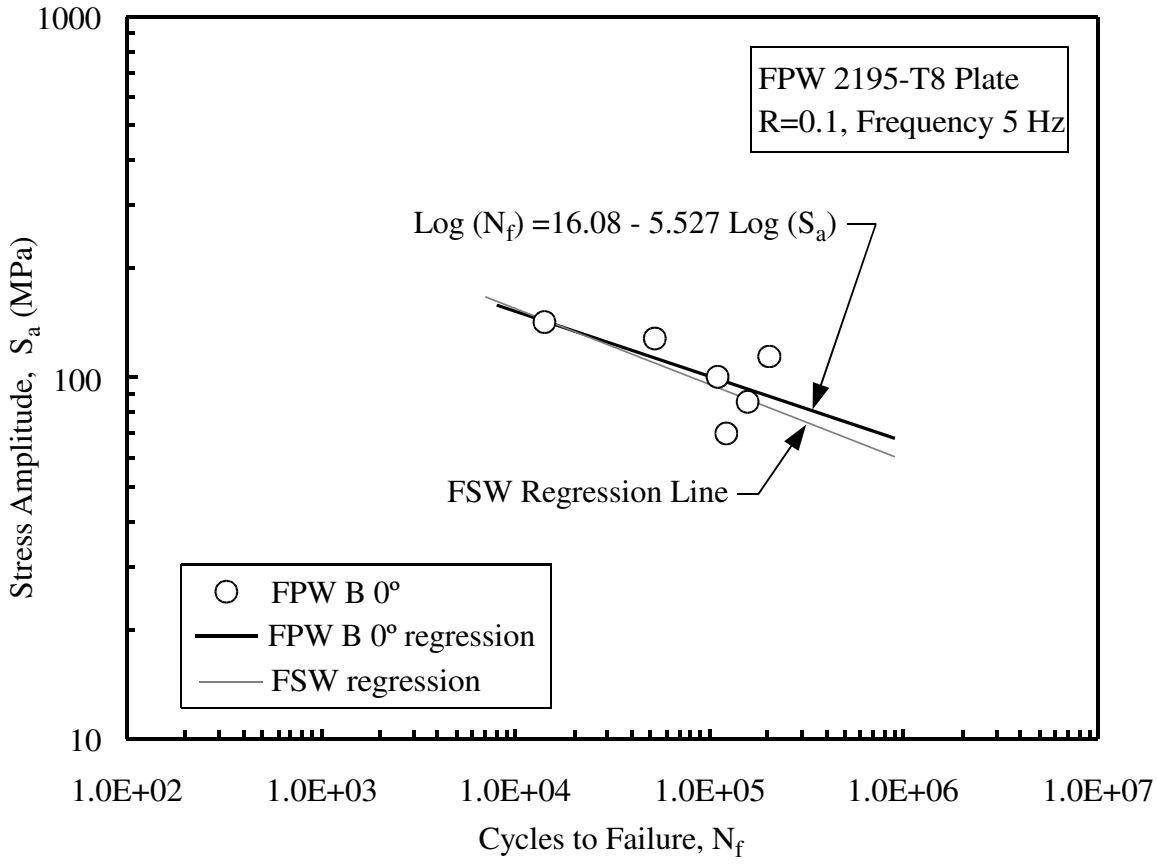

Figure 3.15. S-N curve for FPW B 0º specimens.

Figure 3.16 is a plot of stress amplitude versus cycles to failure for the combined data of all FPW specimens from Group A and Group B except for the data points previously excluded from the regression analysis. The FSW regression line from the FSW fatigue tests is shown for comparison. The FPW regression is seen to be similar in slope and intercept to the FSW regression; however, the error was 0.0777 for the combined data regression line. Comparison of the FPW regression error with the error from FSW regression shows that the error is twice as large, meaning that the FPW fatigue data has more randomness than the FSW fatigue data.

This can be seen by the larger scatter of the FPW data points on the combined S-N plot in Figure 3.16, particularly those of the Group B 0º specimens.

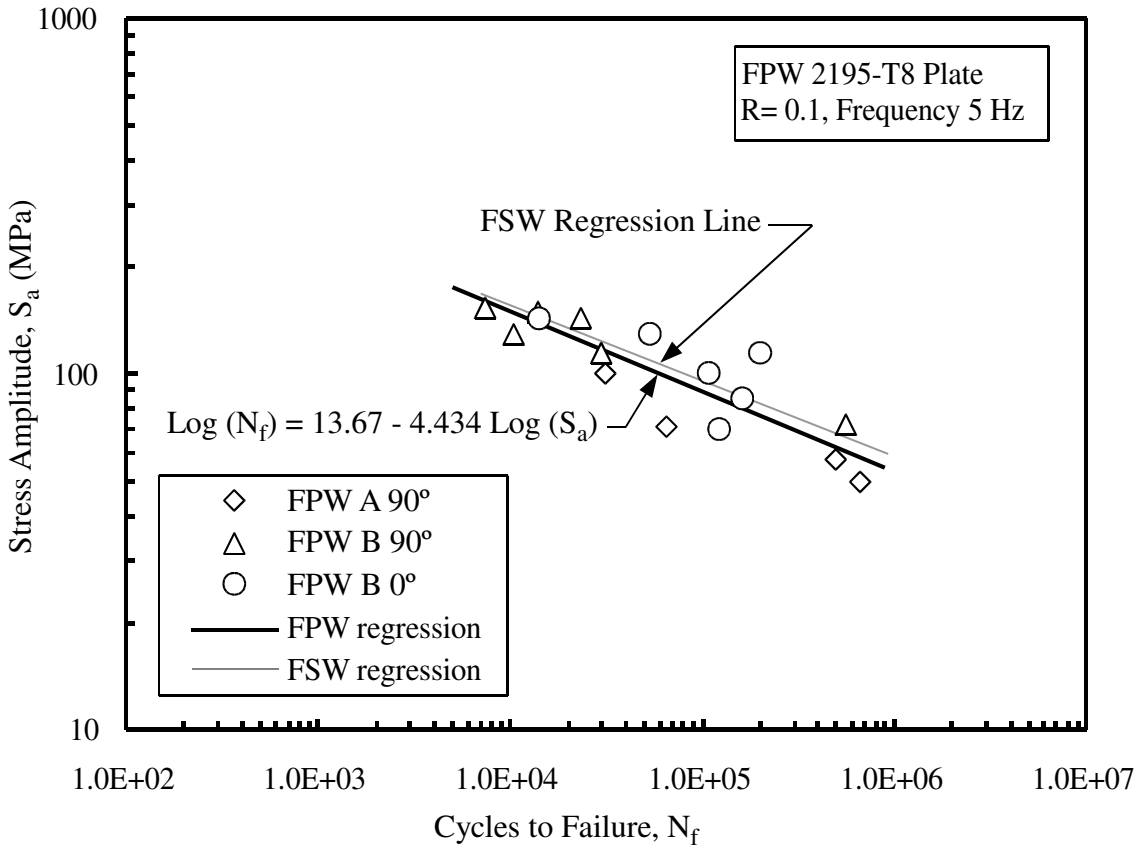

Figure 3.16. S-N curve for combined data of Group A and Group B FPW specimens.

Fatigue crack initiation and propagation

The origin of the fatigue crack initiation and the direction of fatigue crack propagation for each FPW fatigue specimen were identified by visual observation during the fatigue test and/or post-failure visual inspection. The observations are listed in Table 3.3. The table was assembled to show if any significant trends and correlations between the different groups and styles of

specimens could be determined. From Table 3.3 it can be seen that the primary initiation site for fracture of the 90º FPW specimens was on the major diameter side of the FPW, while the 0º FPW specimens all had fractures originate on the minor diameter side. Note that the third column of Table 3.3 shows load as % of UTS, and is referring to the average UTS for the FPW specimens, which was determined to be 342 MPa from the FPW tensile tests.

It was observed that some FPW fatigue specimens had cracks which propagated along the plug weld interface to approximately the center-line of the FSW, at which point the crack began to propagate along a line at an angle to the loading axis of the specimen. Table 3.4 lists the specimens which had an inclination of the crack path, as well as which direction of crack growth with respect to the FSW advancing and retreating direction. Figure 3.15 shows the relationship of the crack propagation angle to the specimen longitudinal axis for both the 90º FPW and 0º FPW specimens. The angle ranged from a minimum of 9° to a maximum of 27°, but tended to be most commonly in the range of 14° to 18°. For some specimens, the crack then propagated past the FSW, FSW HAZ, and into the base metal, while some specimens propagated only into the FSW.

Table 3.3. FPW fatigue specimen fracture initiation and propagation.

			Fracture Initiation							Crack Propagation				
Specimen	Cycles	Load as % of FPW UTS	Major diameter side	Minor diameter side	FPW Interface	FPW HAZ	Outside FPW	Advancing side FSW	Retreating side FSW	Inclined angle	Fracture continued within FSW	Fracture continued along advancing side of FSW	Fracture continued along retreating side of FSW	Other fracture propagation
A-FPW-90°-3	31165	*70*	X		X				X					
A-FPW-90°-4	64689	*50*	X		X			X		X			X	
A--FPW-90°-5	499698	*40*	X					X				X		X
A-FPW-90°-6	668234	*35*	X		X				X	X		X	X	
A-FPW-90°-7	1.5E+06	*30*												
A-FPW-90°-8	1.5E+06	*33*												
A-FPW-90°-9	63287	*33*		X	X				X	X				
A-FPW-90°-10	70327	*33*	X						X		X			
B-FPW-90°-1	23170	*100*	X		X*	X*		X		X	X			
B-FPW-90°-2	933	*110*	X		X			X		X	X			
B-FPW-90°-3	13915	*105*	X			X			X	X				
B-FPW-90°-4	7467	*108*	X		X*	X*			X	X				
B-FPW-90°-7	562594	*50*	X			X			X	X		X		
B-FPW-90°-8	10432	*90*					X			X				X
B-FPW-90°-9	29566	*80*	X					X		X	X			
B-FPW-90°-10	109644	*70*					X							X
B-FPW-0°-11	14175	*100*		X		X				X		n/a	n/a	
B-FPW-0°-12	53098	*90*		X						X		n/a	n/a	
B-FPW-0°-13	202233	*80*		X	X					X		n/a	n/a	
B-FPW-0°-14	109871	*70*		X			X					n/a	n/a	
B-FPW-0°-15	158910	*60*		X			X					n/a	n/a	
B-FPW-0°-16	121993	*50*		X								n/a	n/a	

* Crack initiation involved adjacent region

Table 3.4. Angle of fracture path from axial load direction.

Specimen	ϕ_1	ϕ_2	Direction of Crack Growth
A-FPW-90º-4	17º	18º	Retreating side FSW
A- FPW-90º-6	–	14º	Retreating side FSW
A- FPW-90º-9	20º	18º	Retreating side FSW
B-FPW-90º-1	14º	10º	Retreating side FSW
B-FPW-90º-2	15º	14º	Retreating side FSW
B-FPW-90º-3	20º	–	Advancing side FSW
B-FPW-90º-4	27º	25º	Advancing side FSW
B-FPW-90º-5	–	18º	Advancing side FSW
B-FPW-90º-7	25º	16º	Advancing side FSW
B-FPW-90º-8	12º	9º	Advancing side FSW
B-FPW-0º-11	–	18º	Opposite of FSW direction
B-FPW-0º-12	18º	19º	Opposite of FSW direction
B-FPW-0º-13	15º	–	Opposite of FSW direction

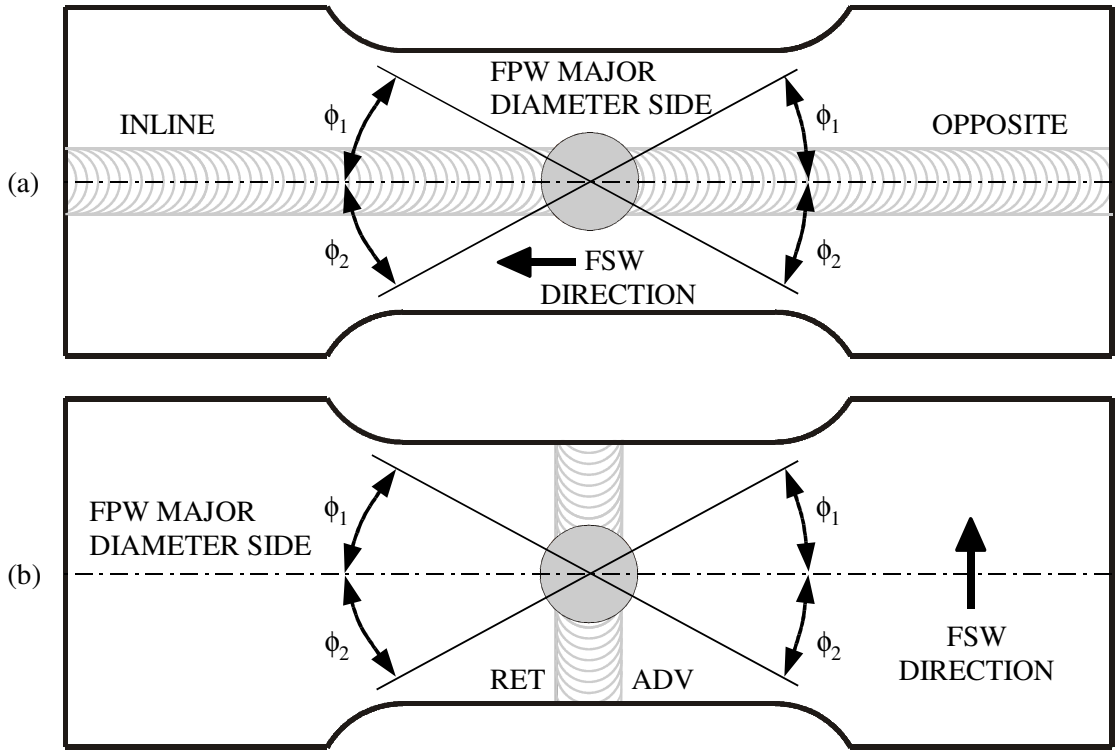

Figure 3.17. Diagram of crack propagation angle ϕ for (a) FPW 0º and (b) FPW 90º specimens

An example of the crack propagation angle for a FPW 90º specimen is shown in Figure 3.18. Some specimens had only one side of the crack grow at an angle to the load axis, with the other side of the crack tending to turn and propagate within the FSW or FSW HAZ region.

It should be noted that specimens B-FPW-90º-8 and B-FPW-90º-10 both had fatigue cracks that originated away from the plug weld at a location near the transitional radius near the grip end of the specimen. The high load amplitude for these specimens was most likely causing the stress concentration effects near the edges of the specimen to become more significant.

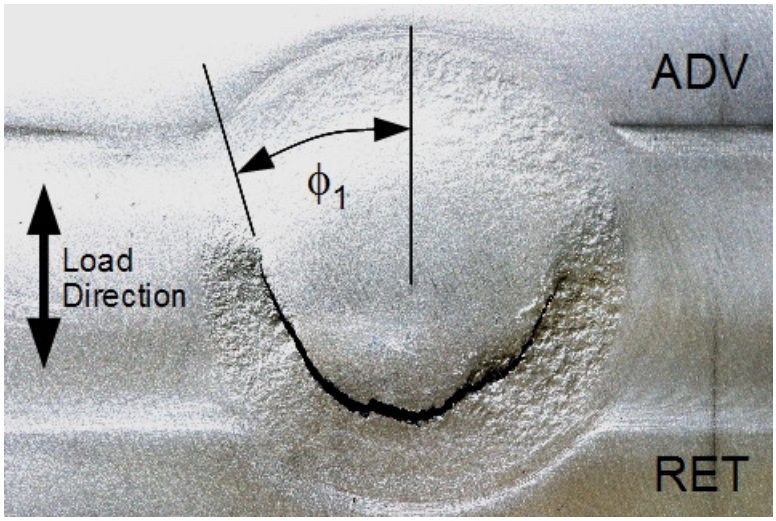

Figure 3.18. Crack propagation angle and plastic strain zone of FPW B 90º specimen.

The Group A 90º specimens had fatigue cracks which initiated within the FPW interface, and the fracture surfaces showed the crack propagation along the plug weld interface. In contrast the Group B 90º specimens tended to have the fatigue crack initiation and propagation occur within the plug HAZ. Specimen B-FPW-90º-1, 2, and 4 showed a mix of initiation and propagation within both the FPW interface and plug HAZ.

DISCUSSION

FSW tensile test

Results from the FSW tensile tests indicate that the FSW process produced a joint with approximately 68% of the UTS of the base metal. The S-N curve for the high cycle regime indicated a reasonable fit of the data to a linear regression line. The presence of weld voids was found to cause a severe reduction in fatigue life for FSW specimens.

Comparison of FSW and FPW Fatigue Properties

The results indicate that FSW specimens that contained a FPW repair exhibit a decrease in ultimate tensile strength and fatigue life. The combined results of the fatigue test of the FSW and FPW specimens, shown in Figure 3.16, reveals the linear regression line for the FPW specimens is moved downward toward the horizontal axis and a reduction in slope from the FSW regression line. This would indicate that the presence of the FPW weld in the specimen results in a shorter fatigue life when compared to specimens that contained only FSW. The decrease in fatigue life is to be expected as the plug weld compromises the existing friction stir weld with a more complex weld interface and HAZ geometry. The magnitude of the decrease is not at a level that would necessarily negate the possibility of using a FPW as a means of repairing FSW defects, but the decrease should be accounted for in design and damage tolerance analysis. When compared to current methods of repair using existing manual TIG welding repair techniques, the friction plug weld repair exhibits higher strength properties [5]. This would indicate that plug welding can be used as a method of repairing keyhole defects and other weld defects without detrimental reduction in the strength and fatigue properties of the structure.

Comparison of the S-N plots for the FPW specimens from Group A with those of Group B would indicate that the plug welding process parameters used to make the Group B test panels resulted in better fatigue properties than the Group A test panels. This would tend to indicate that the strength of the plug weld for Group B plates was higher than that of the Group A plates, and that Group B most likely had fewer defects present in the FPW.

Failure and Fracture Characteristics

The most typical trait noticed amongst the fractured FPW fatigue specimens was the arced shape fracture surface which ranged from quarter-circular to sometimes semi-circular pattern found near the plug weld in the majority of the specimens. This same pattern was also found amongst the FPW tensile specimens. Specimen A-FPW-90º-5 had a unique fracture that originated on the major diameter side of the plug weld adjacent to the advancing side of the friction stir weld. The fracture was unique in that it originated near at the plug weld interface, but the fracture propagated in the FSW HAZ (advancing side) of the base metal along the FSW advancing side in a flat manner without any curvature of the plug weld being evident other than the small amount at the origination point. The fracture surface exhibited evidence of the rolling texture of the base metal in areas away from the crack origin.

Another characteristic found amongst most of the specimens from Group A panels was that the fracture surface showed an angular surface with the plug weld interface clearly defined. Group B specimens did not share this characteristic, but rather had intra-plug HAZ fracture. The only specimens from the Group B plates to display fracture along the FPW interface were specimens B-FPW-90º-2 and B-FPW-90º-8. Specimen B-FPW-90º-2 was tested at higher stress amplitude than specimen B-FPW-90º-8, but the two specimens showed very similar fracture surfaces and fatigue crack growth characteristics.

The other Group B specimens tended to have a fracture surface with a more “fibrous” texture to them with fracture originating in the HAZ of the plug material. The fracture surface tended to be

along the extrusion direction in the thickness dimension of the specimen, while having a curved or arc-shaped path when viewed from the minor or major diameter side of the plug weld.

A notable difference in the location of the fatigue crack initiation site between Group A and B was found. The Group A plates tended to initiate on the major diameter side of the plug at the FPW interface, while the Group B plates tended to have crack initiation within the plug material HAZ on the minor diameter side of the FPW.

Another significant difference between the Group A and Group B FPW 90º specimens was the shape and location of the crack initiation and crack propagation. The Group A FPW specimens all tended to initiate fracture at the FPW interface with the base metal. The fracture propagation tended to be an arced shape following the interface of the plug weld until the plug weld/FSW center-line. The Group B 90º specimens tended to have the fracture initiation in the HAZ of the plug rather than at the plug weld interface. The appearance of the fracture surface showed the extruded texture of the plug material and was not inclined with respect to the specimen's plate surface as was common in the Group A plates. This would seem to indicate that the parameters used to plug weld the Group B plates resulted in higher strength (better weld fusion) as compared with Group A. The fracture path within the plug for Group B specimens appeared to have a more jagged/stepped appearance rather than the smooth appearance of the fracture surface found in Group A. Once the fracture had grown to the FPW interface for Group B specimens, then the fracture tended to propagate along the plug weld interface and/or into the FSW.

The observation of which side of the FSW, either advancing or retreating, where fracture initiated for the FPW-90º specimens is listed in Table 3.3. It can be seen that no clear preferential side for fracture initiation was seen. This is most likely due to the fact that the plug weld is mainly in contact with the base metal at the point of fracture initiation. The microhardness results indicated no distinctive difference in hardness between the advancing or retreating side at these locations of the plug weld [13].

The orientation of the FSW with respect to the load axis may be significant. Comparison of the 0º and 90º specimens from Group B would indicate that the direction of FSW with respect to the loading axis when tested at lower stress amplitudes may result in the FSW being the most likely crack initiation site for specimens with the FSW parallel to the load axis. The 0º specimens tested at lower stress amplitudes had fractures initiate in the FSW instead of the plug weld in those particular specimens. This may be due to plastic strain effects not being the significant cause of fracture initiation, but rather notch and other weld effects playing the more significant role in causing cracks to form.

Another distinguishing feature found in the Group B specimens was the mottled appearance of an annular area encircling the interface part of the plug weld, including the plug HAZ. This mottled appearing area occurred on both the major and minor diameter sides of the plug weld. Figure 3.18 shows the plastic straining typical of Group B specimens. This was likely due to transverse plastic straining taking place within the weld interface and HAZ regions. These areas were found to have lower hardness when compared to base metal and plug material [11, 13] and

would likely have yielded in these areas. The specimens that exhibited this ringed area were all tested at stress amplitudes toward the high end of the range used in fatigue testing, which would induce plastic straining in the transverse direction.

CONCLUSION

The tensile strength and the mid-to-high cycle fatigue behavior of FSW 2195-T8 and FPW 2195-T8 were determined. It was found that the FSW process resulted in an under-matched joint with 68% of the strength of the base metal. The FPW process reduced the strength of the joint further to 57% of the base metal strength. The S-N data plots of the FPW were compared with those of FSW and were found to have similar linear regression lines. However, there is more randomness (data scatter) associated with the FPW fatigue data, when compared to the FSW fatigue data. Both FSW and FPW weld processes were found to be sensitive to weld defects, which resulted in shortened fatigue lives when defects were present. The FPW process does show improvement in both strength and fatigue life when compared to the manual TIG repair process. The load direction and stress amplitude may be significant factors for the location of crack initiation. Higher stress amplitudes tended to show plastic straining effects near the plug weld, while load direction influenced whether the crack initiated at the plug weld or at a location outside of the influence of the plug weld.

REFERENCES

[1] P. Hartley, Friction Plug Weld Repair for the Space Shuttle External Tank, NASA Document ID 20000093962, Johnson Space Center, Marshall Space Flight Center, 2000.

[2] T. Dickerson and J. Przydatek, Fatigue of Friction Stir Welds in Aluminum Alloys that Contain Root Flaws, Int J Fatigue, 25 (2003) 1399-1409.

[3] T. Khaled, An Outsider Looks at Friction Stir Welding, Federal Aviation Administration Report ANM-112N-05-06, 2005, 14-15.

[4] D. Wells, 2008. NASA MSFC, Damage Tolerance Group (EM20), Personal communication.

[5] R. Hafley, J. Wagner, M. Domack, Fatigue Crack Growth Rate Test Results for Al-Li 2195 Parent Metal, Variable Polarity Plasma Arc Welds and Friction Stir Welds, NASA TM-2000-210098, 2000.

[6] P. Mendez, T. W. Eagar, New trends in Welding in the Aeronautic Industry, 2nd Conference on New Manufacturing Trends, Bilbao, Spain, November 2002.

[7] S. Williams, Welding of Airframes using Friction Stir, Air & Space Europe, 3/4 (2000) 64-66.

[8] P.M.G.P. Moriera, A.M.P. de Jesus, M.A.V. de Figueiredo, M. Windich, G. Sinnema, P.M.S.T de Castro, Fatigue Crack Growth behavior of Friction Stir Welded Aluminum-Lithium Alloy 2195, XXVII Meeting of the Grupo Español de Fractura and 12th Portuguese Conference on Fracture, Porto, Portugal, 17-19 March 2010.

[9] R. Nandan, T. DebRoy, H. K. D. H. Bhadeshia, Recent Advances in Friction-Stir Welding – Process, Weldment Structure and Properties, Prog in Mater Science 53 (2008) 980-1023.

[10] E. Colleta, M. A. Cantrell, Frictions Pull Plug Welding: Chamfered Heat Sink Pull Plug Design, U.S. Patent No. US 6880743 B1, 2005.

[11] Z. Li, M. A. Cantrell, R. J. Brown, Process Development and Microstructural Characterization of Friction Plug Welded 2195 and 2219 Alloys. AeroMat 2000 Conference, Seattle, WA, USA, June 2000.

[12] E. Colletta, M. A. Cantrell, Friction Plug Weld Repair Geometric Innovations. Marshall Space Flight Center. NASA Document ID: 20000112928, (2000).

[13] D. Metz, E. R. Weishaupt, B. S. Fairbee, M. E. Barkey, A Microstructure and Microhardness Characterization of a Friction Plug Weld in Friction Stir Welded 2195 Al-Li, ASME J Eng Mater and Tech, In press, [DOI: 10.1115/1.4006066].

[14] R. Crooks, Z. Wang, V. I. Levit, R. N. Shenoy, 1998. Microtexture, Microstructure and Plastic Anisotropy of AA2195, Mater Sci and Eng A257 (1998) 145-152.

[15] Z. Wang and R. N. Shenoy, Microstructural Characterization of Aluminum-Lithium Alloys 1460 and 2195, NASA CR-1998-206914, 1998.

[16] P. Subramanian, N. Nirmalan, L. Young, P. Sudkamp, D. Mika, M. Larsen, M. Othon, P. Dupree, S. Walker, G. Catlin, Fundamental Studies of Microstructure Evolution during Stir Welding of Aluminum Alloys, AFRL Final Technical Report No. AFRL-SR-AR-TR-03-0423, 2003.

[17] Z. Li, W. J. Arbegast, P. J. Hartley, and E. I. Meletis. Microstructural Characterization and Stress Corrosion Evaluation of Friction Stir Welded Al 2195 and Al 2219 Alloys, Proceedings of the 5th International Conference on Trends in Welding Research, Stone Mountain, GA, USA, June 1998.

[18] M. Chaturvedi and D. L. Chen, Effect of Specimen Orientation and Welding on the Fracture and Fatigue Properties of 2195 Al-Li Alloy, Mater Sci and Eng A 387-389 (2004) 465-469.

[19] D. Chen and M. C. Chaturvedi, 2000. Near-Threshold Fatigue Crack Growth Behavior of 2195 Aluminum Lithium Alloy Prediction of Crack Propagation Direction and Influence of Stress Ratio, Metall Mater Trans 31A (2000) 1531-1541.

[20] P. Chen, A. Kuruville, T. Malone, and W. P. Stanton. 1998. The Effects of Artificial Aging on the Microstructure and Fracture Toughness of Al-Cu-Li Alloy 2195. J Mater Eng and Perform 7(5)682-690.

[21] J. Schijve, Fatigue of Structures and Materials, second ed., Springer, 2009.

CHAPTER 4

FATIGUE CRACK GROWTH CHARACTERIZATION OF FRICTION PLUG WELDS IN 2195 AL-LI ALLOY

INTRODUCTION

The aluminum-lithium alloy 2195-T8 has been proven successful in pressure vessel applications in the aerospace field, as demonstrated in NASA's super light weight tank (SLWT) program for the space shuttle. This alloy's low density, high tensile strength, cryogenic fracture toughness are some of its material properties which make it ideal for use in pressure vessel applications. Also, included amongst the material's beneficial properties is the materials weldability. The alloy 2195-T8 has been successfully welded using the friction stir welding (FSW) and variable polarity plasma arc welding (VPPA) processes.

The fabrication and manufacturing procedures used in future aerospace cryogenic pressure vessel programs will most likely rely on friction stir welding for the majority of the large pressure vessel structure joining process [1]. A desirable characteristic for any weld process is the minimization of defects. As with any joining process, a satisfactory method of repairing any weld defects needs to be identified and optimized. It is desired that the repair method should have minimal affect on the surrounding weld and base metal.

A method of repair for FSW that has shown promising results is identified as friction plug welding. This repair process involves removing the defect by drilling a machined hole at the defect location. Next, the hole is filled by simultaneously spinning and pulling a tapered plug into the machined hole creating a friction weld at the interface. The excess plug material is then removed by machining away excess plug material followed by a final manual grinding of the friction plug weld to blend the repair with the surrounding friction stir weld and base metal. The plug weld repair is then inspected by use of non-destructive dye penetrant and phased array ultra-sound techniques to insure that no flaws larger than the minimum detectable size are present in the friction plug weld repair.

The completed plug weld results in a cross-sectional area as shown in Figure 4.1. The plug weld interface line is inclined with relationship to the surface of the base metal plates. A narrow heat affected zone (HAZ) is found on both sides of the friction plug weld interface. Figure 4.2 shows the different interfaces with base metal and FSW zones which encompass the friction plug weld repair. For more detailed information on the FPW process, the reader may refer to the following references [2-4].

The designers and engineers involved with aerospace type cryogenic pressure vessel design have an interest in the prediction of safe life and damage tolerance of a pressure vessel to determine if a flaw of a known size and location could lead to a failure of the pressure vessel. The nature of the fatigue life of pressure vessels in service may tend to be of the low-cycle type with a limited number of load cycle reversals. The fatigue crack growth rate of the welded material and base

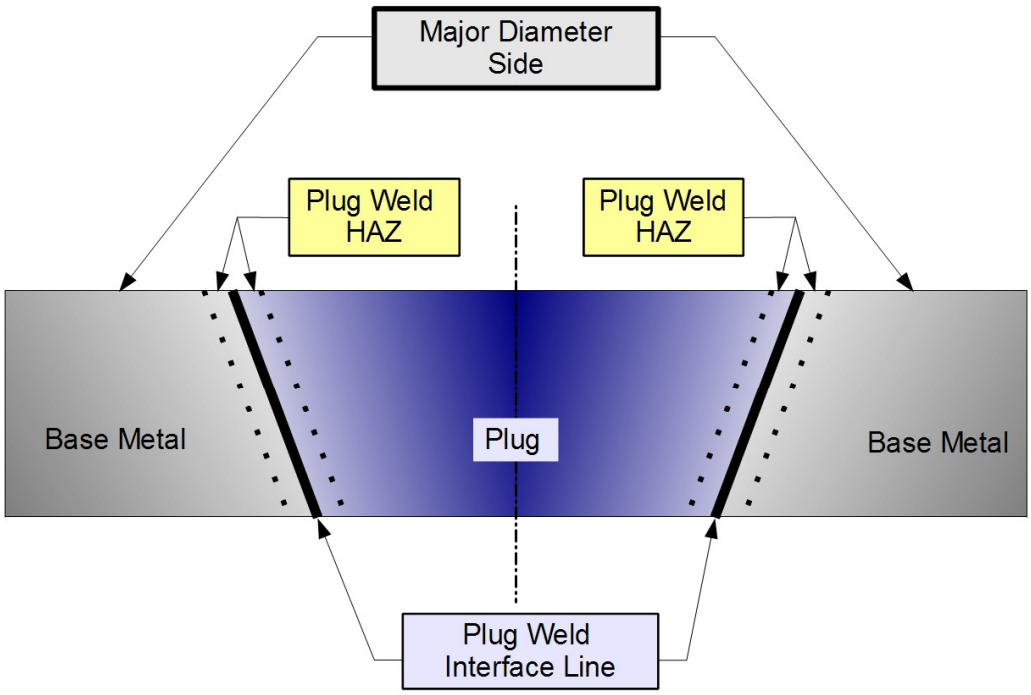

Figure 4.1. Cross-sectional view of FPW.

material must be identified to accurately calculate the safe life and maintain satisfactory safety margins for the pressure vessel design. Pressure vessel designers are usually required to have a leak before burst constraint on the pressure vessel design, which requires knowledge of the welds strength, fracture toughness, and fatigue crack growth rate of the different zones contained within the repair region.

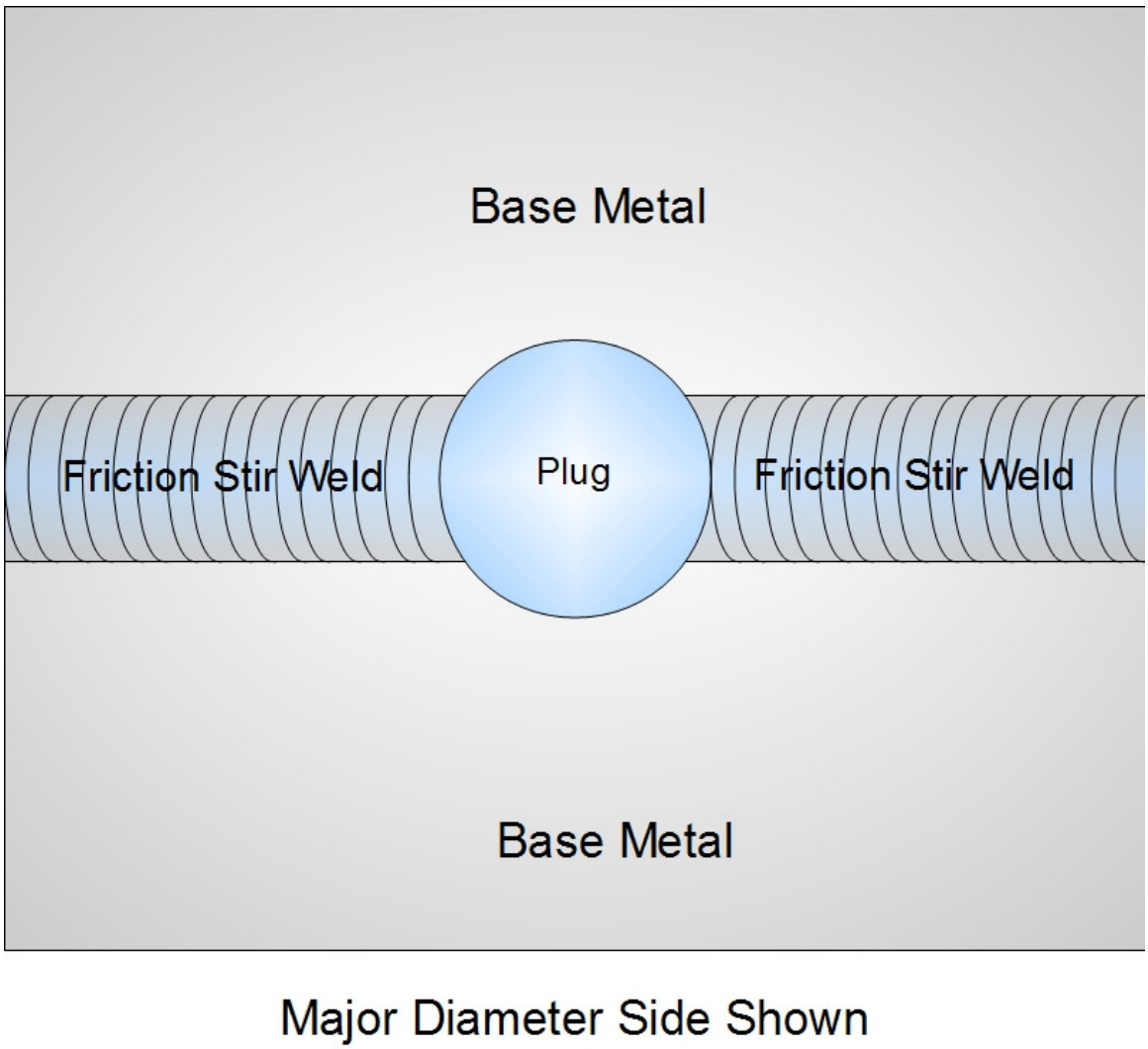

Figure 4.2. Friction plug weld repair in friction stir weld

In the case of single use pressure vessels, the main interest in fracture behavior is often limited to understanding the extent of growth an existing crack may have under high stress, low-cycle conditions. This is in contrast to applications of reusable pressure vessels where the crack growth may span over several repeated mission cycles at various number of load cycles. It is important to characterize the crack growth under load conditions that may well exceed design stresses in an effort to insure proper safety margins are maintained for safe operation. This data would also prove useful to limit the number of missions on a particular vessel to a safety factor, while allowing designers to optimize the weight while maintaining the pressure vessels design safety requirements.

Fatigue crack growth behavior for both 2195-T8 and FSW 2195-T8 has been studied and results published in the literature [6-10]. However, little data been published with regards to the fatigue crack growth rate (FCGR) properties of FSW 2195-T8 plate that has been repaired using the FPW process. Fatigue crack growth data for FSW 2195-T8 containing a friction plug weld would be of interest to design engineer for prediction and evaluation of damage tolerance for structures using this repair process. The focus of this paper is to characterize the observed crack growth of a friction plug weld repair as a representative part of an aerospace pressure vessel under high cyclic load conditions.

As can be seen in Figure 4.1, the cross section of the plug weld would result in difficulty if a standard compact tension C(T) style specimen was used in determining the fatigue crack growth rate for a plug weld. The taper angle of the plug results in a weld fusion line that is inclined with respect to the face of the specimen. Also, the direction of crack growth through the thickness

direction prohibits the use of a C(T) specimen, since the crack depth would not be observable with optical methods. The use of a center cracked tension CC(T) type specimen would permit observation of the crack front; however the crack growth path would likely be different than that found in the actual structure. The observed fatigue cracks in friction plug welds tend to grow in a three-dimensional curved path along the plug weld interface or within the HAZ within the plug material [11].

In the absence of an ASTM accepted test method for the crack growth of a friction plug weld, some means of verifying the growth of crack form a flaw would be needed to reduce the uncertainty involved with using the existing crack growth rate data for the 2195-T8 base metal or friction stir welded 2195-T8 for the estimation of the damage tolerance parameters of the friction plug weld repair. There is a need to test the fatigue crack growth in the actual representative structure in order to estimate the crack growth rate while under actual pressure vessel's representative loading conditions.

In this study fatigue specimens were cyclic loaded to induce a fatigue crack, and then the fatigue specimen was instrumented with a clip gage to measure the crack mouth opening displacement (COD) during remainder of the fatigue test. Note Visual observations of the crack surface geometry were made and recorded during the test procedure for each test specimen. A representative finite element model was created for each specimen's observed changes in crack geometry during the fatigue test. The finite element model was also used to numerically determine the values of COD and stress intensity, K, for each of the specimen's various crack geometries.

The calculated COD determined from the finite element model was compared with the experimental COD, and from this comparison an estimate of the actual crack depth for the specimen was determined. The plot of experimental COD vs. load cycle number was used to determine the number of cycles required to grow the crack from a specific crack depth to the next incremental crack depth. This modeling process for crack depth was used since the crack depth of the specimen was not directly observable during the test procedure [12-13].

The K values calculated from the finite element model were used with a Paris Law for crack growth to determine a relationship between an initial flaw size versus number of life cycles. The combination of finite element modeling and calculation of cycles of crack growth using the Paris Law was used as an indirect method determining the crack depth vs. fatigue cycle.

EXPERIMENTAL PROCEDURE

Overview

The experimental method used in this paper's study was to test a representative part of a pressure vessel structure at high load levels and observe if the crack growth rates of the specimens containing a friction plug weld were characterized by the published crack growth rates for FSW 2195-T8 determined by other researchers. If there was an observed variation, or trend that varied from these published values, then characterize it accordingly.

Material and specimen design

Material strength testing was performed in the accompanying fatigue study [11] to establish baseline ultimate tensile strength (UTS) transverse to the rolling direction for the base metal 2195-T8 Al-Li alloy. The UTS was also determined for the same alloy that had undergone a friction stir welding process, and the UTS determined for a friction stir plug welded specimen consisting of a friction plug weld inserted into a friction stir weld. The properties from the accompanying fatigue study were used to establish the load schedule, and also for use in the material properties of the finite element model of the friction plug weld.

The specimen design and dimension are shown in Figure 4.3. The specimens were cut from friction stir welded plates that contained friction plug welds that were provided by the Materials and Processes Laboratory's Metals Engineering Division, EM30, of NASA's Marshall Space Flight Center. All test plates were made from 6.35 mm thick 2195-T8 Al-Li sheet material. The test plate dimensions were 305 mm x 610 mm. The test plates were all manufactured with process parameters that had been optimized for a spindle speed of 4250 RPM. The spindle speed refers to the rotational speed at which the plug is rotated during the FPW process. The plug used in the manufacture of the welded plates were a M-3 Revision A style plug with a shank diameter of 19.1 mm, and the FSW process parameters were consistent amongst the plates. All test plates were finish ground and had NDE inspection performed by NASA at Marshall Space Flight Center.

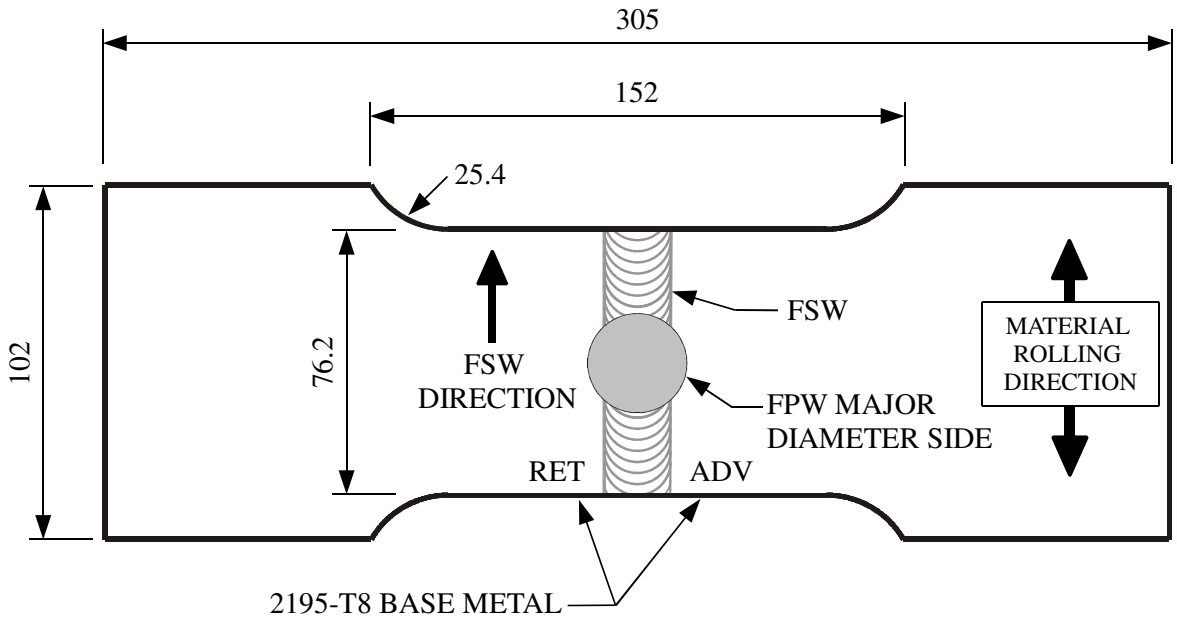

Figure 4.3. FPW specimen design

Fatigue Crack Growth Testing

A total of six specimens containing a friction plug weld were prepared for fatigue crack growth testing. The FCG specimens were all tested using cyclic, sine wave loading with a R-ratio of 0.1 in a SATEC 245 kN test frame with a MTS 407 controller. The fatigue crack growth tests were all conducted with constant load amplitude and under room temperature conditions. A cyclic load frequency of 5 Hz was used for the fatigue crack initiation phase of the testing. The load frequency was reduced to 1 Hz during the data collection phase of the fatigue crack growth test. The clip gage used for measuring crack opening displacement was a MTS model no. 632.02b-20, with an opening of 3.8 mm to 7.6 mm. The clip gage had a calibrated range of 2.5 mm, and was calibrated through the use of a bench micrometer prior to the test procedure. The crack mouth

opening displacement was recorded using LabVIEW 6.2 for data acquisition. The clip gage mounting is shown schematically in Figure 4.4. An image of a specimen with the clip gage mounted during the fatigue testing is shown in Figure 4.5 where a fatigue crack located at the plug weld is visible

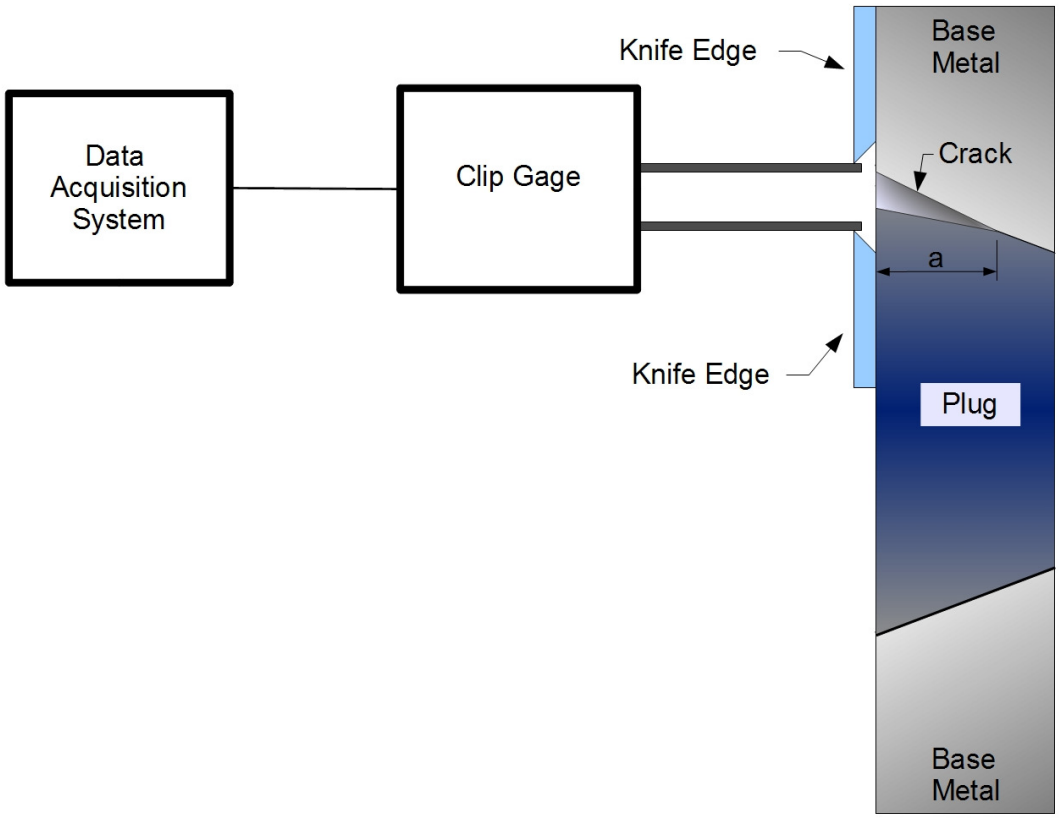

.

Figure 4.4. Schematic of Clip Gage Attachment

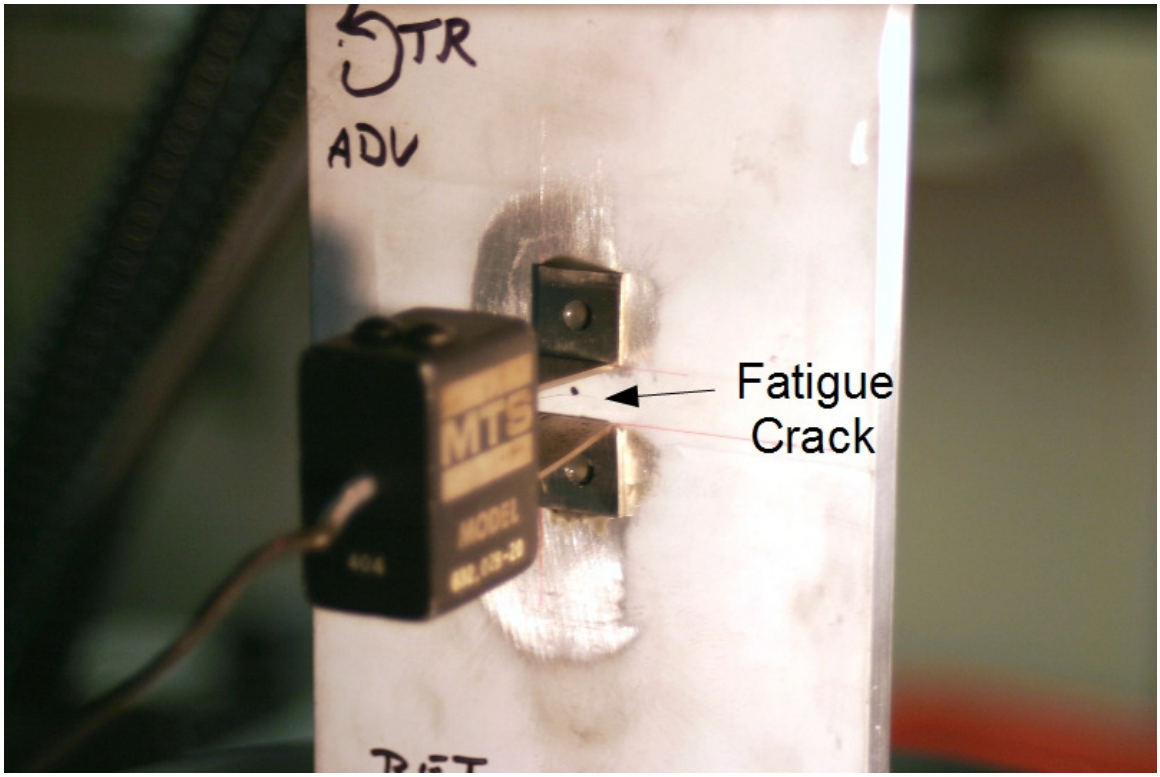

Figure 4.5. FPW specimen during fatigue test with clip gage mounted.

Fatigue starter crack initiation and clip gage mounting

Two methods of fatigue crack initiation and clip gage knife edge mounting were used in this study. The first method was to machine a small, v-shaped, crack starter notch into the specimen on the major diameter side of the plug weld to initiate a fatigue crack at the fusion line of the plug weld. In addition, two holes were drilled and tapped (4-40 UNC) in the specimen near the starter notch for the purpose of mounting the clip gage. The crack starter notch dimensions for test specimens which used this method are listed in Table 4.1. These specimens, however, failed to provide useful data due to fatigue cracks which initiated at the location of the tapped holes used for mounting the clip gage knife edges.

Table 4.1. Fatigue specimen starter notch dimensions.

Specimen	Notch length (mm)	Notch width (mm)	Notch depth (mm)
B-FPW-90º-5	3.8	0.76	0.19
B-FPW-90º-6	8.1	1.14	0.51

Subsequently, the method of initiating a fatigue crack in the specimen was then changed to cyclically loading the specimen to induce a small fatigue crack into the test specimen without the use of a starter notch. The specimen was visually examined during this procedure for the presence of a fatigue crack near the friction plug weld. Upon detection of a fatigue crack, the specimen was removed from the test machine, and the clip gage knife edges were bonded to the specimens using 3M Scotch-Weld DP190 Epoxy Adhesive. The spacing of the knife edges was 7.6 mm. The specimen was then remounted in the testing machine, the clip gage instrumentation installed, and cyclic loading resumed at a reduced frequency of 1 Hz. The clip gage opening data was recorded and synchronized with the load cycle count.

The change in knife edge mounting method was done to alleviate the tendency for the tapped holes to create a failure which did not originate within the friction plug weld. The stress amplitude used for fatigue crack growth testing, clip gage mounting method, and whether data collection was successful for the specimen are listed in Table 4.2.

Table 4.2. Fatigue crack growth specimen data

Specimen	Stress amplitude (MPa)	Total No. of cycles	Fatigue crack starter notched	Knife edge mounting	Successful data collection
B-FPW-90º-5	72	53200	Yes	Tapped hole	No
B-FPW-90º-6	72	82867	Yes	Tapped hole	No
B-FPW-90º-7	100	562594†	No	Bonded	Yes
B-FPW-90º-8	129	10432	No	Bonded	Yes
B-FPW-90º-9	115	29566	No	*	No
B-FPW-90º-10	100	109644	No	*	No

† Fatigue pre-cracked at stress amplitude of 72 MPa for 454500 cycles

* Specimen failed near grip end of specimen

FINITE ELEMENT MODEL OF CRACK GROWTH

Unlike a C(T) type specimen typically used for crack growth measurement, the design of the plug weld fatigue specimens did not allow for any direct means of observation or measurement of the crack depth during the test procedure. A correlation was required that would allow the collected COD data obtained from the clip gage to be indirectly related to the crack depth, *a*. Visual observation of the specimen surface during the test procedure, however, did allow for

recording the manner in which the surface crack length propagated along the major diameter side of the FPW specimens. The fatigue cracks observed in the specimens tested tended to propagate in a semi-circular manner during the test process, and this angle was measured from the center-line of the specimen and recorded during the test procedure. The angles measured for the surface crack were denoted as θ_1 and θ_2 as shown in Figure 4.6.

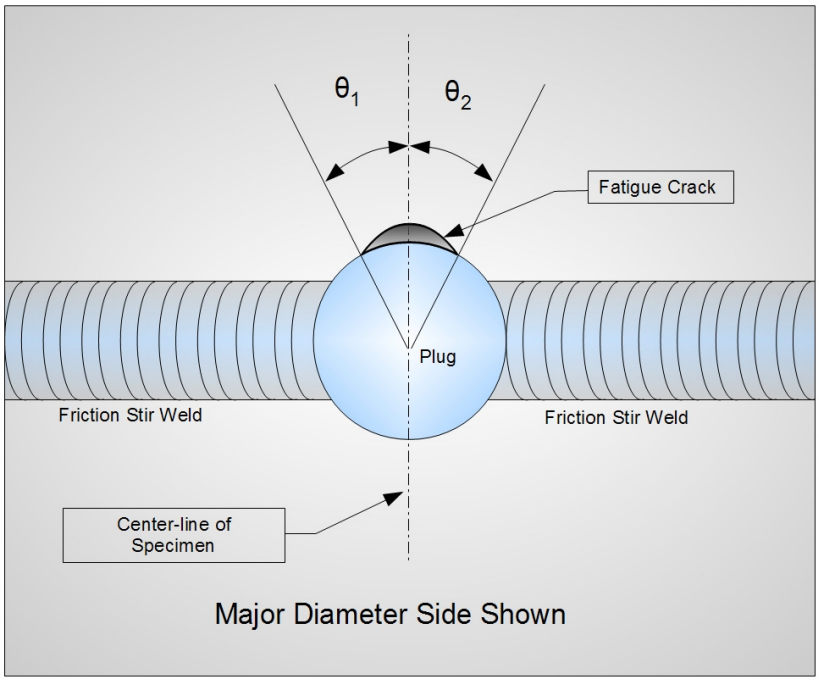

Figure 4.6. Crack angle for FPW fatigue crack.

The finite element software FEACrack version 3.2.012 [14] was used to create a mesh of the plug weld which contained a sharp, semi-elliptical crack with a curved crack front. FEACrack software contains special geometry based input from a graphical user interface to create a finite element model with the crack having a fine mesh. The FEACrack software allows the user to utilize meshing controls for defining the node spacing and mesh density along the crack front. A typical mesh used to model a friction plug weld containing a fatigue crack is shown in Figures

4.7 through 4.9. The finite element model used for the finite element model of the friction plug weld specimen utilized 20 node brick elements. The finite element model of the plug weld was used to simulate the fatigue crack growth of the specimens under cyclic loading. The parameters of crack depth and angle were varied to simulate the fatigue crack growth of the FPW specimen.

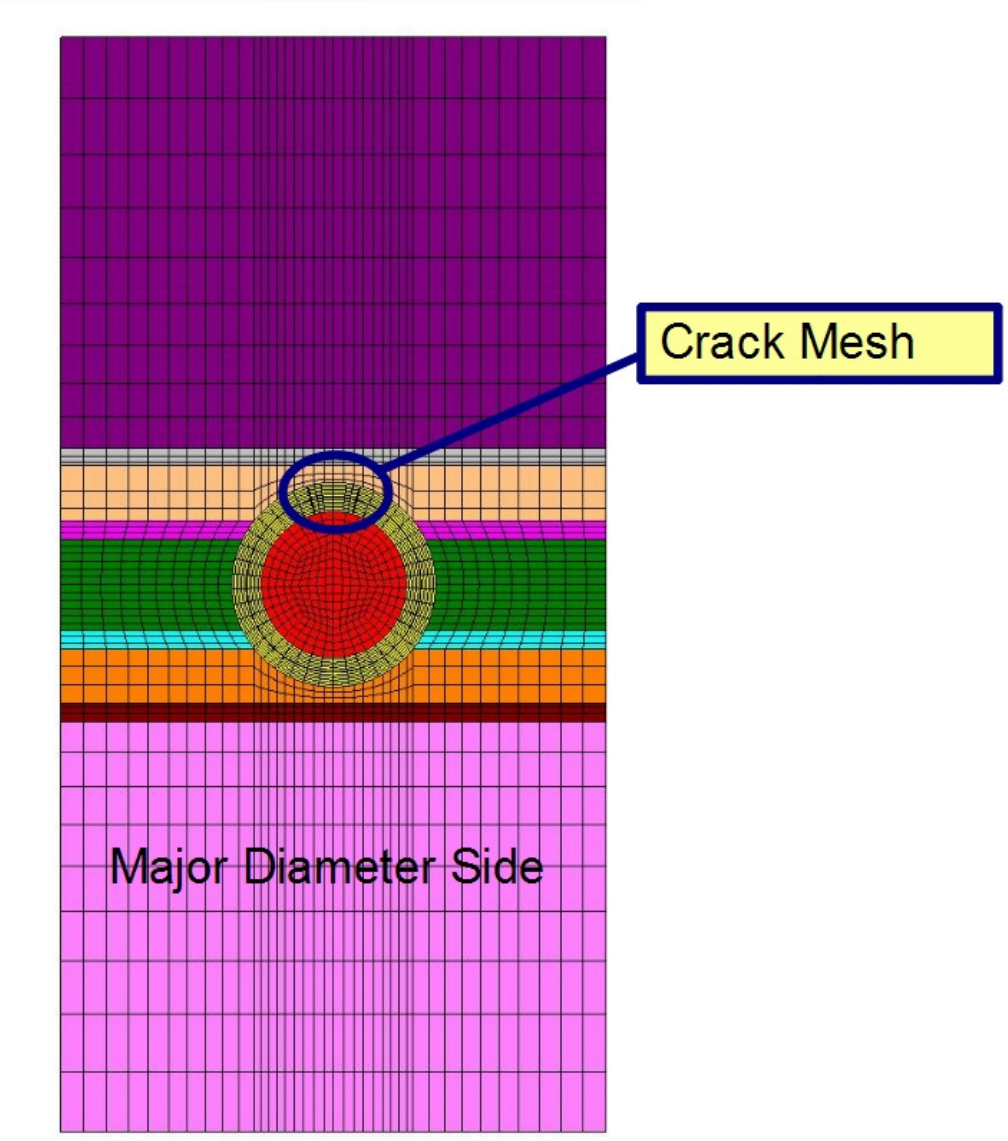

Figure 4.7. Finite element model mesh of FPW fatigue specimen.

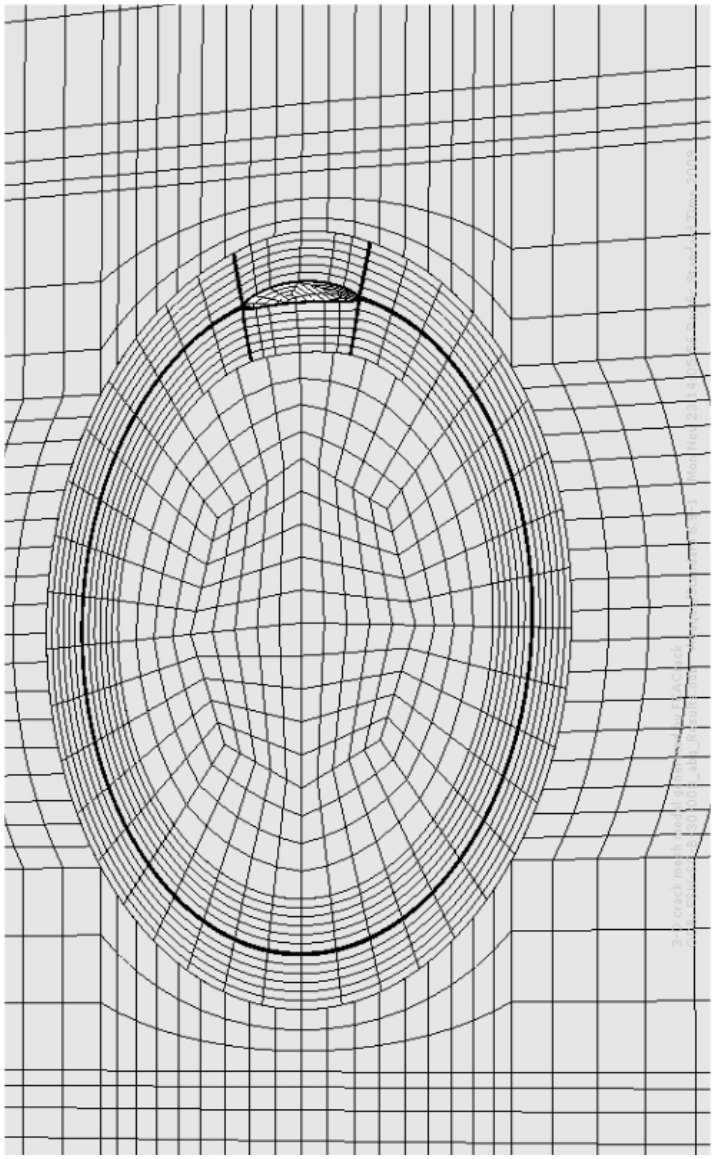

Figure 4.8. Mesh of FPW with crack. (Note: crack opening exaggerated)

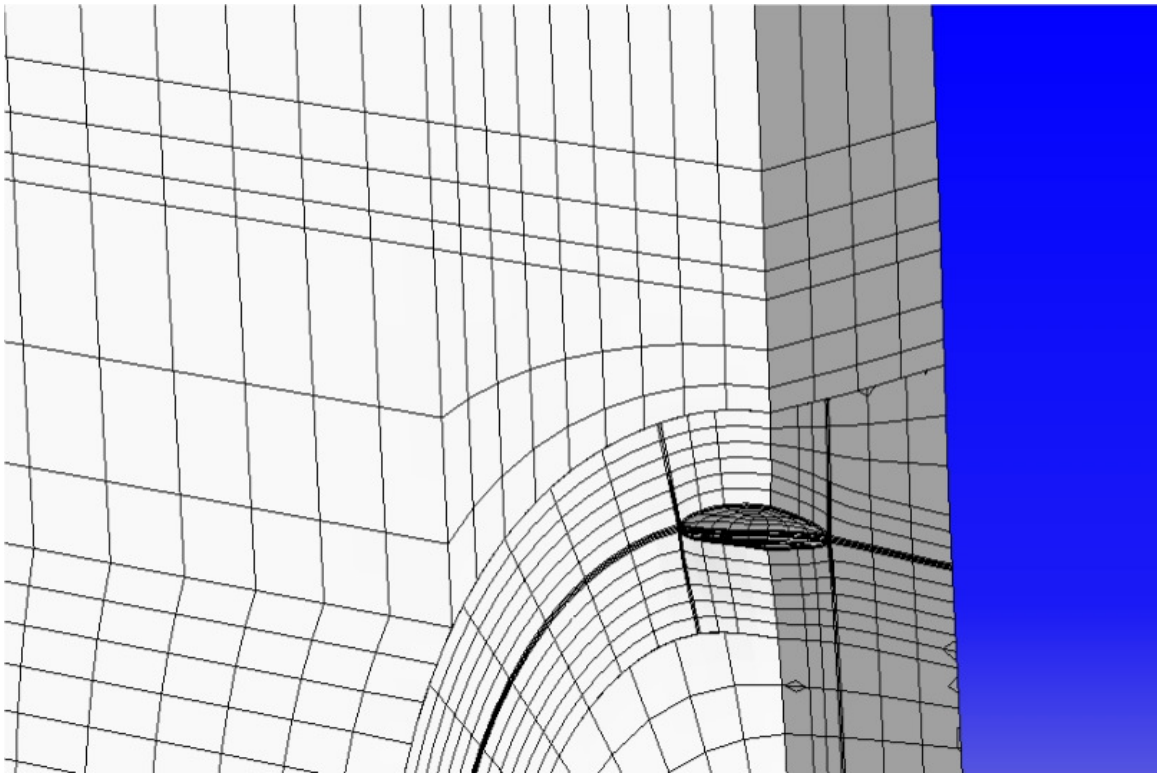

Figure 4.9. Cutaway view of FPW crack mesh.

The FEACrack software first determines the J integral values at the nodes along the crack front, and reports the K values by the relationship [15]

$$K = \sqrt{\frac{JE}{1-\nu^2}} \tag{1}$$

The crack mouth opening displacement was also determined from the finite element model for each set of crack dimensions listed in Table 4.3 and 4.4. The calculated crack opening from FEACrack was then compared with the experimental crack opening data obtained from the test specimens, and this correlation between numerical and experimental COD values allowed for estimation of the crack depth in the specimen for a given experimental COD.

Table 4.3. FEACrack growth model for B-FPW-90º-7.

θ_1 (deg)	θ_2 (deg)	Crack depth, a (mm)	Crack opening (mm)
13	52	0.20	0.00254
20	55	0.51	0.00686
25	55	1.02	0.01194
40	55	1.52	0.0229
55	55	2.03	0.0323
55	55	2.54	0.0442
55	55	3.05	0.0531
60	60	3.56	0.0653
60	60	4.06	0.0739
60	60	4.57	0.0795
60	60	5.08	0.0831
60	60	5.33	0.0844
60	60	5.59	0.0881
60	60	5.84	0.0892
65	65	6.10	0.0942
70	70	6.10	0.0978
80	80	6.10	0.1050

Table 4.4. FEACrack growth model for B-FPW-90º-8.

θ_1 (deg)	θ_2 (deg)	Crack depth, a (mm)	Crack opening (mm)
33	-3	0.20	0.002
35	0	0.51	0.008
40	10	1.02	0.015
40	20	1.52	0.028
40	30	2.03	0.038
40	40	2.54	0.051
40	50	3.05	0.066
40	60	3.56	0.076
45	65	4.06	0.094
50	70	4.57	0.109
50	70	5.08	0.117
50	70	5.33	0.122
50	70	5.59	0.124
50	70	5.84	0.129
50	70	6.10	0.135

The finite element model used to approximate the crack growth for specimen B-FPW-90º-7 was modeled as a curved, semi-elliptical crack growing within the HAZ region in the extruded plug material. The initial flaw size was assumed for the FEA model was for an arc shaped circular flaw originating in the plug weld HAZ within the M3 plug. The starting crack was 0.20 mm in depth, and angles of θ_1 and θ_2 was 13° and 52° respectively.

An estimation of the number of cycles to grow the crack from a given depth a_i to the final depth a_f was determined using the Paris law in a spread sheet calculation. The Paris law for crack growth is given as

$$\frac{da}{dN} = C\Delta K^m \tag{2}$$

where

$$\Delta K = \Delta S\sqrt{\pi a} \tag{3}$$

If the crack growth is such that a Paris relationship is valid, then the number of cycles to grow a crack from an initial crack depth to a final crack depth can be determined using the following equation [16]

$$N = \frac{1}{(C\Delta S\sqrt{\pi})^m}\int_{a_0}^{a_f}\frac{da}{a^{m/2}} = \frac{1}{(C\Delta S\sqrt{\pi})^m} * \frac{1}{(m/2-1)}\left[\frac{1}{a_0^{m/2-1}} - \frac{1}{a_f^{m/2-1}}\right] \tag{4}$$

A flow chart outline of the process is given in Figure 4.10. The values of the constants c and m used for the Paris law crack growth are listed in Table 4.5. The values from the crack growth rate measured for friction stir welded 2195-T8 by Subramanian, et al. are shown for reference [6]. Their work showed that the crack growth rate differed depending on the location within the weld stir zone, HAZ, and base metal.

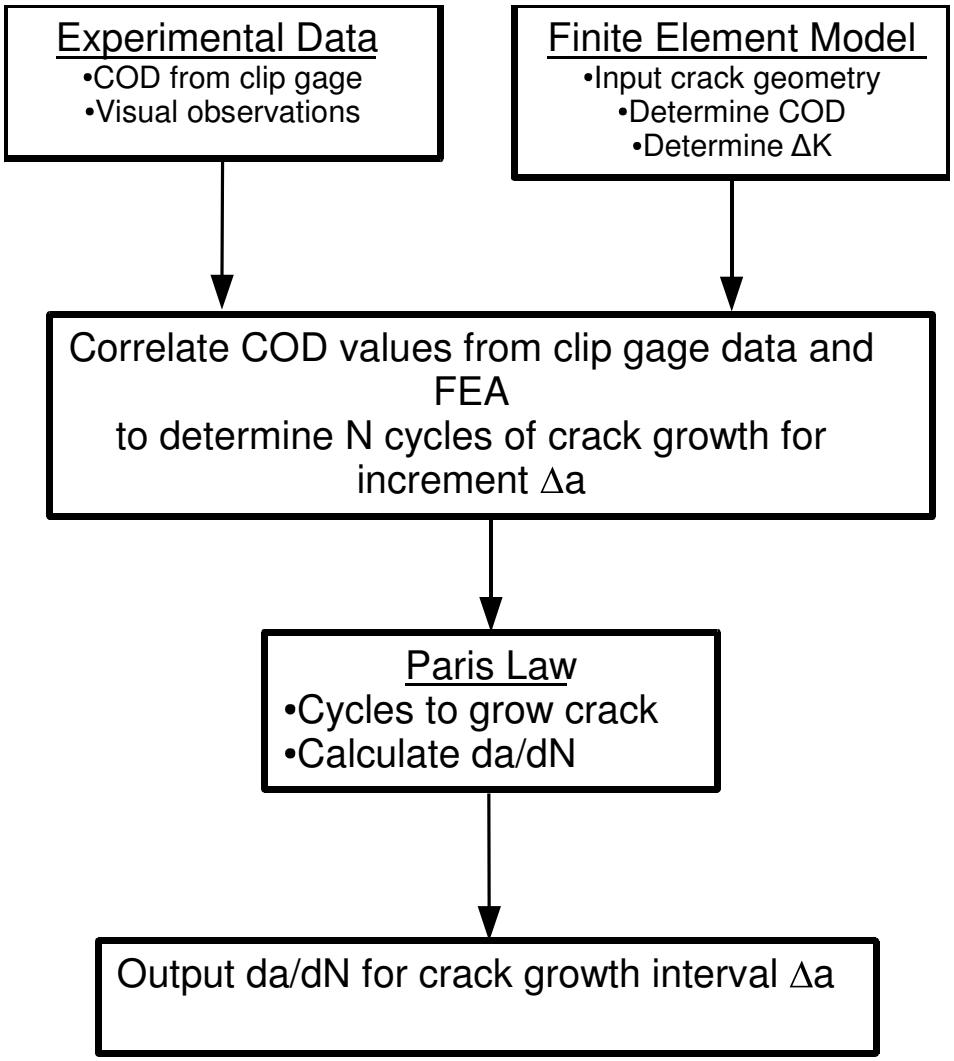

Figure 4.10. Flow chart of numerical crack growth process.

Table 4.5. Paris law parameters for FPW 2195-T8.

Zone	C	m
B-FPW-90°-7	5.86E-8	3.64
B-FPW-90°-8	1.08E-7	3.63
FSW 2195-T8 from C(T) test *		
Base	3.46E-9	4.06
HAZ	1.80E-08	3.64
FSW	3.61E-08	3.62

Note: constants are for (mm/cycle)

* see ref [6]

RESULTS

Fatigue Crack Growth

The specimens B-FPW-90°-7 and B-FPW-90°-8 were the specimens for which the crack opening displacement was successfully recorded. The crack opening displacement versus data cycle is shown for the specimens B-FPW-90°-7 and -8 in Figures 4.11 and 4.12 respectively.

The specimen B-FPW-90º-7 was cyclically loaded without a starter notch at a stress amplitude of 72 MPa, which is 50% of UTS for FPW 2195-T8. A small fatigue crack was observed near the upper left of the major diameter side of the plug weld at 454500 cycles. This crack originated within the HAZ of the plug material. The specimen was removed from the test machine and the knife edges were then adhered to the specimen and the clip gage mounted. The specimen was them remounted in the grips of the test machine and cyclic loading was resumed, but with an increased load level of 100 MPa. The specimen was monitored during the testing, and the progress of the crack noted. Data from the clip gage recording was started at a cycle count of 559713 at which time the crack opening displacement had become greater than 0.005 mm. Crack opening displacement data was then recorded till the removal of the clip gage shortly before the specimen fractured. The crack exhibited breakthrough to the minor diameter side of the friction plug weld specimen at 561579 cycles. The specimen failed at 562594 cycles. The total number of cycles from first observation of the crack until final fracture was 108094 cycles. The number of cycles from recorded crack mouth opening displacement till fracture was 2881 cycles.

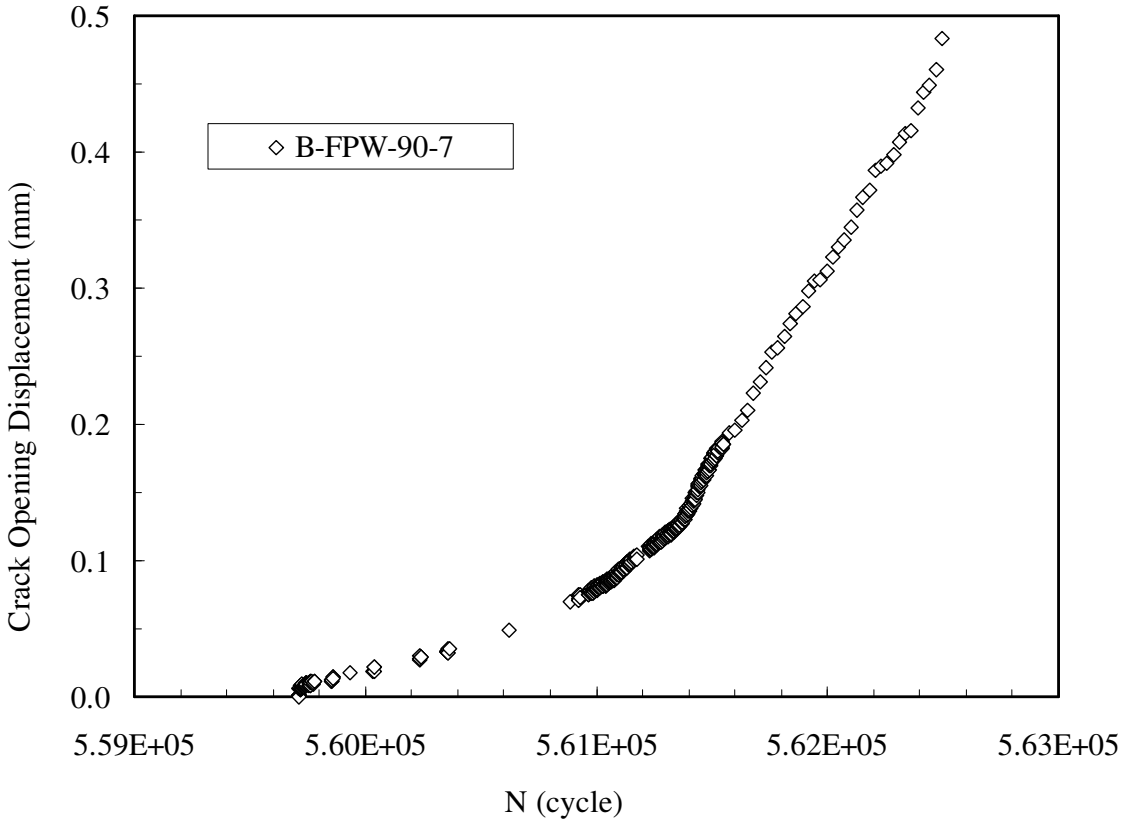

Figure 4.11. Crack opening displacement for B-FPW-90°-7.

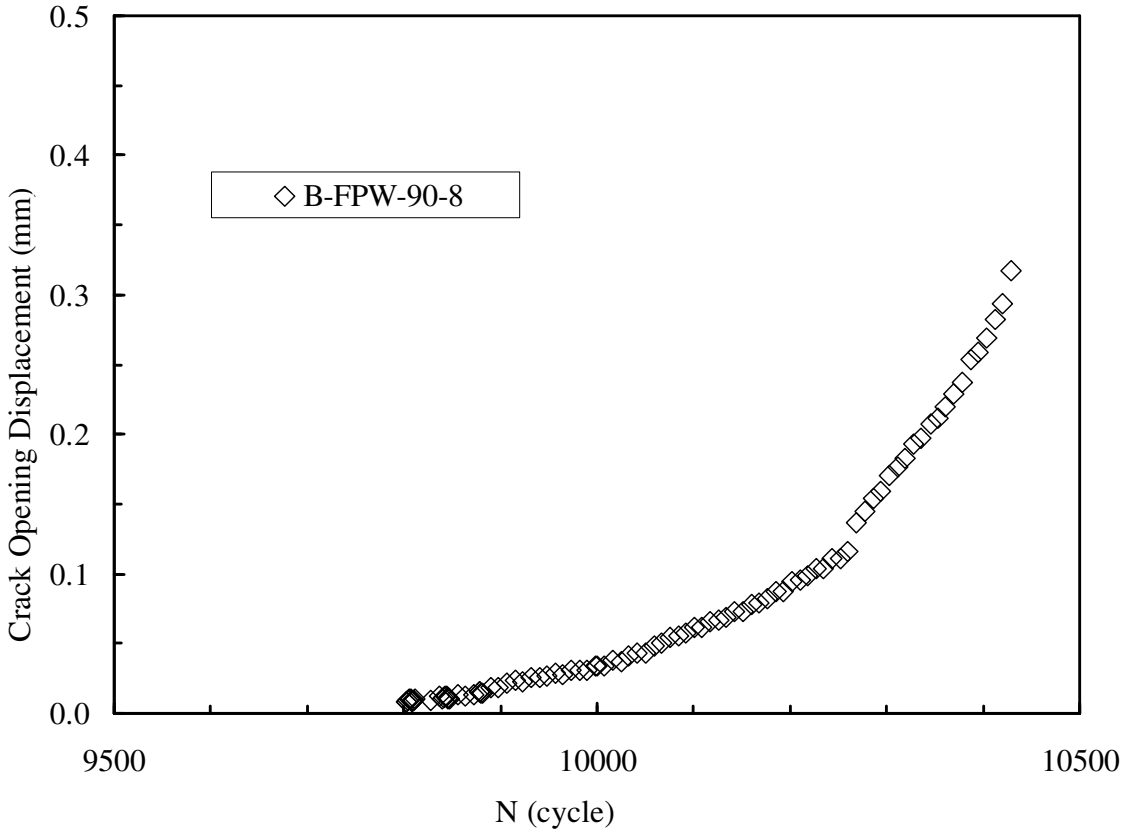

Figure 4.12. Crack opening displacement for B-FPW-90°-8.

Specimen B-FPW-90º-8 was prepared for testing without a starter notch. The specimen was mounted in the test frame, and the load stress amplitude was increased from the previous specimen to 129 MPa. The specimen was observed for the initiation of a fatigue crack, and at a cycle count of 9781 cycles a crack approximately 4 mm long was found to have occurred on the major diameter side of the plug weld. The cyclic load test was paused and specimen was removed from the test frame. The knife edges for the clip gage were then mounted using structural epoxy. The specimen was remounted in the grips of the testing machine, the clip gage mounted, and the cyclic load was again resumed at the same stress amplitude of 129 MPa. The specimen displayed evidence of crack breakthrough on the minor diameter side of the specimen and this occurred at 10292 cycles. Failure of the specimen was considered to occur at 10432 cycles when the minimum valley interlock tripped. It was observed that the fatigue crack had grown to the root side of the plug weld and the crack geometry was now similar to a flat plate with a centrally located hole. The specimen was then monotonically loaded until the specimen fractured.

Fracture surface observation

The fracture surface of specimen B-FPW-90°-7 and -8 are shown in Figures 4.13-16. The fatigue crack initiated in specimen B-FPW-90°-7 within the extruded plug material side of the HAZ region of the FPW. The fracture surface shows a fibrous texture which is typical of failures taking place within this region of the plug weld. The fracture does not show inclination with respect to the specimen face, and follows the extrusion direction of the plug.

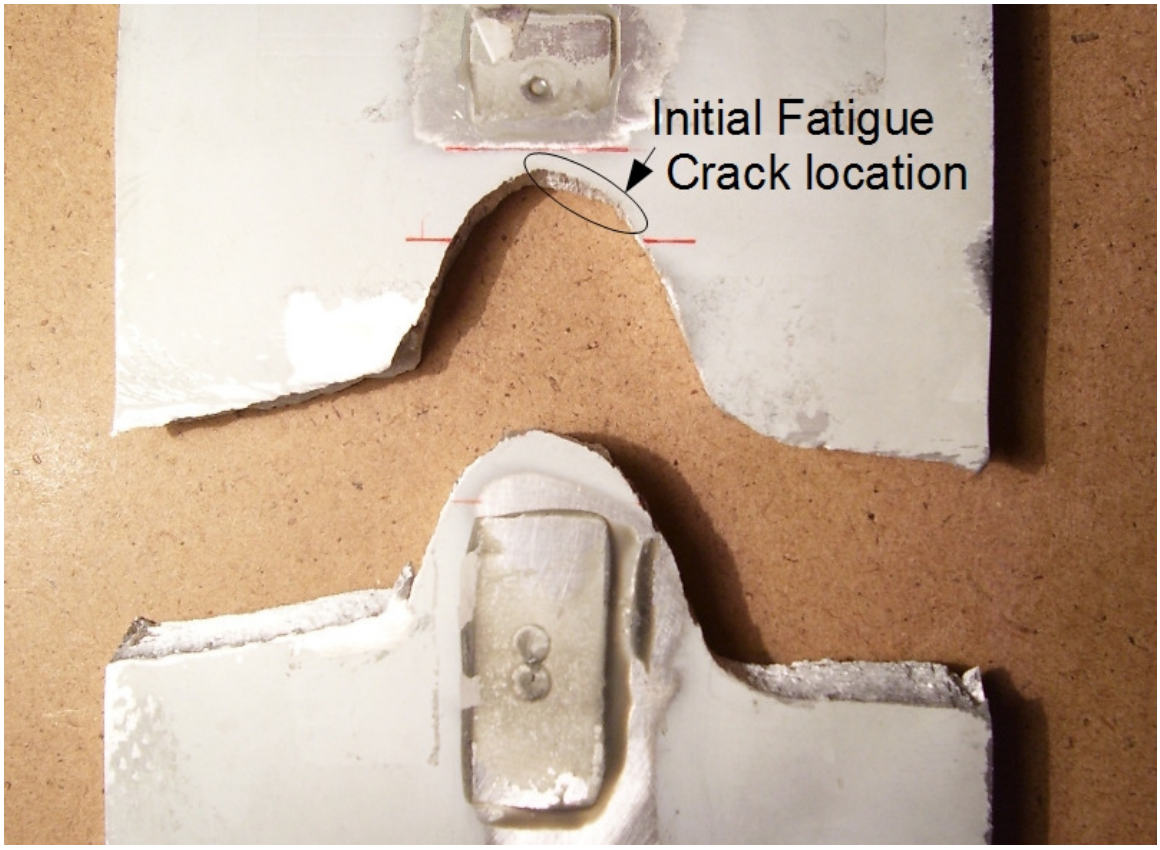

Figure 4.13. Fracture of specimen B-FPW-90°-7.

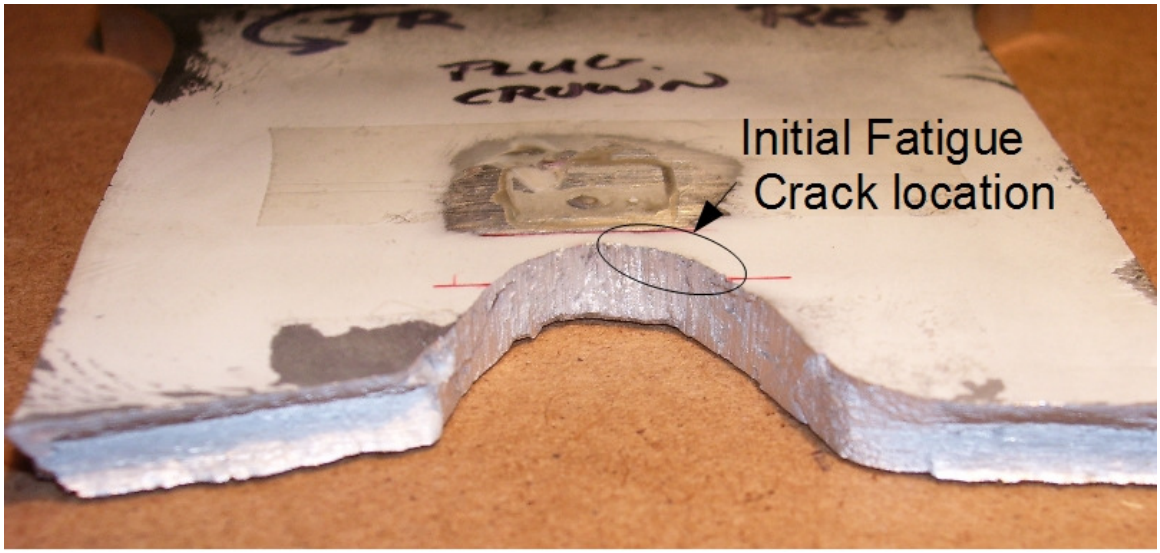

Figure 4.14. Fracture surface B-FPW-90°-7.

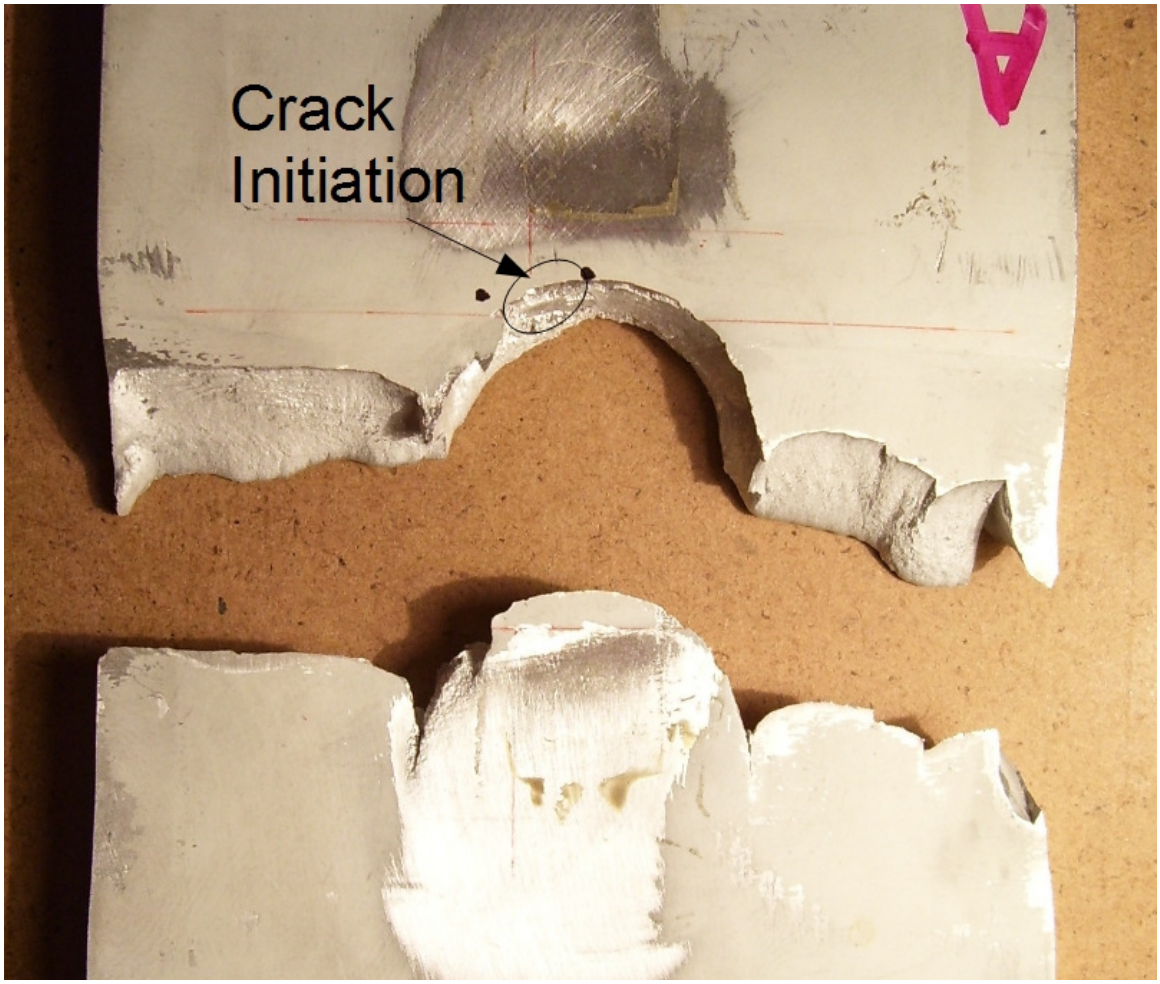

Figure 4.15. Fracture of specimen B-FPW-90°-8.

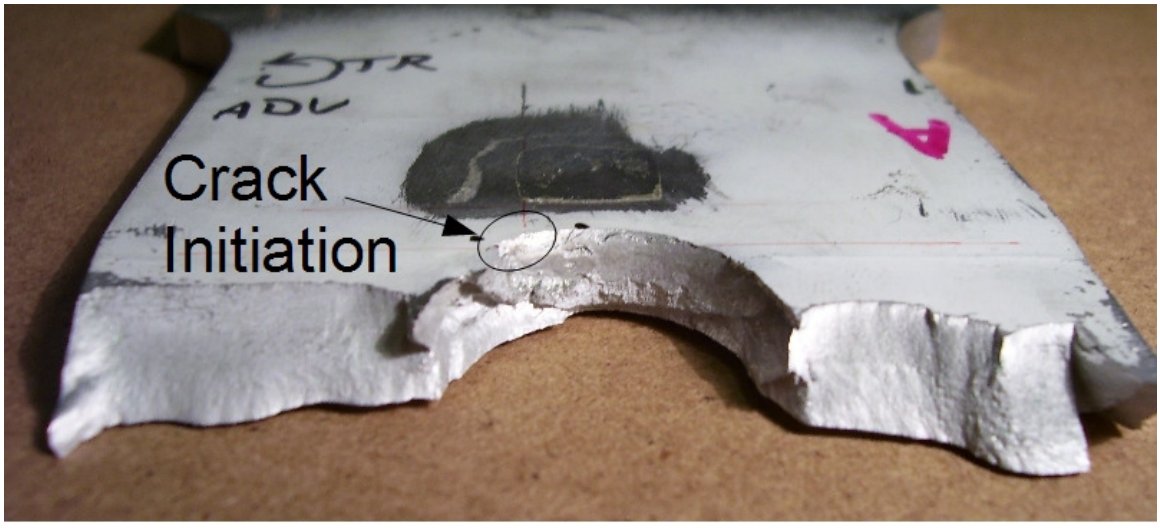

Figure 4.16. Fracture surface of B-FPW-90°-8.

In comparison, the fracture initiated at the plug weld interface for specimen B-FPW-90°-8. The fracture surface shows an inclination with respect to the specimen face and follows the plug weld interface from the major diameter side through the depth of the specimen to the minor diameter side of the plug weld. The surface shows a semi-elliptical pattern of crack growth to the point of break-through. The surface on B-FPW-90-7 was examined visually under 20x magnification and does not exhibit a clearly defined crack initiation region, unlike B-FPW-90°-8 which has a clearly defined initiation area easily identified without the use of magnification.

Estimation of crack growth rate

The data from the COD testing was used to estimate the experimental crack growth rate, da/dN, for the specimens B-FPW-90°-7 and -8. The estimated crack depth, a, which was determined from the correlated COD values obtained from the finite element model, and the cycle count were used to determine the experimental crack growth rate da/dN. The values of ΔK were obtained from the finite element model. Plots of COD vs. cycle number for the specimens B-FPW90°-7 and -8 are shown in Figure 4.15 and 4.16 respectively.

The plot of the determined da/dN versus ΔK for the specimens is shown in Figures 4.15 and 4.16. The crack growth rates for friction stir welded 2195-T8 are shown in these plots in order to compare rates of friction plug welded 2195-T8 [6]. The rates for FSW 2195-T8 were obtained from FCG tests in which C(T) specimens were used. The C(T) specimens had the same R-ratio of 0.1 as was used for the friction plug welded specimens tested in this study.

The experimental crack growth data for FPW shown in Figures 4.17 and 4.18 tends to indicate that the crack growth rate for the friction plug weld specimens tested was similar to that reported for the FSW crack growth rate by other researchers. There is considerable scatter amongst the plotted data points, which most likely reflects the estimation in crack depth and crack growth used in this study.

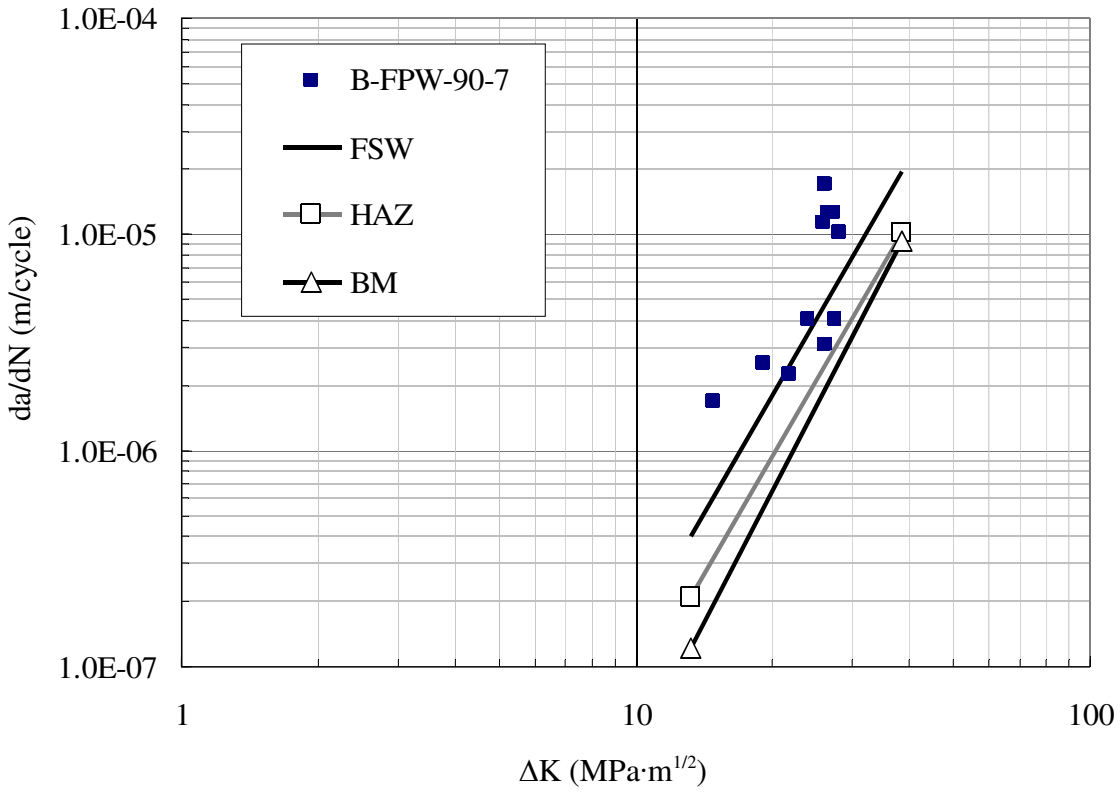

Figure 4.17. Crack growth for B-FPW-90°-7.

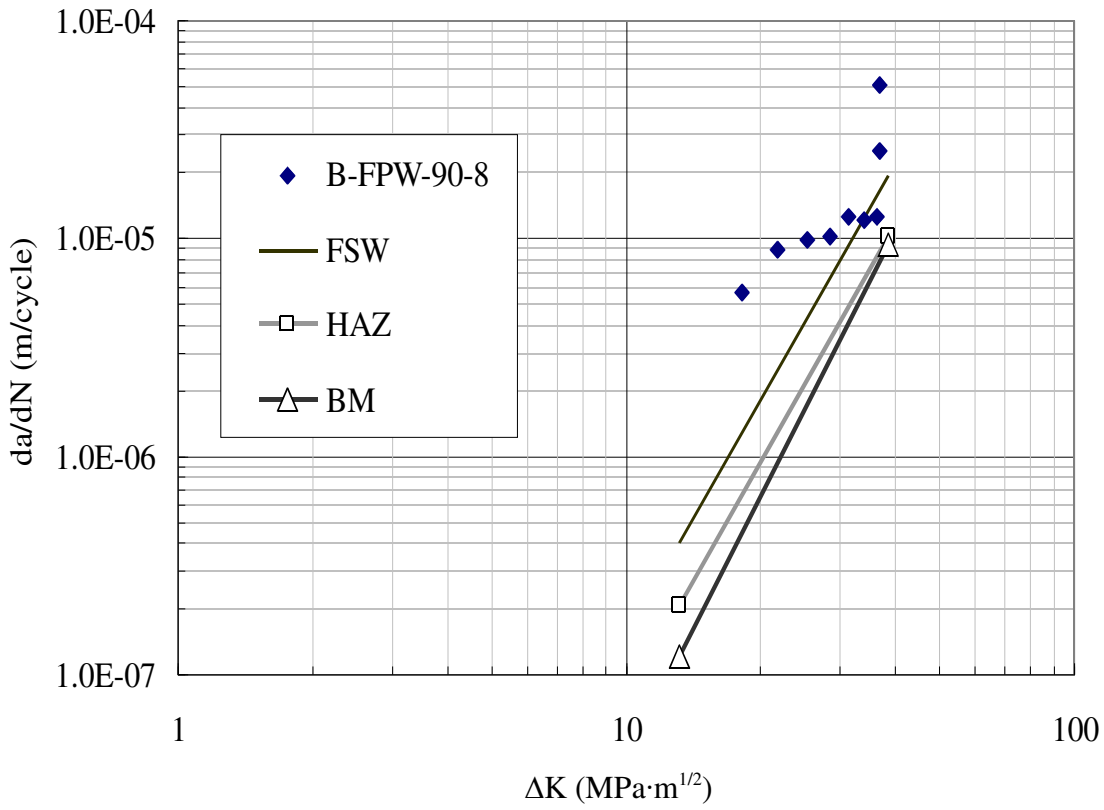

Figure 4.18. Crack growth rate for B-FPW-90°-8.

DISCUSSION

LEFM model and Crack tip plastic zone size

The assumption that the Linear Elastic Fracture Mechanics applied to the portion of crack growth up to breakthrough was made base on the estimated of the plastic zone size ahead of the crack tip being small in relationship to the plate thickness. The size of the plastic zone for cyclic loading is smaller than for monotonic loading [17]. The plastic zone size for cyclic loading under plane stress conditions can be estimated from the following equation

$$r_y = \frac{1}{8\pi}\left(\frac{K}{\sigma_y}\right)^2 \tag{5}$$

where r_y is the radius of he plastic zone, K is the stress intensity factor for the given crack geometry, and σ_y is the yield strength of the material. Calculation of the radius of the plastic zone based for the two specimens tested were r_y of 0.48 mm inch and 0.84 mm for specimens B-FPW-90°-7 and B-FPW-90°-8 respectively. The size of the plastic zone would be indicative that LEFM conditions would apply under the test conditions for most of the fatigue crack growth testing.

In the study of crack growth rate performed by Hafley et al. [7] C(T) specimens of FSW 2195-T8 were used which had thicknesses of 0.25 inch and 0.50 inch. It was reported that no discernible differences in the crack growth rate were observed for the specimens tested due to the thickness of the specimen was found to not have any apparent effect on the fatigue crack growth rate of friction stir welds in 2195-T8.

The calculated crack growth rate for both specimens B-FPW-90°-7 and -8 determined from the

COD method used were found to be higher than that reported for base metal 2195-T8 and FSW 2195-T8. One explanation could be the higher stress amplitudes that were used in this study were causing other damage effects to become significant to the overall crack growth rate. Anderson [15] gives the following equation for high ΔK values associated with region III in the determination of da/dN includes the effects of micro-void coalescence and cleavage in addition to fatigue:

$$\left.\frac{da}{dn}\right|_{total} = \left.\frac{da}{dN}\right|_{fatigue} + \left.\frac{da}{dN}\right|_{MVC} + \left.\frac{da}{dN}\right|_{cleavage} \tag{6}$$

This could be a possible reason why the factor why the da/dN values for both specimens both increase as the ΔK values increased as seen in the plots of da/dN vs. ΔK shown in Figure 4.17 and 4.18.

Another factor affecting the crack growth rate may have been the residual stresses found in both a friction stir weld and friction plug welds [18,19] The location of localized residual stresses may cause an increase in crack growth rate as the crack progresses through the specimen.

Since data for only two of the specimens tested was obtained, it is not possible to compare several specimens at the same load amplitude. Future tests could be improved with a non-contacting method of measuring crack opening displacement using optical tracking methods. Additionally, implementation of a potential drop type of method to determine the crack depth would aid in reducing uncertainty regarding crack depth. Another possible improvement would

be to use load markers at specific points during the test procedure to aid in determination of da/dN values. Although with specimens that fracture within the plug HAZ, identification of the load markers could prove difficult with optical methods.

The specimens B-FPW-90°-7 and -8 both showed a similar distinct change in the COD displacement versus cycle number near the break-through transition where the crack front propagated to the minor diameter side of the plug weld as seen in Figures 4.13 and 4.14. The change in sudden change in COD would most likely have been caused by the crack transition from a curved, semi-elliptical crack to more of a flat plate with a centrally located hole. This transition in crack geometry would have a large increase in local stresses near the edge of the hole, which would directly influence the COD and crack growth rate. The stress intensity value would increase due to the increased stress level near the edge of the hole.

The crack growth rate for the plug welded repairs at lower cyclic stress most likely would be similar to those friction stir welded 2195-T8. The determination of fatigue life and damage tolerance for pressure vessels containing plug weld repairs would need to consider the apparent faster growth rate in the analysis, where as lower cyclic stress levels could most likely use the published data on crack growth rate for determination.

A plot of fatigue life prediction for the two specimens is shown in Figure 4.19. This plot was generated using the results from the Paris law determination of crack growth. The plots show the expected fatigue life of the specimens tested if an initial flaw size were present. The specimen B-FPW-90°-7 was tested at a lower stress amplitude than B-FPW-90°-7, and because of the lower

stress level it has a longer expected fatigue life for the same size initial flaw size. The plot helps illustrate that a reduction in stress amplitude and flaw size can extend the expected fatigue life of the friction plug weld repair.

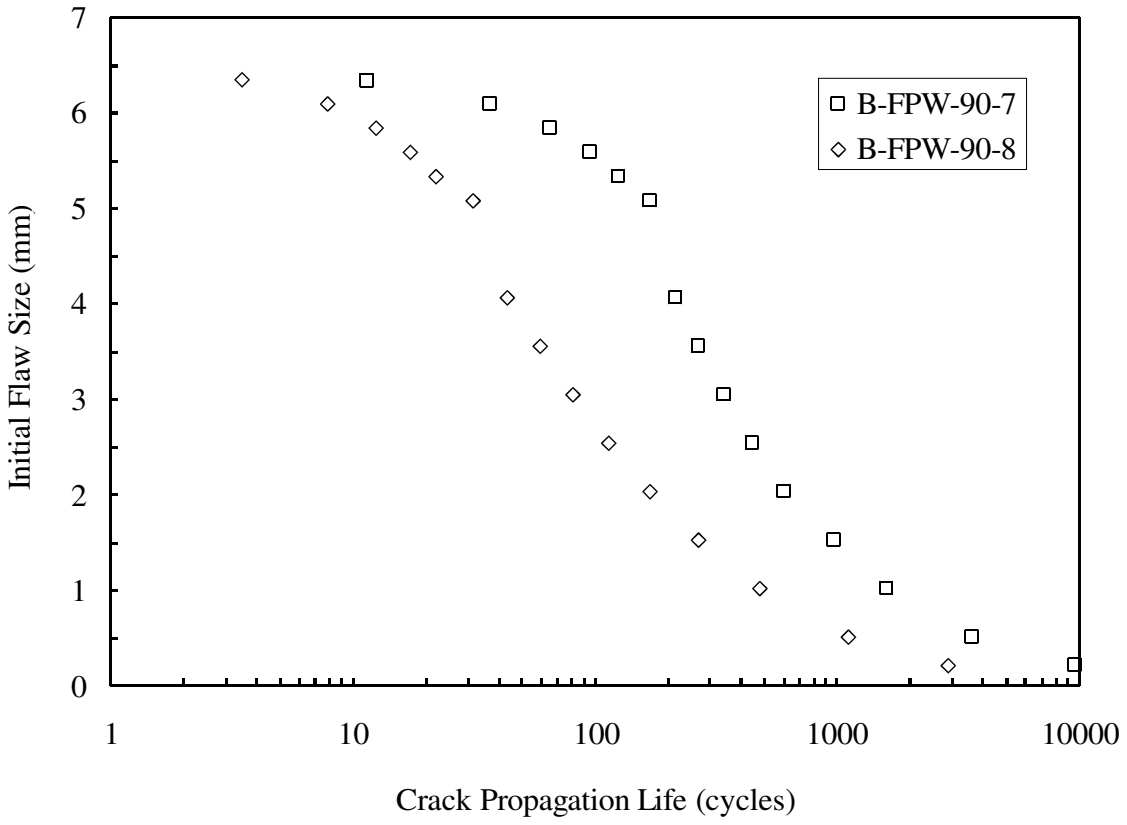

Figure 4.19. Plot of crack propagation vs. initial flaw size for FPW 2195-T8.

CONCLUSION

The crack growth rates of two specimens containing friction plug welds placed in friction stir welded 2195-T8 plate weld specimens was observed to be faster than that of the base metal and friction stir welded 2195-T8 that had been reported by other researchers. The more complex geometry, contact areas, containing different weld joint properties, residual stress, overlapping HAZ zones, and possible small weld voids present in the weld may have lead to the observed difference in crack growth rate. The two specimens tested had differing points of crack origin, but similar crack growth rates were observed.

The lack of a means to observe the progression of the crack front through the material prompted the implementation of an alternate method to indirectly approximate the crack depth. The crack opening displacement data obtained through the use of a clip gage was used in conjunction with a finite element model approximation of COD for representative crack geometry to estimate the crack depth for the corresponding experimental COD. Visual observation of the crack angle observed on the major diameter side of the specimen, and recorded observation of the corresponding cycle number were used to help estimate growth of the specimens tested.

The crack opening displacement method used in this study served as a means for estimating an observed crack growth rate in a friction pug weld specimen that was representative of a repaired section within a pressure vessel. Results show that the fatigue crack growth rate observed was consistent with that reported by other researchers for friction stir welded 2195-T8. An adjustment to the fatigue crack growth rate used in damage tolerance analysis for friction plug weld repairs

using extruded 2195-T8 plugs in friction stir welded 2195-T8 would be recommended when high levels of stress amplitudes are anticipated within the structure.

REFERENCES

[1] Cook, J. R. (2006) NASA Ares I Crew Launch Vehicle Upper Stage Configuration Selection Process. *57th International Astronautical Conference*, October 2-6, 2006, Valencia, Spain.

[2] Coletta, E. R. and Cantrell, M. A. (2000) "Friction Plug Weld Repair Geometric Innovations," Marshall Space Flight Center, NASA Document ID: 20000112928.

[3] Hartley, P. (2000) Friction Plug Weld Repair for the Space Shuttle External Tank, NASA Document ID 20000093962, Johnson Space Center, Marshall Space Flight Center, 2000.

[4] Colleta, E. and Cantrell, M.A., Friction Pull Plug Welding: Chamfered Heat Sink Pull Plug Design, U.S. Patent No. US 6880743 B1, 2005.

[5] Mulvihill, R. J., Safie, F. M., Application of the NASA risk assessment tool to the evaluation of the Space Shuttle external tank re-welding process, *Reliability and Maintainability Symposium, 2000. Proceedings. Annual*, Los Angeles, CA Jan 4-7, 2000.

[6] Subramanian, P., Nirmalan, N., Young, L., Sudkamp, P., Mika, D., Larsen, M., Othon, M., Dupree, P., Walker, S., and Catlin, G. (2003) Fundamental Studies of Microstructure Evolution during Stir Welding of Aluminum Alloys, NASA Technical Report No. 20031028177.

[7] Hafley, R., Wagner, J., and Domack, M. (2000) Fatigue Crack Growth Rate Test Results for Al-Li 2195 Parent Metal, Variable Polarity Plasma Arc Welds and Friction Stir Welds, NASA TM-2000-210098.

[8] Blankenship, C. P. and Starke, E. A. (1991) The Fatigue Crack Growth Behavior of the Al-Cu-Li Alloy Weldalite 049, *Fatigue Fract. Eng. Mater. Struct.*, **14**, 103-114.

[9] Moriera, P. M. G. P., de Jesus, A. M. P., de Figueiredo, M.A.V., Windich, M., Sinnema, G., and de Castro, P.M.S.T. (2010) Fatigue Crack Growth behavior of Friction Stir Welded Aluminum-Lithium Alloy 2195, XXVII Meeting of the Grupo Español de Fractura and 12th Portuguese Conference on Fracture, Porto, Portugal, 17-19 March 2010.

[10] Chen, D. and Chaturvedi, M.C. (2000) Near-Threshold Fatigue Crack Growth Behavior of 2195 Aluminum Lithium Alloy Prediction of Crack Propagation Direction and Influence of Stress Ratio, *Metall. Mater. Trans*. **31A**, 1531-1541.

[11] Metz, D. F. and Barkey, M. E. (2012) Fatigue behavior of friction plug welds in 2195 Al-Li alloy. *Int. J. Fatigue* **43**, 178-187.

[12] Vaidya, W. V., Angamuthu, K., and Kocak, M. (2010) Utilizing COD_{max} as an Indirect Fatigue Crack Length Measurement Parameter for M(T) Specimens of an Airframe Aluminum Alloy AA6056, *MP Materials Testing*, **52,** 771-777.

[13] Sullivan, A. M. and Crooker, T. W. (1977) A crack-opening-displacement technique for crack length measurement in fatigue crack growth testing–development and evaluation, *Engineering Fracture Mechanics*, **9**, 159-166.

[14] FEACrack Software, Quest Integrity Group, LLC, 2465 Central Ave Suite 110, Boulder, CO, 80301 USA.

[15] Anderson, T. L. (2005) *Fracture Mechanics Fundamentals and Applications.* CRC Press, Boca Raton, FL.

[16] Schijve, J. (2009) Fatigue of Structures and Materials. Springer.

[17] Bannantine, J. (1989) *Fundamentals of Metal Fatigue Analysis.* Prentice Hall, New Jersey.

[18] Sutton, M. A., Reynolds, A. P., Wang, D. Q., and Hubbard, C. R. (2002) A study of residual stresses and microstructure in 2024-T3 aluminum friction stir welds.

[19] Kroninger, H. R. and Reynolds, A. P. (2002) R-curve behavior of friction stir welds in aluminum-lithium alloy 2195, Fatigue Fract. Eng. Mater. Struct. **25**, 283-290.

CHAPTER 5

CONCLUSION

The purpose of this study was to characterize the mechanical, fatigue and crack growth of friction stir welded 2195-T8 Al-Li that contained friction plug weld repairs. The mechanical properties were determined by uni-axial tensile tests of specimens for base metal, friction stir weld, and friction plug welds. The results show that the tensile strength of the friction plug weld reduced the strength of the friction stir weld. This reduction was likely due to lack of fusion with the surrounding base metal and friction stir weld and voids introduced by the plug weld repair.

Fatigue tests were performed on friction stir weld specimens and friction stir weld specimens that contained a friction plug weld repair using constant amplitude loading. Results from the fatigue tests show that the fatigue life of a friction stir weld that contains a friction plug weld repair was reduced from that of those that did not have a friction plug weld repair. The process parameters used during the friction plug weld can influence the fatigue life. Optimized plug weld parameters resulted in improved fatigue lives for plug welded specimens. There was an increased amount of scatter in the fatigue data for the plug welded specimens compared with specimens that did not contain plug welds.

The crack growth properties of friction plug welds at high stress levels were investigated by the use of a crack mouth opening displacement method. Comparison was made to the crack growth rates for or friction stir welded 2195-T8 in the following zones: base metal, heat affected zone, and stir zones. The investigation showed that a plug weld tends to have a higher rate of crack growth when compared to the crack growth rate of a friction stir weld.

Based on the results of the study, the following conclusions can be stated:

1. The microhardness of the region at the plug weld interface was seen to be reduced from the base metal hardness by approximately 35%.
2. The thickness of the recrystallized zone at the plug weld interface varied in thickness from 20- 122 μm. The taper angle of the plug may cause significant changes in thermal gradients during the plug weld procedure.
3. The process parameters used to make a friction plug weld repair have a direct influence on the mechanical properties of a friction stir weld. A reduction in tensile strength was noted for specimens that contained non-optimized friction plug welds.
4. The fatigue properties of friction plug weld repairs are dependent on the process parameters used to make the friction plug weld repair. The fatigue life is reduced for non-optimized plug welds.
5. The crack growth rate for friction plug welds at high stress levels should be considered in the evaluation of damage tolerance for the intended application in aerospace pressure vessels.

REFERENCES

[1] Hartley, P. (2000) Friction Plug Weld Repair for the Space Shuttle External Tank, NASA Document ID 20000093962, Johnson Space Center, Marshall Space Flight Center, 2000.

[2] Wells, D., 2008. NASA MSFC, Damage Tolerance Group (EM20), Personal communication.

[3] Coletta, E. R. and Cantrell, M. A. (2000) "Friction Plug Weld Repair Geometric Innovations," Marshall Space Flight Center, NASA Document ID: 20000112928.

[4] Colleta, E. and Cantrell, M.A., Friction Pull Plug Welding: Chamfered Heat Sink Pull Plug Design, U.S. Patent No. US 6880743 B1, 2005.

[5] Li, Z., Cantrell, M. A., and Brown, R. J., Process Development and Microstructural Characterization of Friction Plug Welded 2195 and 2219 Alloys. AeroMat 2000 Conference, Seattle, WA, USA, June 2000.